REPORT R-474 JUNE, 1970 UILU-ENG 70-219

CSL COORDINATED SCIENCE LABORATORY

THE INTERNAL STRUCTURE OF SHOCK WAVES

BRUCE L. HICKS
SHEE-MANG YEN
BARBARA J. REILLY

UNIVERSITY OF ILLINOIS - URBANA, ILLINOIS

THE INTERNAL STRUCTURE OF SHOCK WAVES

Bruce L. Hicks, Shee-Mang Yen and Barbara J. Reilly

This work was supported in part by the Joint Services Electronics Program (U.S. Army, U.S. Navy & U.S. Air Force) under Contract DAAB 07-67-C-0199; and in part by ONR N00015-67-A-0305-0001.

TABLE OF CONTENTS

THE INTERNAL STRUCTURE OF SHOCK WAVES

Bruce L. Hicks, Shee-Mang Yen and Barbara J. Reilly

Abstract

The non-linear Boltzmann equation has been solved for shock waves in a gas of elastic spheres. The solutions were made possible by the use of Nordsieck's Monte Carlo method of evaluation of the collision integral in the equation. Accurate solutions were obtained by the same method for the whole range of upstream Mach numbers M_1 from 1.1 to 10 even though the corresponding degree of departure from equilibrium varies by a factor greater than 1000. Many characteristics of the internal structure of the shock waves have been calculated from the solutions and compared with Navier-Stokes, Mott-Smith and Krook descriptions which, except for low Mach numbers, are not based upon the Boltzmann equation itself.

Among our conclusions are the following:

1. The reciprocal shock thickness is in agreement with that of the Mott-Smith shock (u^2-moment) from M_1 of 2.5 to 8. The density profile is asymmetric with an upstream relaxation rate (measured as density change per mean free path) approximately twice as large as the downstream value for weak shocks and equal to the downstream value for strong shocks.

2. The temperature density relation is in agreement with that of the Navier-Stokes shocks for the lower Mach numbers in the range of 1.1 to 1.56. The Boltzmann reciprocal shock thickness is smaller than the Navier-Stokes value at this range of Mach number because the viscosity-temperature relation computed is not constant as predicted by the linearized theory.

3. The velocity moments of the distribution function are, like the Mott-Smith shock, approximately linear with respect to the number density; however, the deviations from linearity are statistically significant. The four functionals of the distribution function discussed show maxima within the shock.

4. The entropy is a good approximation to the Boltzmann function for all M_1. The solutions obtained satisfy the Boltzmann theorem for all Mach numbers. The increase in total temperature within the shock is small, but the increase is significantly different from zero.

5. The ratio of total heat flux q to q_x (associated with the longitudinal degree of freedom) correlates well with local Mach number for all M_1 in accord with a relation derived by Baganoff and Nathenson. The Chapman-Enskog linearized theory predicts that the ratio is constant. The (effective) transport coefficients are larger than the Chapman-Enskog equivalents by as much as a factor of three at the mid-shock position.

6. At $M_1=4$, and for 40% of velocity bins, the distribution function is different from the corresponding Mott-Smith value by more than three times the 90% confidence limit. The rms value of the percent difference in distribution function is 15% for this Mach number. The halfwidth and several other characteristics of the function $\int f dw_y dv_z$ differ from that of the Chapman-Enskog first iterate, and many of the deviations are in agreement with an experiment by Muntz and Harnett.

7. The ratio of the collision integral (found from our solution of the Boltzmann equation) to that calculated from Mott-Smith velocity distribution functions is approximately 0.8 near the cold side for the majority of the velocity bins and varies below and above one elsewhere in a shock for $M_1=4$. Comparison of the Boltzmann collision integrals with the Krook expression indicates that

the latter expression is inadequate in several respects for representing qualitatively the characteristics of either the gain term or the loss term of the Boltzmann collision integral, near the upstream and downstream region of the shock. Therefore, in these regions, the solutions of the Krook equation will not agree with solutions of the Boltzmann equation.

8. A three-dimensional, computer-generated graphical display was found to be useful in representing variations of the distribution function f and the collision integral in the velocity space and for studying their characteristics.

INTRODUCTION

Nordsieck's Monte Carlo Method

A shock wave is a commonly occurring, well-defined, non-equilibrium phenomenon in gas dynamics. It is therefore desirable to be able to determine any of its properties that are currently of physical interest and to be able to determine others as they are needed in the future. Unfortunately, experiment yields only a few properties of shock waves and, until recently, calculations of the structure of strong shocks have been based upon assumptions whose validity has not been established.

Nordsieck's development of an accurate Monte Carlo evaluation of the collision integral in the non-linear Boltzmann equation has radically altered this situation, both for shock wave calculations and for other rarefied gas dynamics problems. No longer is it necessary to assume near-equilibrium or near-free-molecule flow, nor to assume the validity of equations that substitute for the full, non-linear Boltzmann equation. Nordsieck's evaluation of the collision term (gain and loss terms separately) makes possible direct solution of this basic equation, a possibility that has been largely ignored in the century since it was derived by Boltzmann.

Nordsieck's method was developed in 1958 and was first described in the literature in 1966.[1] Brief accounts of the application of the method to strong shock waves have appeared there and in the Proceedings of the Sixth Rarefied Gas Dynamics Symposium.[2] Applications to other problems have been made by Hicks and Yen.[3,4,5,6] Part of an extensive analysis of the systematic and random errors of the method and its applications was described in a paper published in 1968.[7] More recent analysis of the errors and improvements of the method have been described in a CSL report.[8]

Using Monte Carlo evaluation of the nonlinear collision integrals, we solved the non-linear Boltzmann equation, during 1968-1969, for shock waves in a gas of elastic spheres. We used the same numerical methods for eight Mach numbers in the range 1.1 to 10. In the present paper we describe selected results from these calculations.

There are several reasons for publishing only selected results of these shock wave calculations, the most obvious being the large volume of results, larger than it is possible to reprint in a journal. Only a small fraction of the calculated values of the Boltzmann collision integral, for example, can be reported here. Furthermore, no direct comparison with experimental results are possible until new theory is developed that predicts the effects upon the collision integral of changing the intermolecular forces or until differential cross sections for realistic, slightly "soft" molecular fields are known. It is also impossible to predict exactly which detailed computed properties of shock structure will be needed in the future to compare with other calculations and with experiment. Using our basic Boltzmann program, however, which solves the Boltzmann equation, and the AVERR program, which gives detailed information about moments and functions derived from them, we can relatively easily calculate the specific details of shock structure when they are needed.

For these reasons we have chosen to describe here those characteristics of shock waves having the greatest physical interest at present. These characteristics are named in the section headings. With one exception we discuss first those characteristics which are most commonly treated in gas dynamics, namely, shock thickness and density gradients, (these two properties alone do not, of course, provide full characterization of a shock wave). We then discuss less familiar characteristics, like Boltzmann flux and longitudinal transport of heat,

concluding with a description of the microscopic properties of the shock as defined by the velocity distribution function and its spatial derivative.

It is useful to preface our discussion of these characteristics with general remarks on our methods. For a number of reasons (summarized in a CSL report[9]) we find it desirable to use the local particle density n as the independent variable rather than x, the position coordinate. Except in Sect. 2, then, we consider variations of the different shock properties as functions of n rather than of x. We use the dimensionless variable $\hat{n} = (n-n_1)/(n_2-n_1)$.

The solutions we discuss are iterative solutions of the Boltzmann difference equation, which we have reason to believe approximate well the solutions of the differential equation.[7,9] The difference equation is solved by embedding Nordsieck's Monte Carlo method of evaluating the collision integral in an iterative scheme of finding velocity distribution functions (everywhere in the shock wave and at all positions in velocity space) which produce two sides of the Boltzmann equation that are equal within about 1%. We have studied the convergence of the iterative scheme and made strong uniqueness tests of our solutions. The results of weaker tests have been published.[7]

The units we use are the values, denoted by the subscript 1, of various properties of the upstream gas. Thus n_1, T_1 are the units of number density n and temperature t. The unit of length $\ell_1 = 1/(2\pi n_1\sigma^2)$ = (mean free path)$_1/\sqrt{2}$. The unit of velocity $c_1 = \sqrt{(2\pi kT_1/m)}$ = (mean speed)$_1 \times (\pi/2)$. The unit of time is therefore (mean free time)$_1 \times (\sqrt{2/\pi})$ and of the velocity distribution function is n_1/c_1^3. In these units the Boltzmann equation for the shock wave is

$$v_x \partial f/\partial x = a - bf = \int (FF'-ff') \left|\bar{k}\cdot\bar{v}_r\right| d\bar{v}' (d\bar{k}/4\pi),$$

where $f = f(\bar{v},x)$ is the velocity distribution function; x is the distance variable, perpendicular to the shock; the unit vector $\bar{k}$ gives the direction of the line of centers during a collision; $\bar{v}_r = \bar{v}' - \bar{v}$; and f,f',F,F' denote the four values of f corresponding to the four velocities, $\bar{v},\bar{v}',\bar{V},\bar{V}'$. Integration is over the whole 4π solid angle in order that the $\bar{k}$ integration limits may be independent of $\bar{v}$ and $\bar{v}'$. The notation bf reminds us that this second part of the collision integral is proportional to $f(\bar{v},x)$, a fact of importance in devising a stable method of integrating the differential equation.

In all calculations we used 226 bins in velocity space. For this subdivision of velocity space it is possible to make meaningful calculations up to a Mach number $M_1 = 10$ but not much higher. We used the LS and the MB corrections and the "single sample" technique (described elsewhere[8]) throughout the calculations in the entire M_1 range of 1.1 to 10. For each M_1, runs were made for each of four large, independent collision samples (2^{13} collisions per sample), yielding estimates of the mean value and the statistical error of <u>any</u> quantity derived from either the velocity distribution functions or the collision integrals. The rms probable errors of the velocity distribution function, calculated by our solution of the Boltzmann equation, were determined for each Mach number and are about 3% for a Mach number of 4. The probable errors in various moments of the velocity distribution and of the collision integral are smaller by factors of ten to one hundred. This level of accuracy is obtained on the CDC 1604 digital computer (50 microsecond multiplication time) in a run lasting about two hours, for each Mach number.

The values of the mean and the statistical error of each function derived from the velocity distribution function or the collision integral is calculated by the AVERR program. This program computes the means and errors of

101 functions for each set of four collision samples, for each position in the shock and for each value of the Mach number. We discuss seventeen of these functions in later sections of the paper.

The overall method is summarized in Fig. 1. As shown in this figure, properties and transport properties of shock waves are calculated from the moments of the distribution function; gradients, from the moments of the collision integrals; and transport coefficients, from both of the two moments.

Remarks on other Determinations of Shock Properties

Much of our discussion of the results will make use of comparisons with Mott-Smith shock waves. We have tested the accuracy of the Mott-Smith solutions in satisfying the Boltzmann equation and have found that our Monte Carlo solutions satisfy the Boltzmann equation more accurately by a factor of 100. Since we know the magnitudes of the random errors of our solutions, we can state unequivocally, in the comparison with the Mott-Smith solution, which differences are significant and which are not. The comparison with Mott-Smith results is of interest because we have found that the qualitative features of the Mott-Smith velocity distribution functions are correct and that some of the Mott-Smith moments give surprisingly good accuracy despite the error in the distribution function itself.*

Furthermore, the Mott-Smith shock is easy to interpret physically, and it possesses the simple property that each moment of the velocity distribution function is a linear function of n, the particle density. Use of the Mott-Smith

---

*It is, therefore, clear that it would not be possible to establish accuracy of any proposed solution $f(\bar{v},x)$ solely on the basis of the moments of the distribution function.

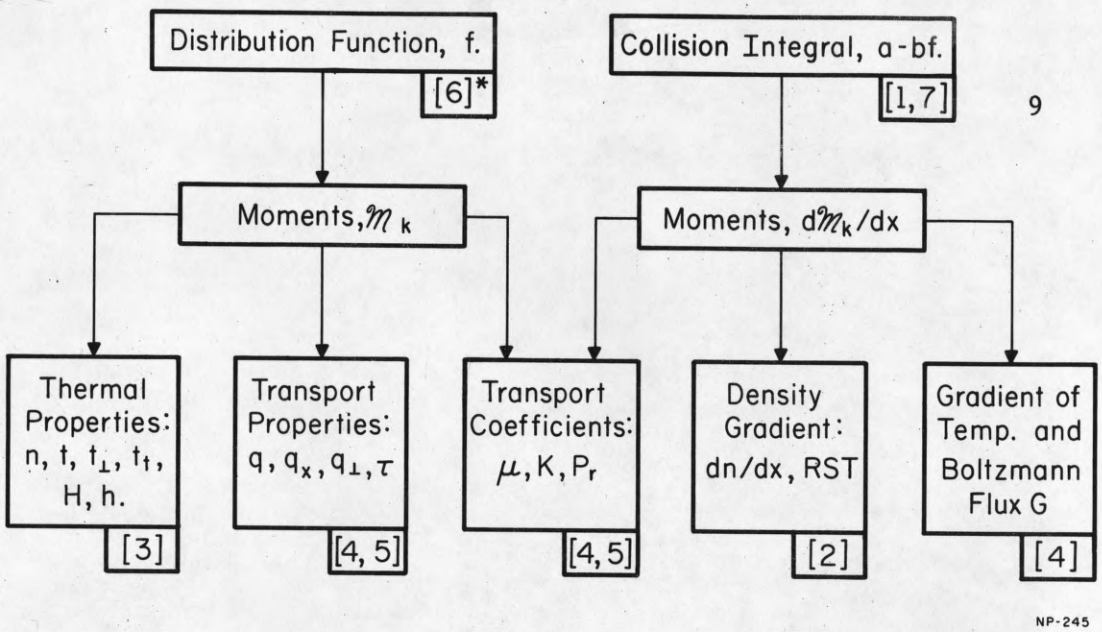

Fig. 1 Overall method of computation of shock wave properties from the solution of the Boltzmann equation.

Definitions of Symbols

f	velocity distribution function
a-bf	Boltzmann collision integral
n	particle density
x	coordinate perpendicular to the plane of the shock
$\mathcal{M}_k$	k-th moment of f
$d\mathcal{M}_k/dx$	k-th moment of df/dx
RST	reciprocal shock thickness
G	Boltzmann flux
h	H/n
H	Boltzmann function
t	temperature
$t_\perp$	lateral temperature
t_t	total temperature
q	heat flux
τ	stress
μ	viscosity coefficient
k	thermal conductivity

subscripts

x	associated with x component
$\perp$	associated with perpendicular component
t	total

*Number of the section where this shock property is discussed.

model thus permits us to present detailed results, especially in Sections 7 and 8, in a rather compact form. Also, since many other proposed shock wave solutions have been compared with Mott-Smith results, the difference between our Monte Carlo solutions and these solutions can also be easily predicted.

1. Measures of Departure from Equilibrium

Shock waves are interesting phenomena in rarefied gas dynamics because their interiors exhibit large departures from thermal equilibrium. It is therefore appropriate to discuss measures of this departure before discussing other aspects of shock waves.

A monatomic gas is in a state of thermal equilibrium if it has a Maxwell-Boltzmann velocity distribution function. One measure, then, of the departure of a gas from thermal equilibrium is the deviation of its velocity distribution function $f(\bar{v})$ from the Maxwell-Boltzmann form.

We may write the deviation as

$$\delta f = f - f_{eq} \tag{1.1}$$

where f_{eq} is a Maxwell-Boltzmann function that corresponds to the same values of density n, gas velocity u and temperature (or total energy) t. Since the Krook model of the collision integral is proportional to δf, this measure is essentially just the Krook collision integral, although f is <u>not</u>, in general, a solution of the Krook equation.

A monatomic gas is also known to be in a state of thermal equilibrium if the Boltzmann collision integral vanishes. Thus a second measure of the departure from thermal equilibrium is the deviation of the collision integral from zero. We write this in fractional form as

$$\delta\gamma = (a - bf)/a = 1 - (bf/a) \tag{1.2}$$

where each quantity a, bf and $\delta\gamma$ is a function of $\bar{v}$.

In certain circumstances we are interested in the variation of δf and of $\delta\gamma$ throughout velocity space. Usually, however, we would use more global measures of departure from equilibrium, which we obtain by integrating (or summing or bounding) δf, $(a-bf)$, or $\delta\gamma$ over velocity space. Among these global measures are the following:

a) rms values of δf;

b) rms values of $\delta\gamma$ or of related functions;

c) maximum values of $\delta\gamma$;

d) heat flux q and stress τ and other properties which can be calculated from moments of f;

e) moments of $(a-bf)$.

Our calculations yield values of each of these measures of departure from equilibrium, but we shall discuss just two of them, the second and fifth ones in this section and the fourth one in Sections 3,4, and 5.

In our studies of the relative departure from equilibrium we have found it convenient to use a certain function of $\delta\gamma$ or of the ratio a/bf. This function is

$$\psi(a/bf) = (a-bf)/(a+bf) = \delta\gamma/(2-\delta\gamma). \qquad (1.3)$$

Its value runs from -1 (for a/bf=0) to +1 (for bf/a=0). For a gas in equilibrium its value is zero. The global measure of departure from equilibrium that we use is the rms value of $\psi(a/bf)$ over velocity space, which we call ψ_{ab}. The values of ψ_{ab}, for different Mach numbers and different positions in the shock waves, show us the degree of the local departure of the gas from thermal equilibrium.

Fig. 1.1 summarizes the degree of departure from thermal equilibrium at three positions in shock waves for Mach numbers ranging from 1.1 to 10. We notice first the very large range of values of ψ_{ab}, from 1.3×10^{-3} near the hot side ($\hat{n} = 7/8$) of the weakest shock ($M_1 = 1.1$), to 0.32 near the cold side ($\hat{n} = 1/8$) of the strongest shock ($M_1 = 10$). These two values of ψ correspond, roughly, to values of $|\delta\gamma|$ equal to 3×10^{-3} and 0.5, respectively. Our development of Nordsieck's method of evaluation of the collision integral has made it possible to solve the Boltzmann equation over this very wide range of non-equilibrium conditions.

A second characteristic of the curves in Fig. 1.1 is noteworthy: for Mach numbers larger than about 1.2 the departure from equilibrium, as measured by ψ_{ab}, is larger near the cold side ($\hat{n} = 1/8$) than in the center of the shock ($\hat{n} = 1/2$). Inspection of the isolines of ψ_{ab} show that the origin of this effect lies in the large values of $|\psi|$ (or of bf/a) for negative values of v_{xa}, that is, corresponding to the molecules with backward velocity relative to the shock that are being (rapidly) produced by the collisions. This non-equilibrium phenomenon, due to "diffusion" of such high speed molecules backward or toward the cold side of a shock wave or other rarefied gas flow, has provoked the interest of researchers for many years.

Krook[10] suggested the use of a local Knudsen number $(Kn)_\ell$ which may be defined as

$$(Kn)_\ell = \frac{\ell}{\Phi}_1 \left(\frac{d\Phi}{dx}\right) \qquad (1.4)$$

where ℓ = local mean free path and Φ = any macroscopic property (dimensionless).

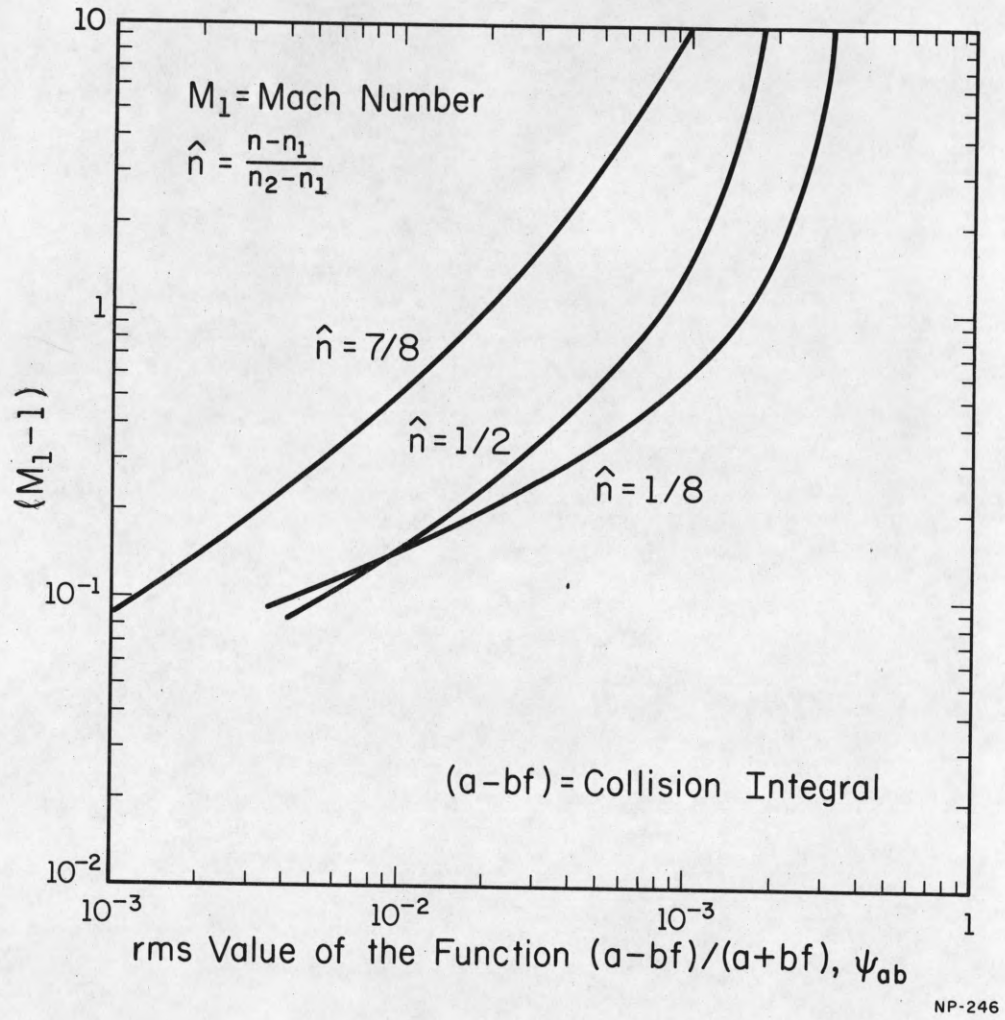

Fig. 1.1 Maximum departure from thermal equilibrium in weak and strong shock waves.

Since $\ell = [\int a d\bar{v}]/[n \times \text{ref. velocity}]$ and $d\Phi/dx = \int (a-bf)\phi d\bar{v}/v_x$, we are able to calculate any such local Knudsen number from moments of the collision integral. When $(Kn)_\ell$ defined on the basis of density (i.e., $\Phi=n$) was calculated, it was found, in contrast to ψ_{ab}, that the departure from equilibrium measured this way is larger near the hot side than the cold side.

2. Shock Thickness and Density Gradients

As noted in the Introduction, we will use n rather than x as independent variable in giving a detailed discussion of shock structure. The present section will concern itself with relation between n and x. Discussion of this relation will show the nature of the $x \rightarrow n$ transformation and will also exhibit characteristics of the density profile in the shock waves. A comparison of Boltzmann and Navier-Stokes density gradients, for $M_1 = 1.2$, will be given in Section 6.

The density is a sigmoid function of x which is approximated by the hyperbolic tangent function first suggested by Mott-Smith.[11] The density profiles, for two Mach numbers are shown in Fig. 2.1. These calculated curves are not symmetrical, but the asymmetry is not easy to see in an n vs x plot. Also, choice of origin is arbitrary, which makes objective comparison among n-x curves from various sources rather difficult. Plotting dn/dx vs $\hat{n}$ (density gradient profile), to be discussed shortly, removes both of these difficulties.

Just one characteristic of the density profile (or of the density gradient profile) is usually used to represent shock structure, namely, the RST (reciprocal shock thickness). It is also the characteristic most commonly determined by experiment. In defining RST we first introduce the reduced density

$$\hat{n} = (n - 1)/(n_2 - n_1) \qquad (2.1)$$

which ranges from 0 on the cold side (n=1) to 1 on the hot side ($n=n_2$).

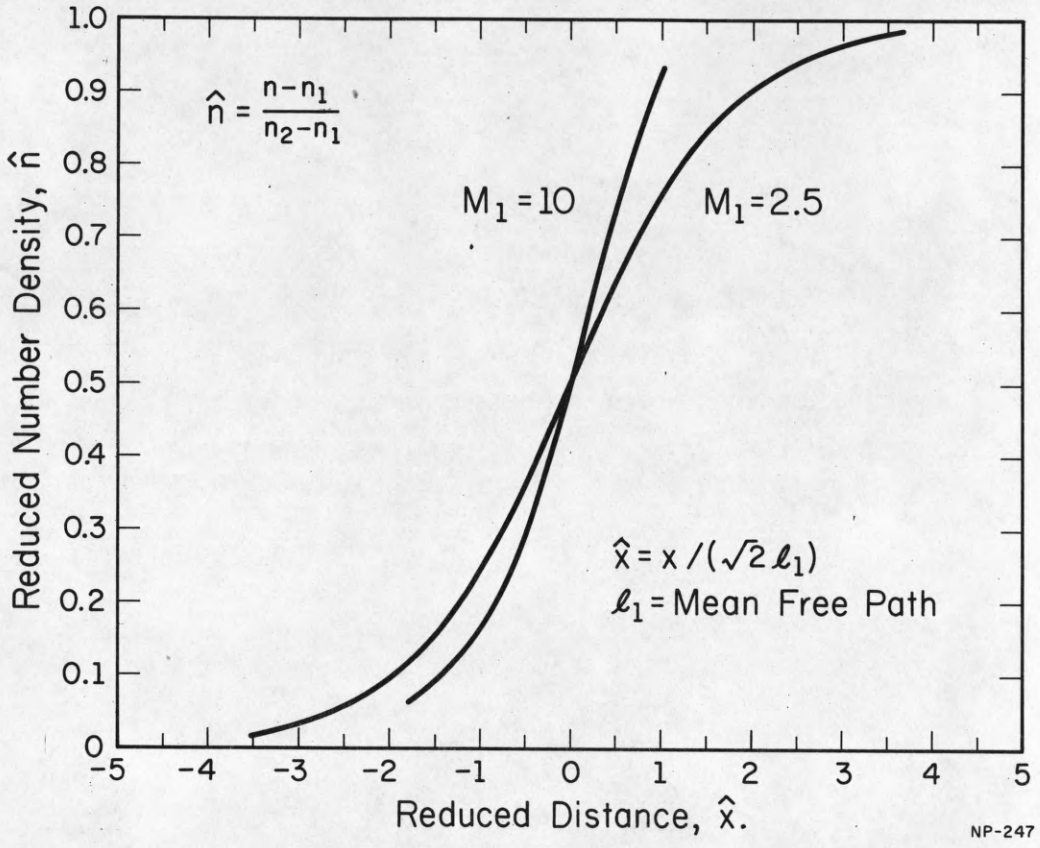

Fig. 2.1 Variations of reduced number density $\hat{n}$ with reduced distance $\hat{x}$.

This reduced density gradient $d\hat{n}/dx$ has a maximum value $[d\hat{n}/dx]_{max}$ somewhere within the shock. Then*

$$RST = \sqrt{2}\,[d\hat{n}/dx]_{max} \,. \tag{2.2}$$

The unit of RST here is the upstream mean free path.

Many theoretical calculations of the shock wave have been made on the basis of different collision laws. In order that the RST on the basis of these calculations could be compared with each other (or with experimental values for different gases), it has been suggested that a reference mean free path other than the upstream value be used. For low Mach numbers, Sherman[12] suggested the use of the mean free path for M = 1, assuming that the maximum slope occurs at the same location with M = 1. For large Mach numbers, Ziering[13] has found that, for Mott-Smith shocks, the RST is insensitive to the collision law if the mean free path at the point where $\hat{n} = \frac{1}{2}$ is used as the reference value in defining the shock thickness.

Our solutions of the Boltzmann equation for shock waves in a gas of elastic spheres lead to the values of RST in Figs. 2.2 and 2.3. We should like to point out these values of RST were evaluated from the moment of the collision integral, not from the n-x curve.

As shown in Fig. 2.2, the RST for low Mach numbers are smaller than the corresponding Navier-Stokes results.† Since the characteristics of the

---

*To be more specific we might call this the (density) RST to suggest that reciprocal shock thicknesses based on the profiles of other gas properties are different from RST for density.

†The RST curve for Navier-Stokes for M_1=1-2 is obtained from calculations of algebraic theory.[14] This curve deviates, on the average, by 1.6% from Wang-Chang's result[15] for M_1=1-1.2; by 3.8% from Grad's result[16] for M_1=1.2; and by less than 1% from Schmidt's numerical results[17] for M_1=1.2-2.

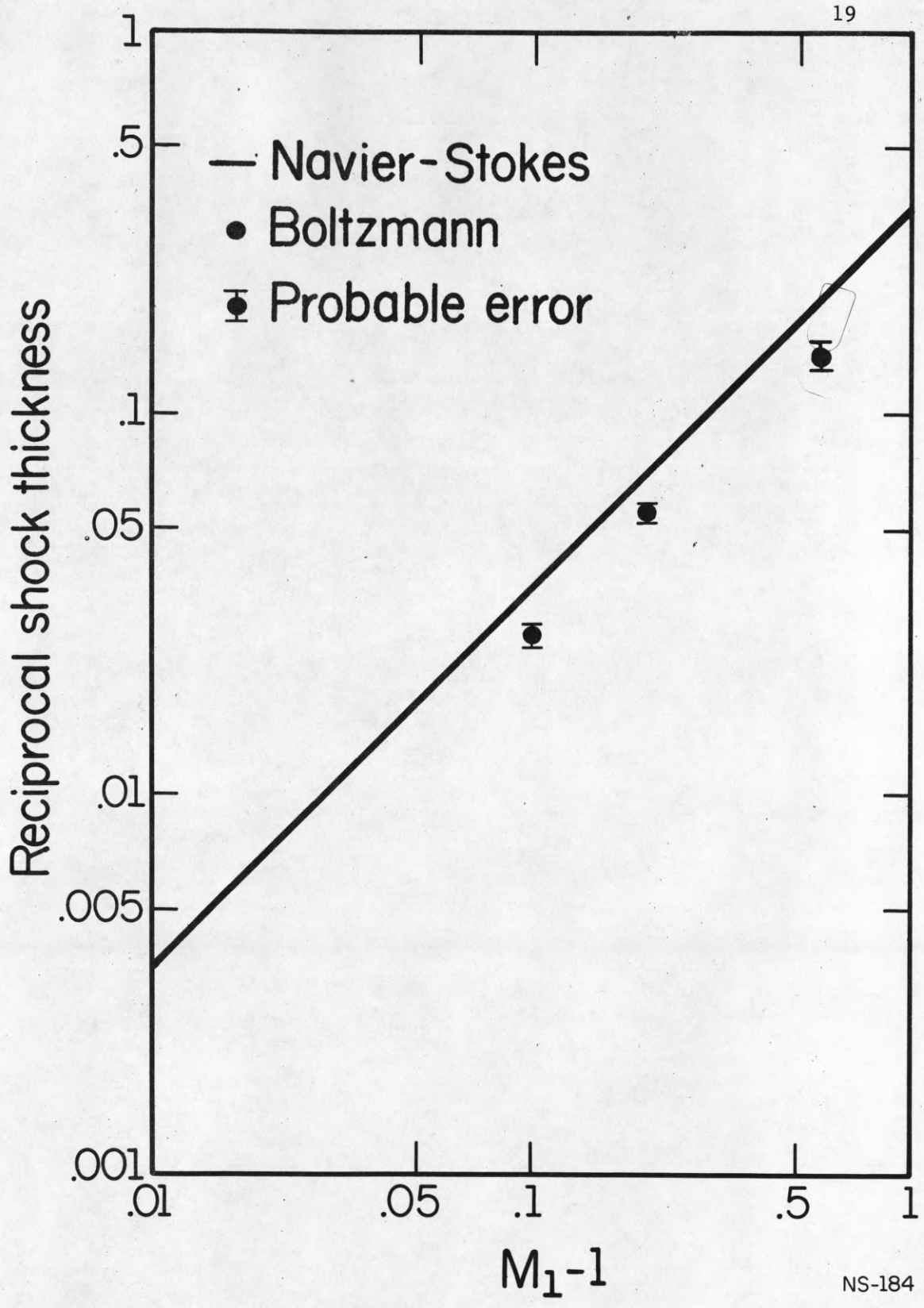

Fig. 2.2 Variation of reciprocal shock thickness with Mach number M_1 for weak shocks.

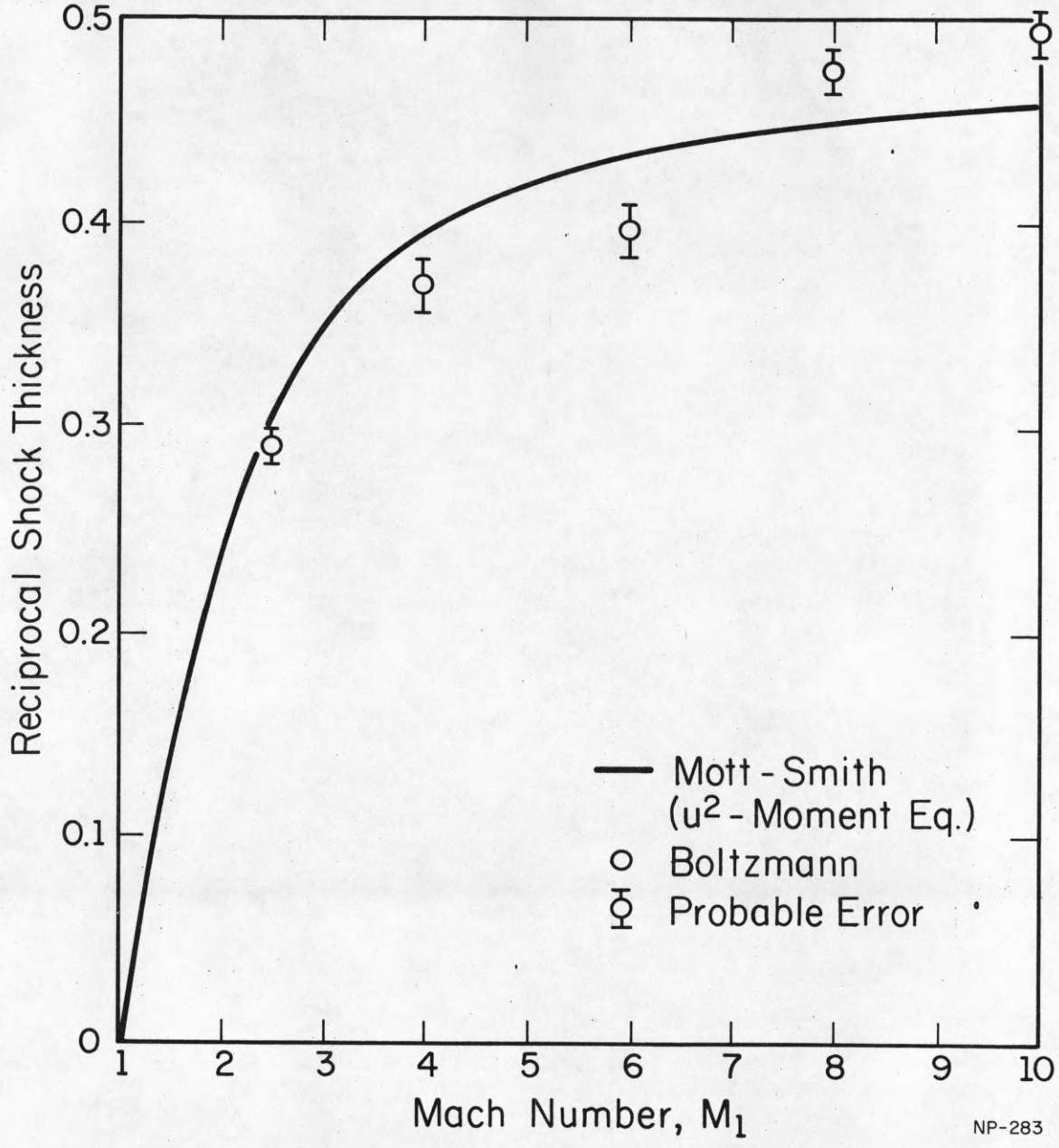

Fig. 2.3 Variation of reciprocal shock thickness with Mach number M_1 for strong shocks.

Navier-Stokes shock can be described by the t-n curve and the transport coefficients together with the n-x curve, the interpretation of our comparative results for low Mach numbers will be made in Section 6 in which the results on dt/dn and the transport coefficients are presented. However, we do want to point out here that the variation of properties with respect to the number density n in a Navier-Stokes shock depends on the integral curve, i.e., the t-n relation and thus on the Prandtl number Pr, while the determination of the variation with respect to x requires, in addition, the μ-t relation. Sherman and Talbot[18] studied the RST at low Mach numbers. They measured the temperature profile for M_1 = 1.335 - 1.713 and obtained the density (or velocity) shock thickness by using the theoretical t-n relation.

For values of $M_1 > 2.5$, as shown in Fig. 2.3 we compare values of RST only with the Mott-Smith results (with u^2-moment). The Boltzmann and Mott-Smith values agree with the 90% confidence limits.† The fact that the Boltzmann RST curve and the Mott-Smith RST curve are not far apart, for intermediate values of the Mach number, does <u>not</u> imply that other shock characteristics calculated by the Monte Carlo method and the Mott-Smith method also are in approximate agreement.

The RST, of course, shows only one characteristic of the density profile.* It tells nothing about the physically interesting relaxation rates in the wings of shock nor about the asymmetry of the density gradient profiles. The degree of asymmetry of the profiles is exhibited directly in plots of our

---

†The 90% confidence limit $\epsilon_{90} = 3.07(\epsilon_{50})$. ϵ_{50} = probable errors which are given in all figures.

*Grad[16] suggested a definition of the shock thickness based on the integral properties of the profile.

calculated values of dn/dx vs $\hat{n}$, as in Figs. 2.4 and 2.5. The density profiles, if needed, can be calculated by numerical integration $\int_{\hat{n}=\frac{1}{2}}^{\hat{n}} (dx/d\hat{n})d\hat{n}$, as shown in Fig. 2.1.

We remark first that the four curves for each individual Monte Carlo sample are smooth and of similar shape (i.e., the four curves are "nested"). It is therefore permissible to make somewhat more detailed analysis of the shape of the (average) density gradient curves than would be justified by the values of ϵ_{50} shown in Fig. 2.3.

Comparison of ordinates for symmetrically placed values of $\hat{n}$ affords a more powerful test of asymmetry. On this basis we see that the gradient curves are asymmetric for all Mach numbers except $M_1 = 2.5$. The asymmetry produces larger upstream than downstream gradients for $M_1 < 2.5$ and smaller upstream than downstream gradients for $M_1 > 2.5$. These qualitative results for high Mach numbers were anticipated in our algebraic theory[14] of 1967.

We can connect the asymmetry within the shock to the density relaxation rates in the shock wings by generalizing part of the Mott-Smith Ansatz. As $x \to -\infty$ we assume that

$$\frac{dx}{d\hat{n}} \sim \frac{a_1}{\hat{n}} \tag{2.3}$$

and as $x \to +\infty$

$$\frac{dx}{d\hat{n}} \sim \frac{a_2}{1-\hat{n}} \tag{2.4}$$

which follows directly from linear dependence of f on $\hat{n}$ (in Mott-Smith's Ansatz, where $a_1 = a_2$). A simple form for the $\hat{n}$ dependence of $dx/d\hat{n}$ that satisfies

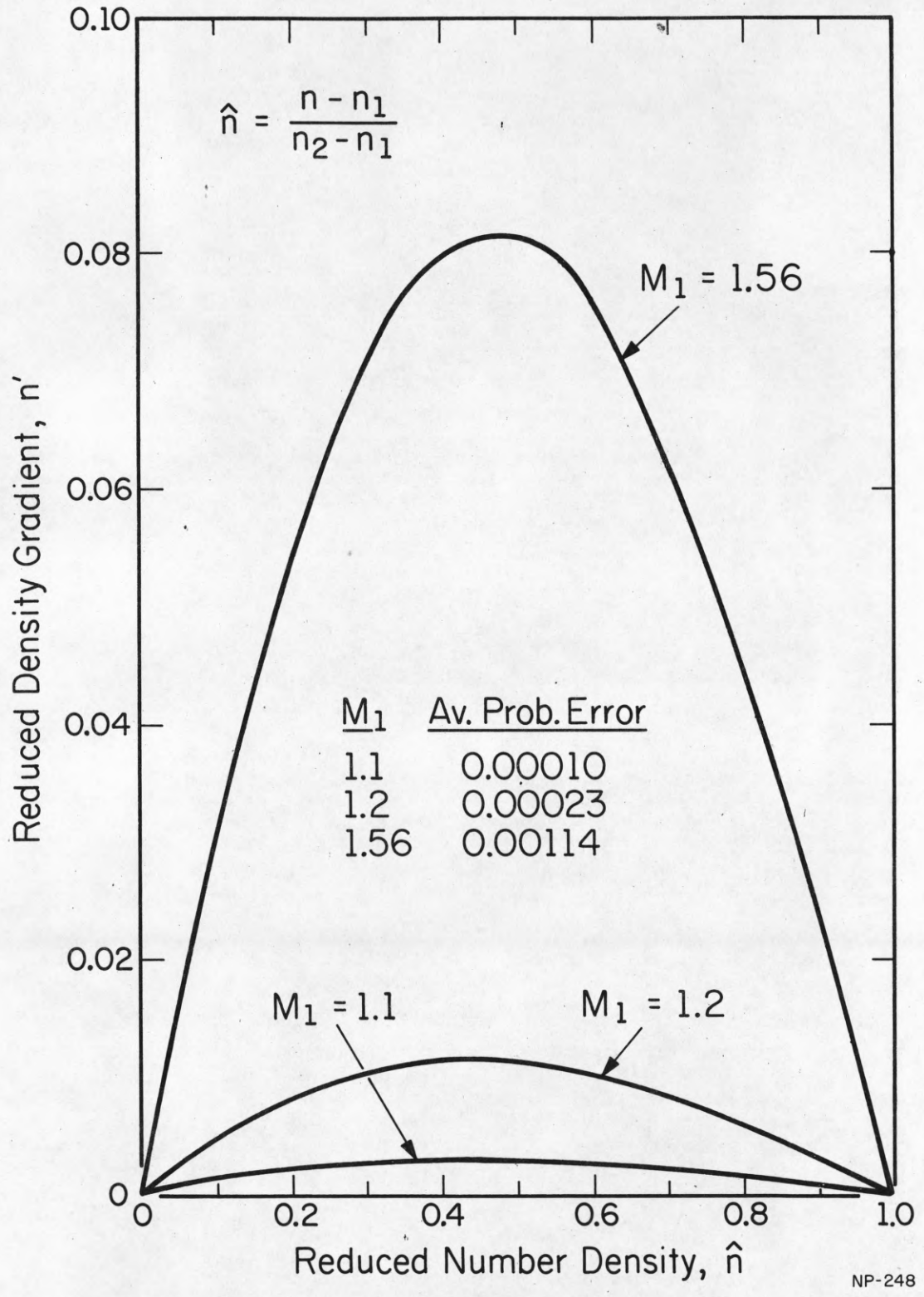

Fig. 2.4 Variation of density gradient with reduced density $\hat{n}$ for M_1 = 1.1, 1.2, and 1.56.

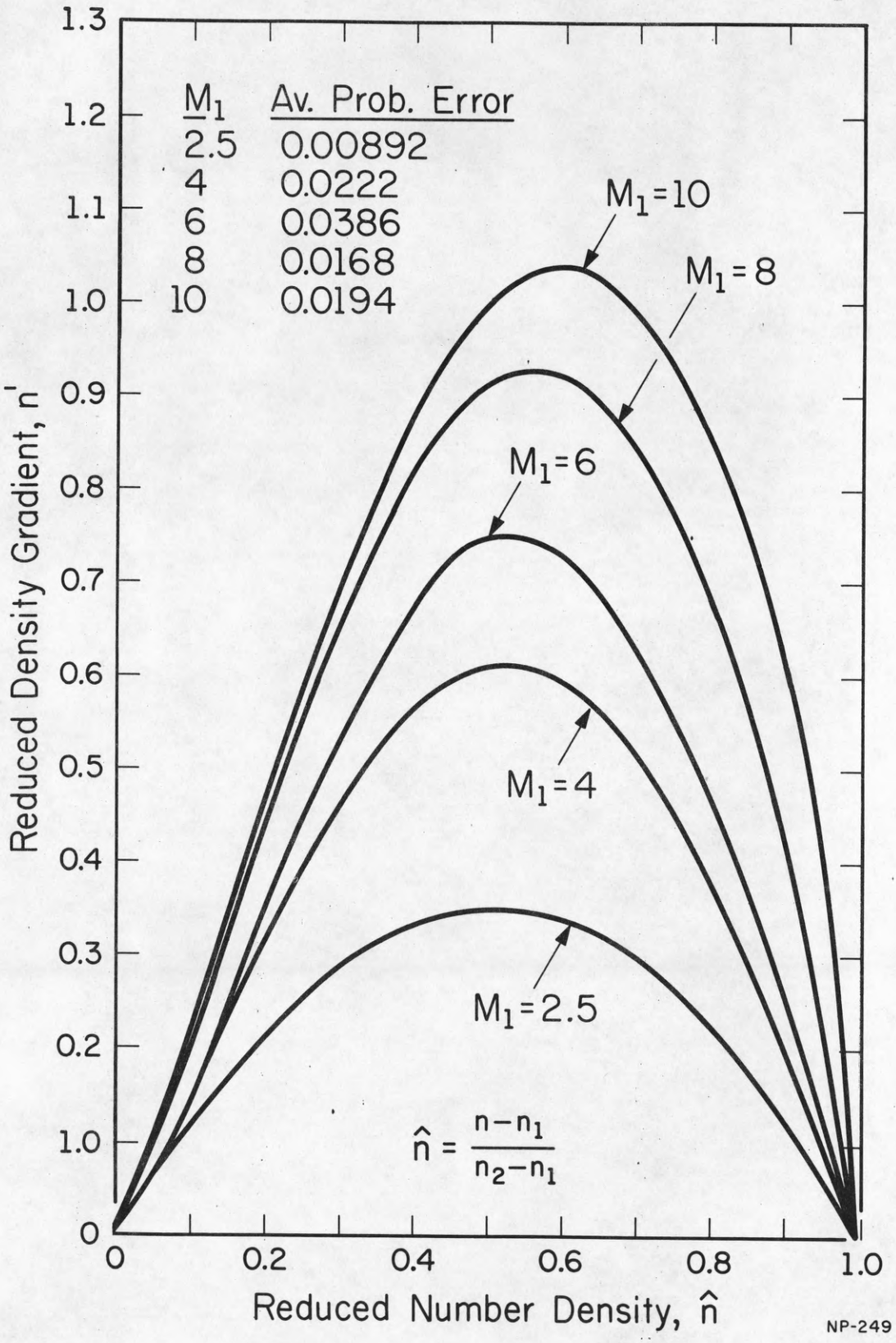

Fig. 2.5 Variation of density gradient with reduced density $\hat{n}$ for M_1 = 2.5, 4, 6, 8, and 10.

both of these conditions is

$$\frac{dx}{d\hat{n}} = \frac{a_1}{\hat{n}} + \frac{a_2}{1-\hat{n}} = \frac{a_1 + (a_2-a_1)\hat{n}}{\hat{n}(1-\hat{n})} \tag{2.5}$$

The linear expression $a_1 + (a_2-a_1)\hat{n}$ is thus a correction factor for the symmetric function $\hat{n}(1-\hat{n})$. For $a_2 > a_1$ (slower relaxation per unit path downstream than upstream) the gradient curves are skewed to the left, while for $a_2 < a_1$ (faster relaxation downstream than upstream) the gradient curves are skewed to the right. Applying these results to Figs. 2.4 and 2.5, we see qualitatively that for $M_1 < 2.5$ the upstream relaxation rate must be greater than the downstream rate, and the reverse is true for $M_1 > 2.5$.

The new Ansatz leads to simple formulas for $n'_{\frac{1}{2}}$, n'_{max} and $\hat{n}_{max}$

$$n'^{-1}_{\frac{1}{2}} = 2(a_1 + a_2) \tag{2.6}$$

$$n'_{max} = (\sqrt{a_1} + \sqrt{a_2})^2 \tag{2.7}$$

$$\hat{n}_{max} = \sqrt{a_1}/(\sqrt{a_1} + \sqrt{a_2}) \tag{2.8}$$

Thus $n'^{-1}_{\frac{1}{2}}$ is proportional to the arithmetic mean of a_1 and a_2 and that n'^{-1}_{max} is proportional to the sum of the geometric and arithmetic means.

The new Ansatz describes our data qualitatively but not quantitatively. To represent the Monte Carlo results within the tolerance given by the 90% limits we modify it again, assuming now

$$\hat{B} = [\hat{n}(1-\hat{n})]^{-1}(d\hat{n}/dx) = [\frac{1}{a_1+(a_2-a_1)\hat{n}} + \Delta_B \hat{n}(1-\hat{n})] \tag{2.9}$$

The resulting values of $\hat{B}_1 = a_1^{-1}$, $\hat{B}_2 = a_2^{-1}$, and Δ_B are shown in Table 2.1. The three coefficients are each proportional to (M_1-1) for $M_1 \leq 1.56$.

Table 2.1 Parameters of the Density Profile in Shock Waves

M_1	$\hat{B}_1$	$\hat{B}_2$	Δ_B	$\hat{B}_{\frac{1}{2}}$ (Boltzmann)	$\hat{B}_{\frac{1}{2}}$ (M-S;u^2)
1.1	0.088	0.053	0.044	0.077	0.086
1.2	0.176	0.105	0.088	0.154	0.169
1.56	0.40	0.29	0.24	0.40	0.44
2.5	0.62	0.69	0.49	0.78	0.86
4.0	0.70	1.00	0.76	1.02	1.12
6.0	0.74	1.37	0.96	1.20	1.22
8.0	0.74	1.85	1.08	1.36	1.27
10.0	0.74	2.3	1.18	1.45	1.29

The relaxation rate $\hat{B}_2$ is proportional to M_1 for $M_1 >$ about 7. The relaxation rate $\hat{B}_1$ seems to approach an asymptotic value of about 0.7 as $M_1 \to 10$. The two rates appear to be equal for $M_1 \sim 2.1$, in agreement with our earlier, qualitative conclusion. In the wings ($\hat{n} \leq 1/16$ or $\geq 15/16$) the values of $[\hat{B}-\Delta_B\hat{n}(1-\hat{n})]^{-1}$ computed from solution of the Boltzmann equation show large deviations above and below the values of $[a_1+(a_2-a_1)\hat{n})$. In the intermediate range ($1/16 < \hat{n} < 15/16$) the two sides of the equation agree to within less than the 90% confidence limits of the left hand side.

We emphasize that the values of $\hat{B}_o$, $\hat{B}_1$ and Δ_B in the table are tentative. When used in Eq. (2.9) they describe our present Monte Carlo results. But the strong evidence for asymmetry and the estimates made of the magnitude of the relaxation rates in the wings will, we hope, stimulate further experimental and theoretical studies of the density gradient profiles of shock waves.

Shock wave theories for low Mach numbers describe $\hat{B}$ by various functions of $\hat{n}$. For example, $\hat{B}$ for Grad's thirteen moment shock is a linear function of $\hat{n}$

with positive coefficients. The fact that the asymmetry for this shock is to the right is obvious; however, the relaxation in the wings cannot be explicitly determined. As the Mach number approaches one, the density profile becomes symmetrical for all shock wave theories for low Mach numbers; therefore, the first order theory for very low Mach number gives a constant value of $\hat{B}$.

3. Shock Properties as Functions of Mach Number

In Sections 3, 4 and 5 we shall be discussing a number of functions derived from our solution of the Boltzmann equation for shock waves. In preparation for this discussion we shall now define a number of properties which are derived from the velocity distribution function $f(\bar{v},x)$. We shall then describe the behavior, as functions of M_1, of certain of these properties, especially those which possess extrema within the shock waves.

From six moments of the velocity distribution function f we can calculate all of the ordinary macroscopic properties of the non-equilibrium gas. The six moments are $n = \mathcal{M}_1$, and $\mathcal{M}_2$, $\mathcal{M}_3$, $\mathcal{M}_4$, $\mathcal{M}_6$ and $\mathcal{M}_9$ where

$$\mathcal{M}_k = \int f \, \Phi_k \, d\bar{v} \tag{3.1}$$

and

$$\Phi_1 = 1 \qquad \Phi_3 = v_x^2 \qquad \Phi_6 = v_x^3$$

$$\Phi_2 = v_x \qquad \Phi_4 = v_x v^2 \qquad \Phi_9 = v_\perp^2$$

The moments $\mathcal{M}_2$, $\mathcal{M}_3$ and $\mathcal{M}_4$ are the invariants. The reduced, dimensionless properties derived from the six moments are:

gas velocity	$u = \mathcal{M}_2/n$	(3.2)
lateral temperature	$t_\perp = \pi \mathcal{M}_9/n$	(3.3)
stress	$\tau = \frac{2}{3}n(t_\perp - t_x)p_1$	(3.4)
total heat flux	$q = (2\pi\mathcal{M}_4/\mathcal{M}_2) - 3t_x - 2t_\perp - 2\pi u^2$	(3.5)
longitudinal heat flux	$q_x = (2\pi\mathcal{M}_6/\mathcal{M}_2) - 3t_x - 2\pi u^2$	(3.6)

In accordance with our definition of units in the Introduction, the units of the dimensional quantities (corresponding to the dimensionless quantities u, t, τ and q) are, respectively, u_1, t_1, p_1, and u_1^2.

To calculate the gas temperature t we need to have t_x, the longitudinal temperature, but this, as seems not to be generally realized, is a function of n which can be derived explicitly from the first two conservation equations:[19]

$$t_x = 2\pi[-u^2 + (\mathcal{M}_3/n)] \tag{3.7}$$

The temperature and pressure are then given by

$$t = \frac{1}{3}t_x + \frac{2}{3}t_\perp \tag{3.8}$$

$$p = nt \tag{3.9}$$

The temperature t_g, associated with the mass velocity, is defined by

$$t_g = 2\pi u^2 \tag{3.10}$$

Knowing n and t we can calculate any thermodynamic property of the equilibrium reference gas, such as entropy S per unit volume, for example:

$$S = n[\log_e(nt^{-3/2}) - 3/2] \tag{3.11}$$

The foregoing discussion shows that $t_\perp$ occupies a special place in shock theory. Unlike t_x, its dependence on n <u>cannot</u> be derived from conservation

equations but must be calculated from a solution f of the Boltzmann equation for the shock and subsequent calculation of $\mathcal{M}_9/n$ by numerical integration. But once $t_\perp(n)$ is known, then the temperature t, and the properties τ/p_1 and q can be computed, as functions of n from Eqs. (3.1)-(3.8).

The dependence of $t_\perp$, at the mid-shock position, on M_1 is shown in Fig. 3.1. Similar curves could be drawn for other positions in the shocks. There is a small but significant departure of the Boltzmann points from the Mott-Smith curve. This difference is enlarged when translated to $(t_\perp - t_x)$ or τ/p_1 or q. Except for weak shocks, $t_\perp$ has reached >70% of its downstream value at the mid-shock position. The variation of $t_\perp$ with $\hat{n}$ is represented (indirectly) in Section 4 by the variation of $d\hat{t}/d\hat{n}$ with $\hat{n}$.

Our calculations show that each of some nine moments of f is nearly a linear function of n, that is, f and its moments are rather similar to the Mott-Smith f and its moments, which are <u>exactly</u> linear functions of n. The maximum deviations from linearity amount to -0.59% and 1.8% for the moments $\mathcal{M}_6$ and $\mathcal{M}_9$, for example, for $M_1 = 2.5$. The Monte Carlo fluctuations are much smaller than these deviations. Rather than showing, in this section, the detailed variation of the moments $\mathcal{M}_6$ and $\mathcal{M}_9$ with n, we will instead discuss the characteristics of the derivatives of various related quantities in Sections 4 and 5.

There are two other important macroscopic properties of the non-equilibrium gas, the two Boltzmann functions

$$H = \int f \log_e f \, d\bar{v} \tag{3.12}$$

and

$$G = \int v_x f \log_e f \, d\bar{v} \tag{3.13}$$

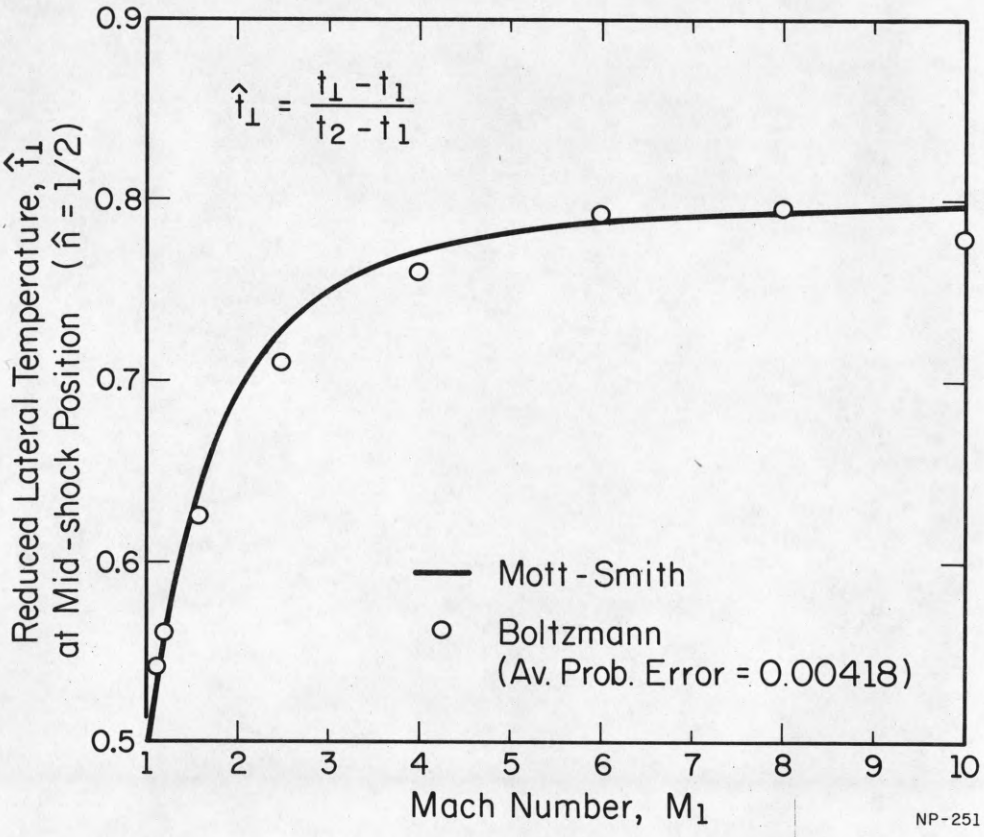

Fig. 3.1 Variation of reduced lateral temperature $\hat{t}$ at mid-shock position ($\hat{n} = \frac{1}{2}$) with Mach number M_1.

These are seldom discussed because their calculation requires knowledge of the velocity distribution function, (which can only be calculated accurately by our method, for gases that are far from equilibrium), and because the integrations must be performed by quadrature.

The Boltzmann Theorem for a steady state flow, as in a shock wave, says that G must monotonically decrease through the shock. We shall make a sensitive test of the conformity of our results to this theorem in Section 4. We shall see shortly that H (and the related function h = H/n) also possess certain other interesting properties in shock waves.

With these preliminaries out of the way we shall now discuss four properties, each a functional of f, and each exhibiting a maximum within the shock waves.

The first functional $(t_x - t_\perp) = -3\tau/2n$ refers to non-equilibration of temperature, that is, the lack of equality between t_x and $t_\perp$. In Fig. 3.2 the value of $(\hat{t}_x - \hat{t}_\perp)$ at the mid-shock position is plotted as a function of M_1. Since $(t_\perp = t_x)$ at the up- and downstream boundaries of a shock wave, $(t_x - t_\perp)$ must pass through an extremum somewhere inside the shock. The curve for the Mott-Smith temperatures is shown for comparison and is seen to differ by a small but statistically significant amount.

It was noticed many years ago (Nordsieck, 1959; Hicks, 1963; Yen,[19]) that the longitudinal temperature t_x, as a function of n in the shock [Eq. (3.7)], possesses a maximum, for $M_1^2 = 1.8$. We represent this overshoot in Fig. 3.3 by plotting $[(\hat{t}_x)_{max} - \hat{t}_2]$ at the mid-shock position as a function of upstream Mach number M_1. According to the results of our Boltzmann calculations the lateral temperature $t_\perp$ does not show a maximum, for any Mach number or position in the

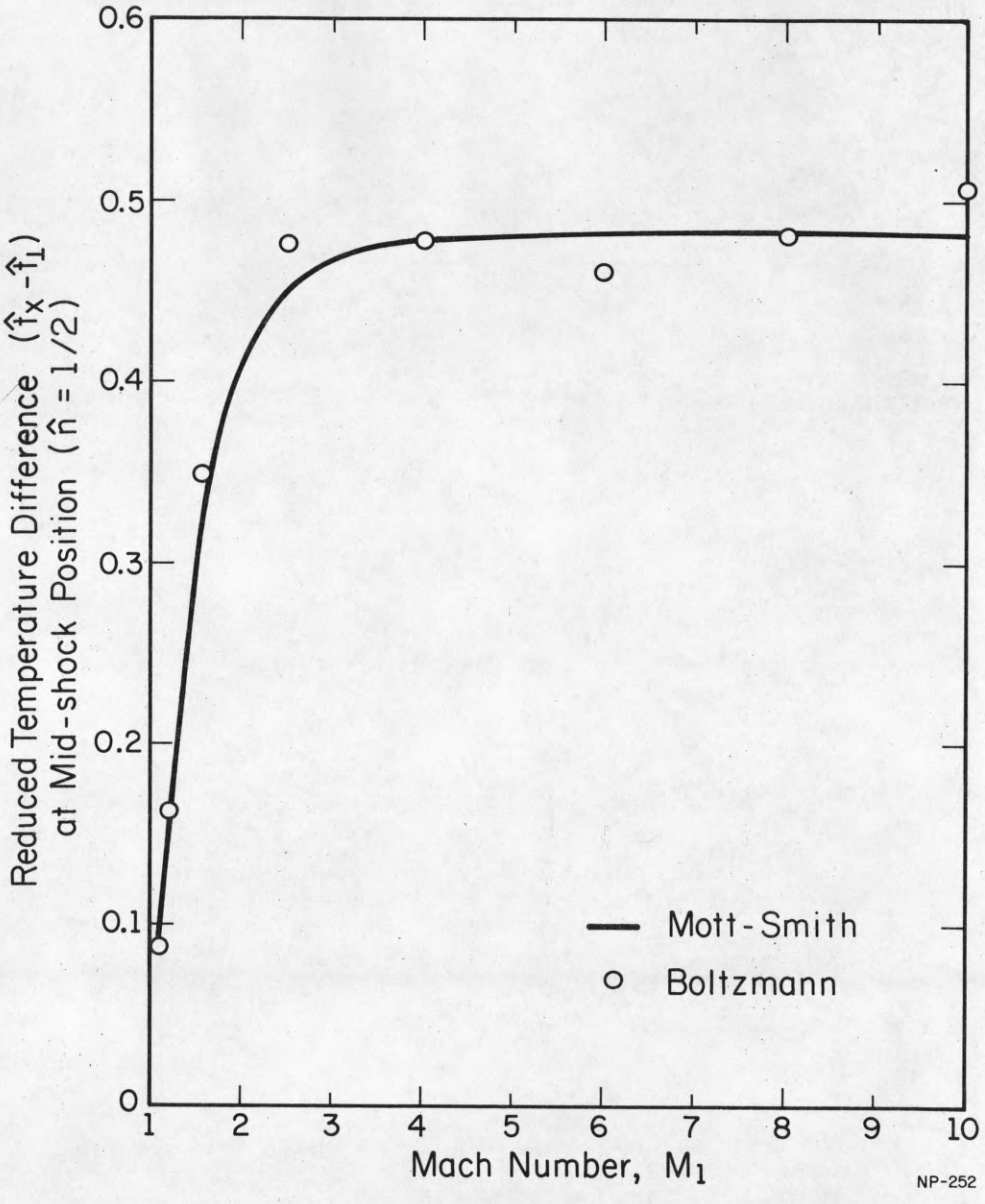

Fig. 3.2 Variation of departure of isotropicity in reduced temperature, $\hat{t}_x - \hat{t}_\perp$, at mid-shock position ($\hat{n} = \frac{1}{2}$) with Mach number M_1.

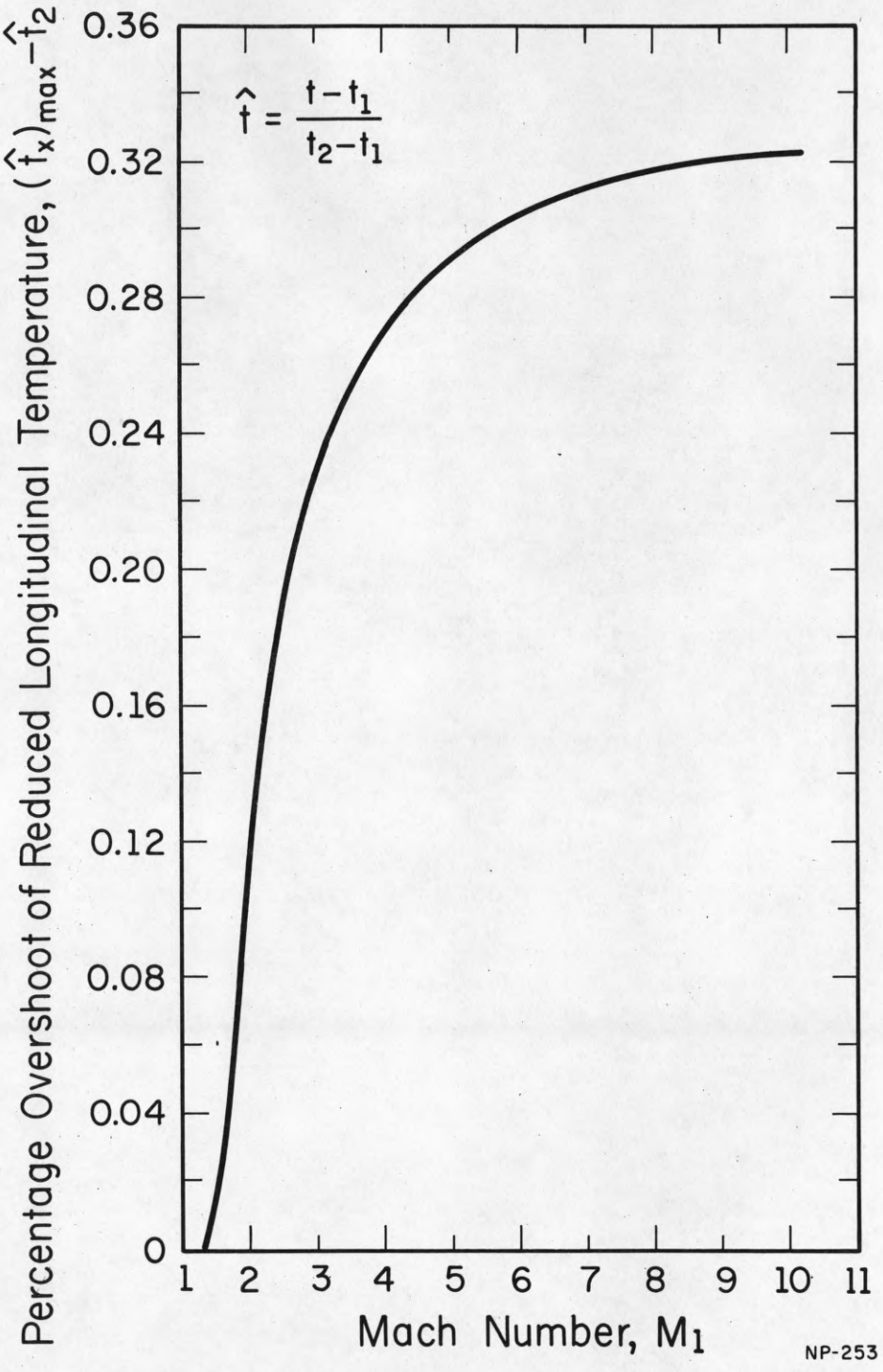

Fig. 3.3 Variation of overshoot of reduced temperature associated with longitudinal random motion, $(\hat{t}_x)_{max} - \hat{t}_x$, at mid-shock position ($\hat{n} = \frac{1}{2}$) with Mach number M_1.

shock. The existence of a maximum of t_x thus assures that for $M_1^2 > 1.8$, the temperatures are not equilibrated.

The total temperature

$$t_t = t + \frac{4\pi}{5}\left(\frac{\mathcal{M}_2}{n}\right)^2 \tag{3.14}$$

Its variation, thus depends on two moments, $\mathcal{M}_1$ and $\mathcal{M}_9$. We have found that it has a maximum for all the Mach numbers studied. As shown in Fig. 3.4, the maximum overshoot, defined by $(t_t)/(t_t)_1$, is less than 8.5%.

For weak shocks, the Boltzmann function H per unit volume and the entropy S per unit volume are nearly equal. For strong shocks, the difference between the two functions is thus a global measure of departure from thermal equilibrium. (See also Section 1.) At the up- and down-stream boundaries the two functions are exactly equal, so that, just as in the case of $(t_\perp - t_x)$ the difference must possess an extremum inside the shock. The difference $(\hat{H}-\hat{S})$ is plotted in Fig. 3.5, for the mid-shock position, to show its general behavior as a function of M_1.

It was also noticed some time age[20] that the value of s, the entropy per molecule, calculated from the Navier-Stokes description of a shock wave, possesses a maximum within the shock wave for all Mach numbers. The maximum is caused by the change of sign of the (large) heat conduction term $d(kdT/dx)/dx$ which dominates the (smaller) positive, viscous dissipation term $(4\mu/3)(du/dx)^2$. It is therefore of interest to examine the behavior of the corresponding Boltzmann function $h = H/n$. We find that it has the same qualitative behavior as $s = S/n$, as is shown by the h overshoot plot of Fig. 3.6, where the measure of overshoot is $\hat{h}-\hat{h}_2$.

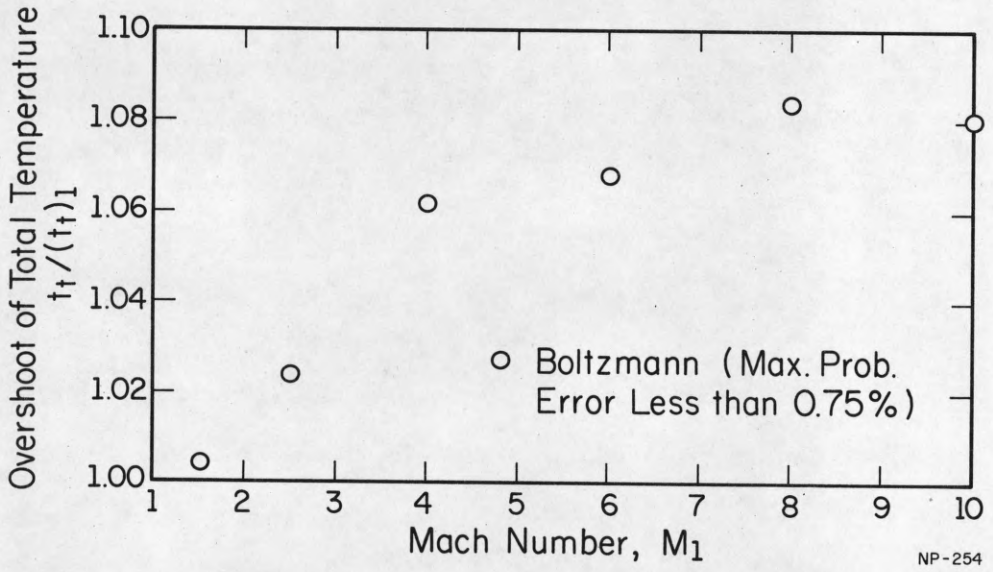

Fig. 3.4 Variation of maximum overshoot of total temperature, $(t_t/(t_t)_1$, with Mach number M_1. (See Fig. 3.6 for locations of these maxima.)

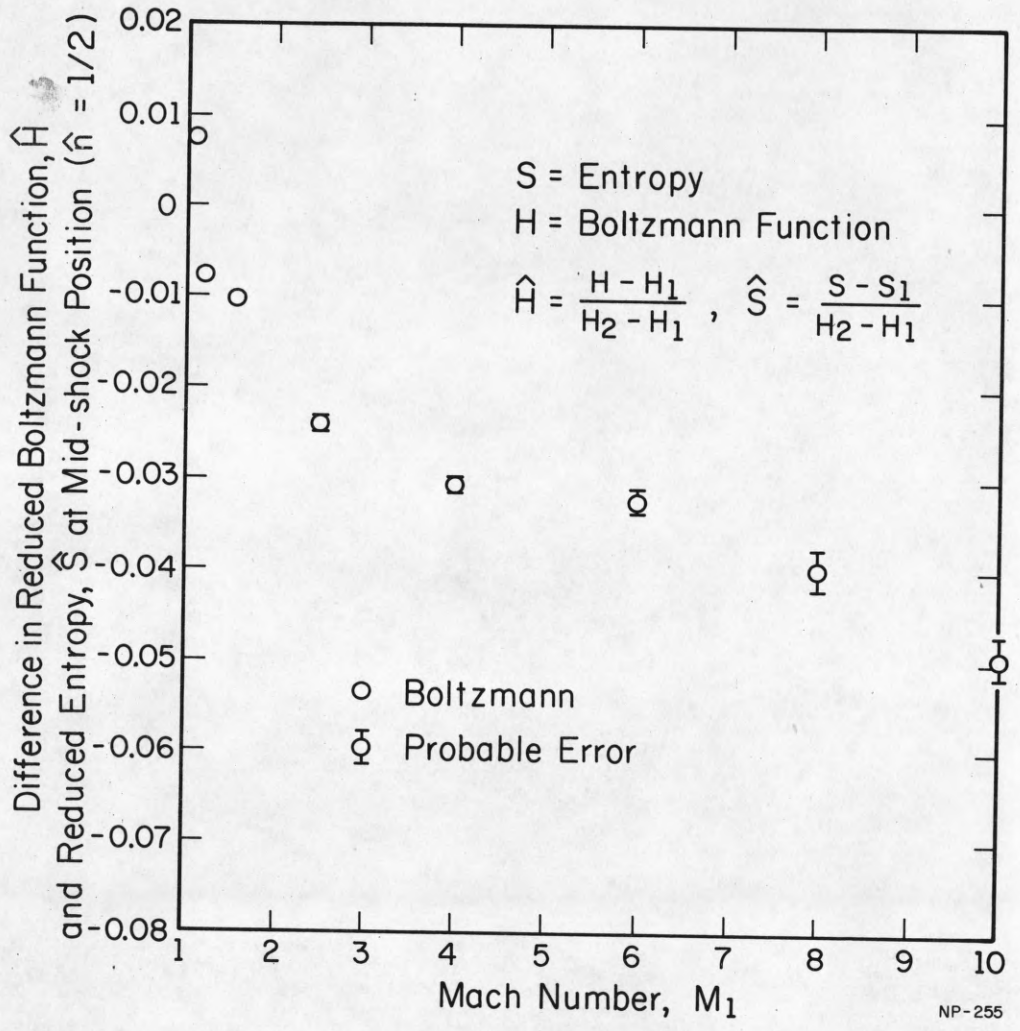

Fig. 3.5 Variation of difference in reduced Boltzmann function $\hat{H}$ and reduced entropy $\hat{S}$ at mid-shock position ($\hat{n} = \frac{1}{2}$) with Mach number M_1.

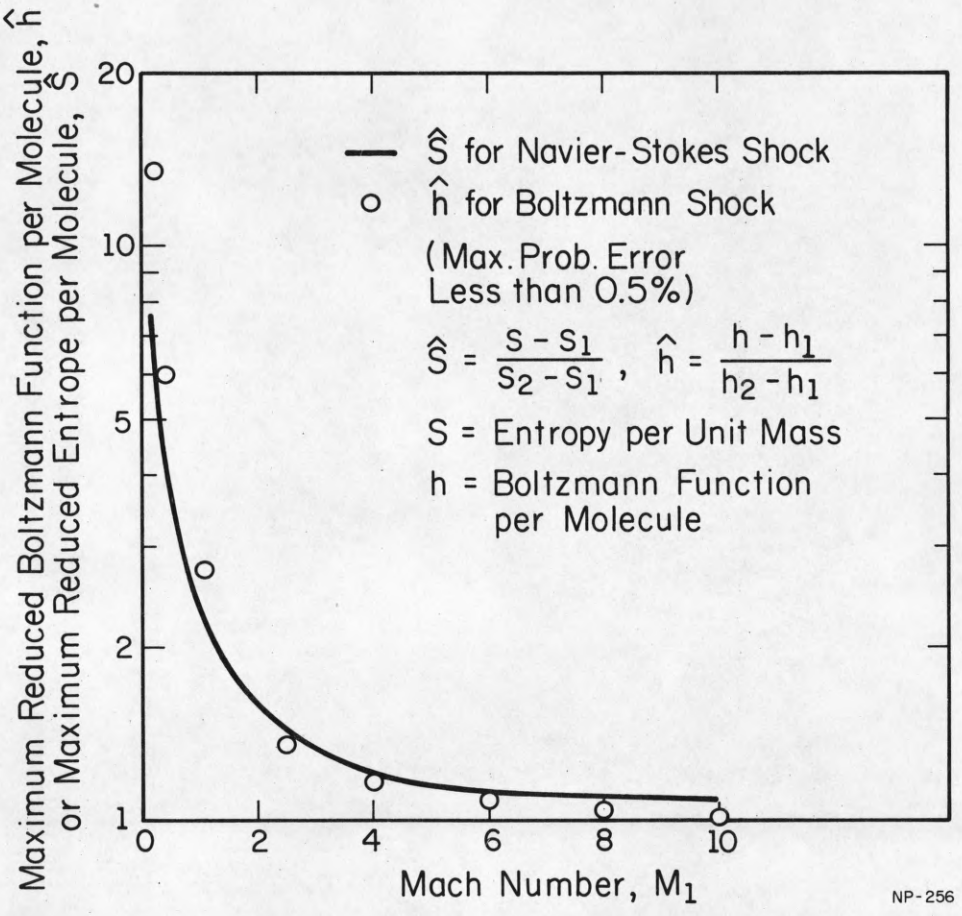

Fig. 3.6 Comparison of maximum of reduced Boltzmann function per molecule $\hat{h}$ with the Navier Stokes of maximum entropy per unit mass.

We have now discussed many of the functions that possess maxima within the shock wave: n' in Section 2, and $(t - t_x)$, t_x, t_t, $\hat{H}$-$\hat{S}$, and $\hat{h}$ in the present section. In Fig. 3.7 we compare the positions of the maxima of four of these functions, n', t_x, t_t, and h, for different Mach numbers. We shall discuss the stress τ and the heat flux q in Section 5 but show here the positions of the maxima of τ and q and the position at which the local Mach number M becomes one in Fig. 3.8.

It is clear that no one position (value of $\hat{n}$) within shock waves has a special significance for all shock properties and all Mach numbers.

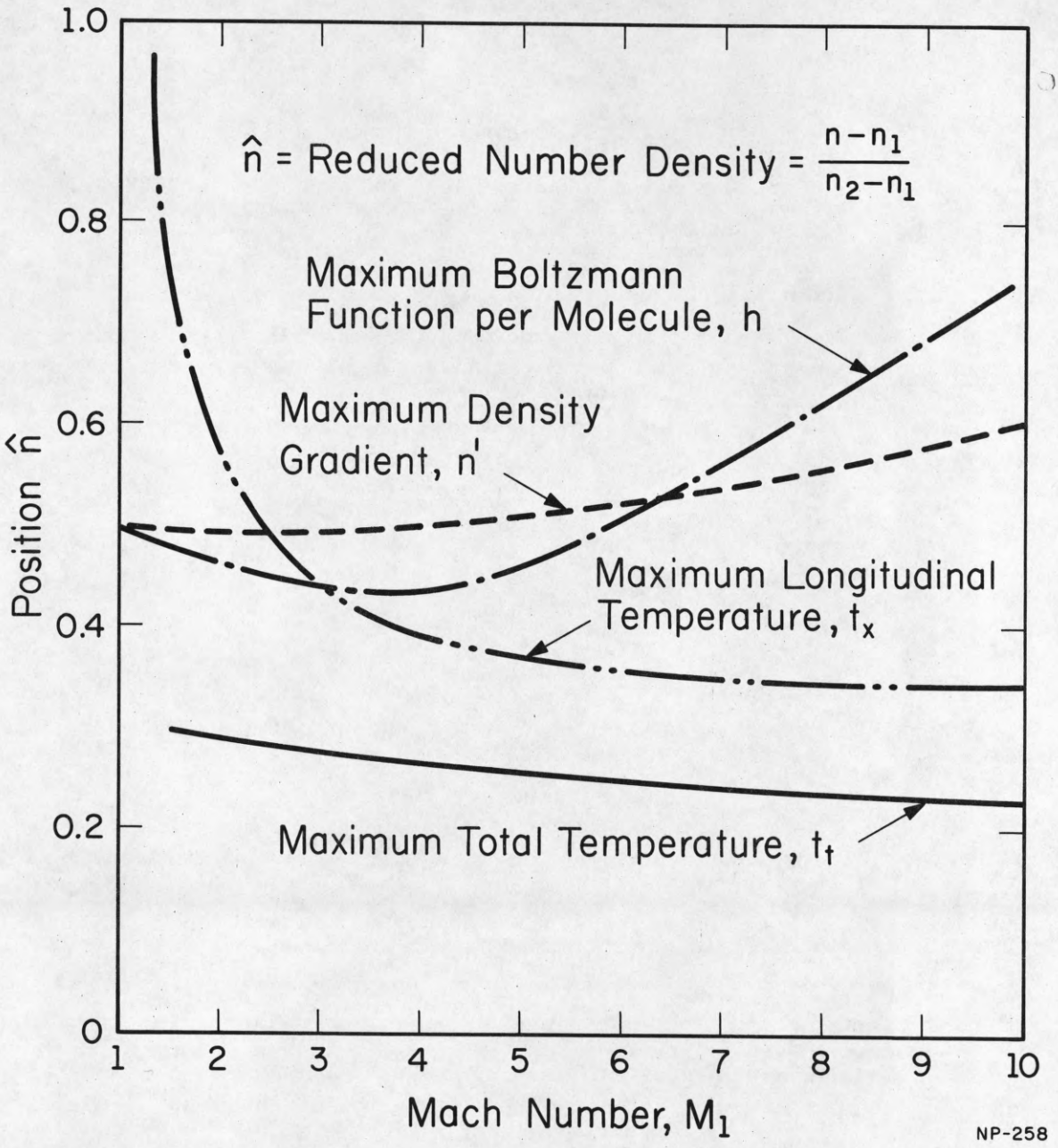

Fig. 3.7 Variation of location of the maximum with Mach number M_1 for the following: longitudinal temperature t_x, Boltzmann function h, density gradient n', and total temperature t_t.

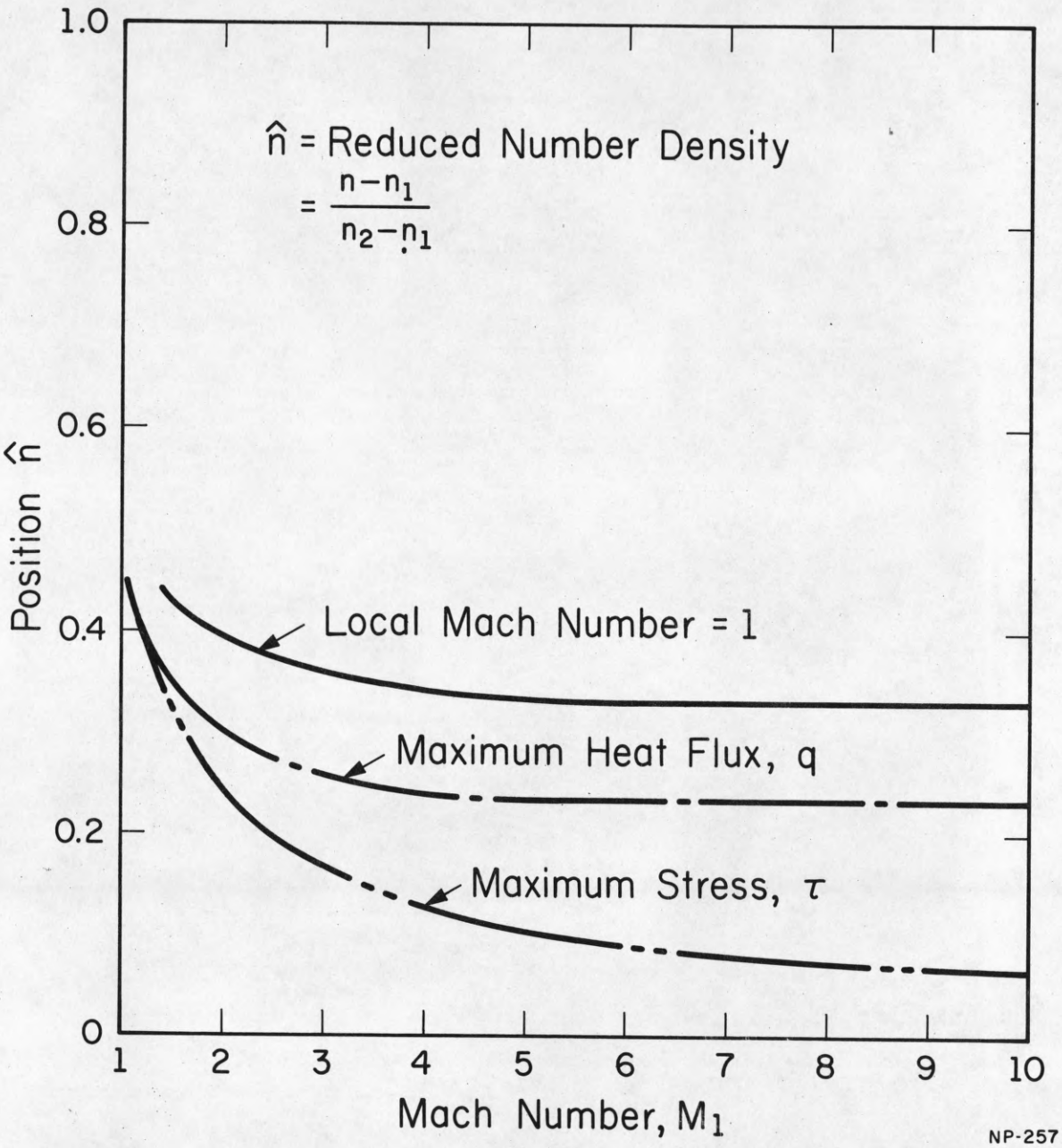

Fig. 3.8 Variation of locations of maximum stress t, maximum heat flux q, and local Mach number = 1 with Mach number M_1.

4. Profiles of the Gradients of Shock Properties

In Section 2 we discussed the dependence of number density upon position in the shock and upon Mach number M_1.

In Section 3 we examined the behavior of various characteristics of shocks, evaluated at the mid-shock position ($\hat{n} = \frac{1}{2}$), as a function of the Mach number M_1. In this section we will look at the detailed variations, for each Mach number, of several shock characteristics as functions of the independent variable n. The functions are the Boltzmann flux

$$G = \int v_x f \log f \, d\bar{v} \tag{4.1}$$

the temperature t, and the total temperature $t_t = t + t_g/5$. In each case we shall study the n-derivatives of the function.

According to the Boltzmann Theorem for steady flow of a gas

$$dG/dx \leq 0 \tag{4.2}$$

throughout the gas. Since dn/dx is positive throughout each shock wave (see Section 2) the Theorem can also be stated in the form

$$dG/dn \leq 0 \tag{4.3}$$

One test of the physical validity of our solutions of the Boltzmann equation is the question, "Do the solutions satisfy the Boltzmann Theorem?". The answer, for our solutions is "yes" for the complete range of Mach number from 1.1, where the largest value of $d\log_e G/dn$ is about 10^{-5} to a Mach number

of 10 where this derivative is as large as 0.306. The rather similar Mott-Smith velocity distribution functions also satisfy the theorem. (This has not been shown analytically but is a result of our numerical calculations.) Agreement with the Boltzmann Theorem is clearly one criterion that any supposed solution of the Boltzmann equation should satisfy.

The detailed variation of dG/dn with n is conveniently represented in terms of the reduced quantity $d\hat{G}/d\hat{n}$, which is plotted vs $\hat{n}$ for four Mach numbers in Fig. 4.1. Notice that $d\hat{G}/d\hat{n}$ is almost independent of M_1 at the mid-shock position, for M_1 greater than about two.

The derivative dt/dn is a function worth studying for several reasons. First, the Navier-Stokes treatment of the shock wave is based on this function. Secondly, the value of this derivative fixes the quantitative nature of the singularities at each boundary of the Navier-Stokes shock. Finally, this function enters explicitly into the formula for the (effective) Prandtl number that we shall discuss in Section 5. We shall therefore compare the values of dt/dn obtained from the Navier-Stokes and from our solutions of the Boltzmann equation.

The values of $d\hat{t}/d\hat{n}$, the reduced derivative, are plotted vs $\hat{n}$ for six Mach numbers in Figs. 4.2 and 4.3. The Navier-Stokes values of the derivative are marked on the plots at $\hat{n} = 0$ and 1 and agree well with the Boltzmann values for low Mach numbers. The curves are dashed where the sharp cold peak produces large quadrature errors.

The derivative dt/dn is related to the number density and the derivative of the total temperature t_t by the equation

$$dt/dn = (4\pi/5)(m_2^2/n^3) + dt_t/dn$$

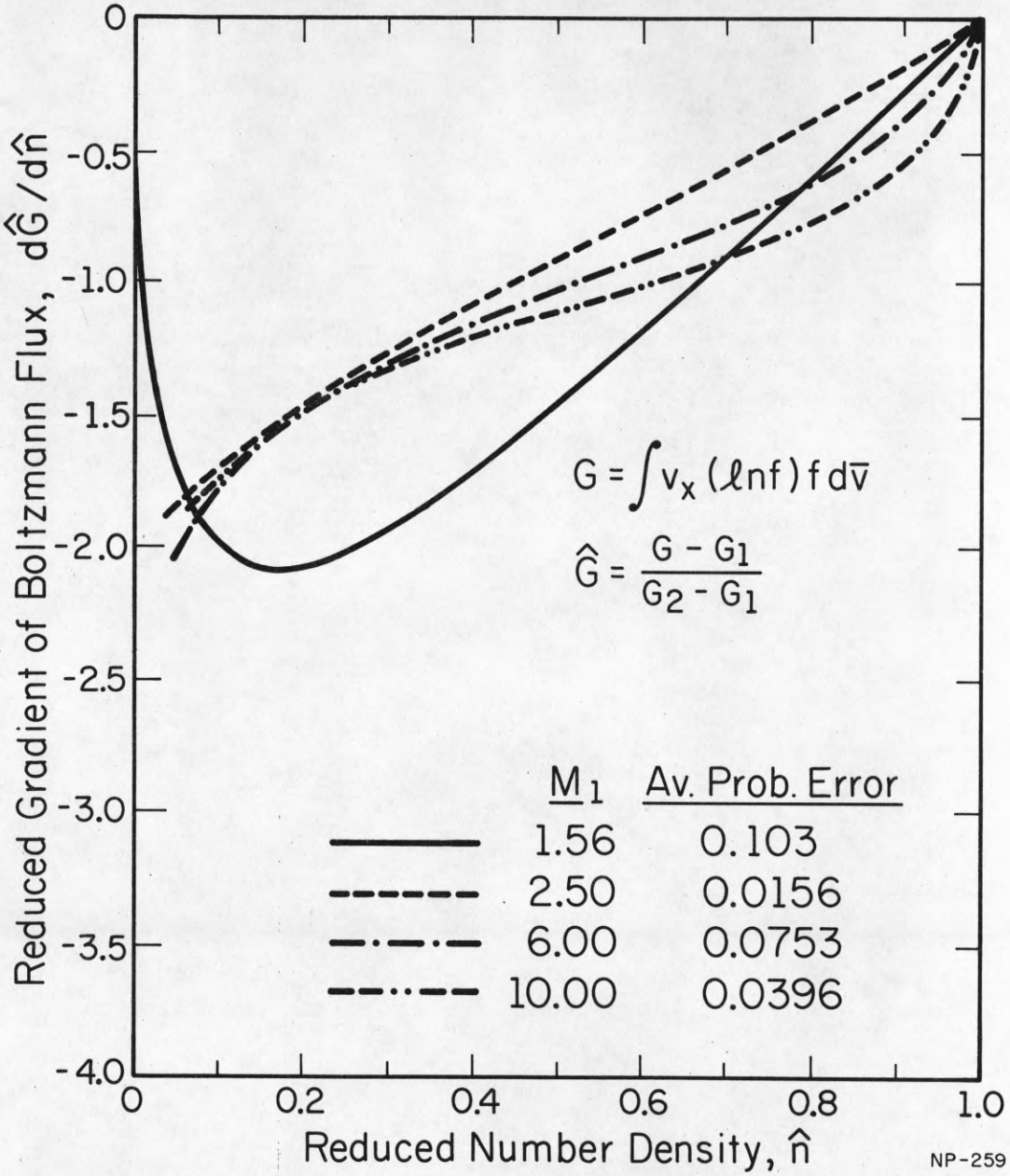

Fig. 4.1 Variation of the gradient of reduced Boltzmann flux $d\hat{G}/d\hat{n}$ with reduced density $\hat{n}$ for M_1 = 1.56, 2.5, 6, and 10.

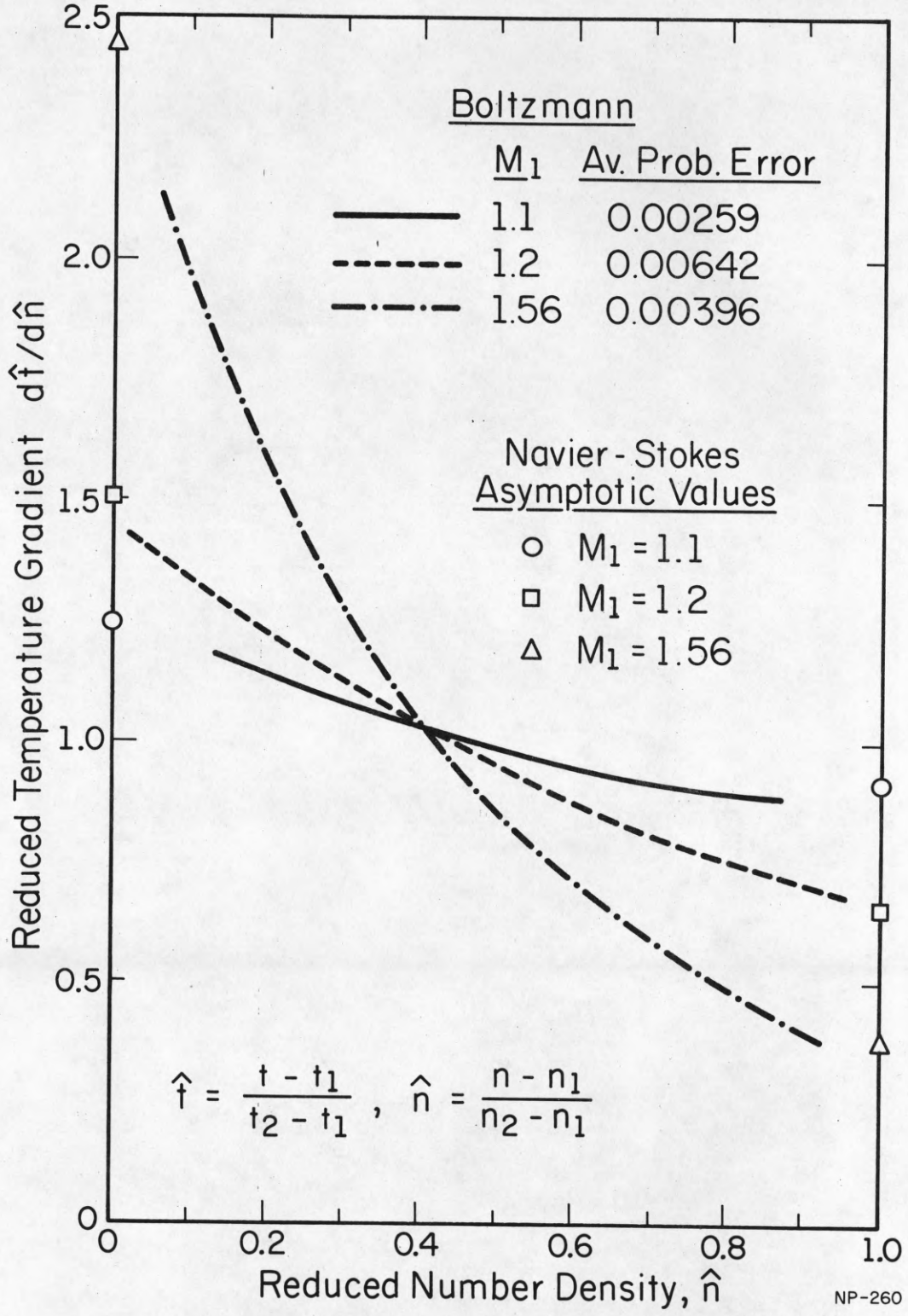

Fig. 4.2 Variation of the gradient of reduced temperature, $d\hat{t}/d\hat{n}$, with reduced density $\hat{n}$ for M_1 = 1.1, 1.2, and 1.56.

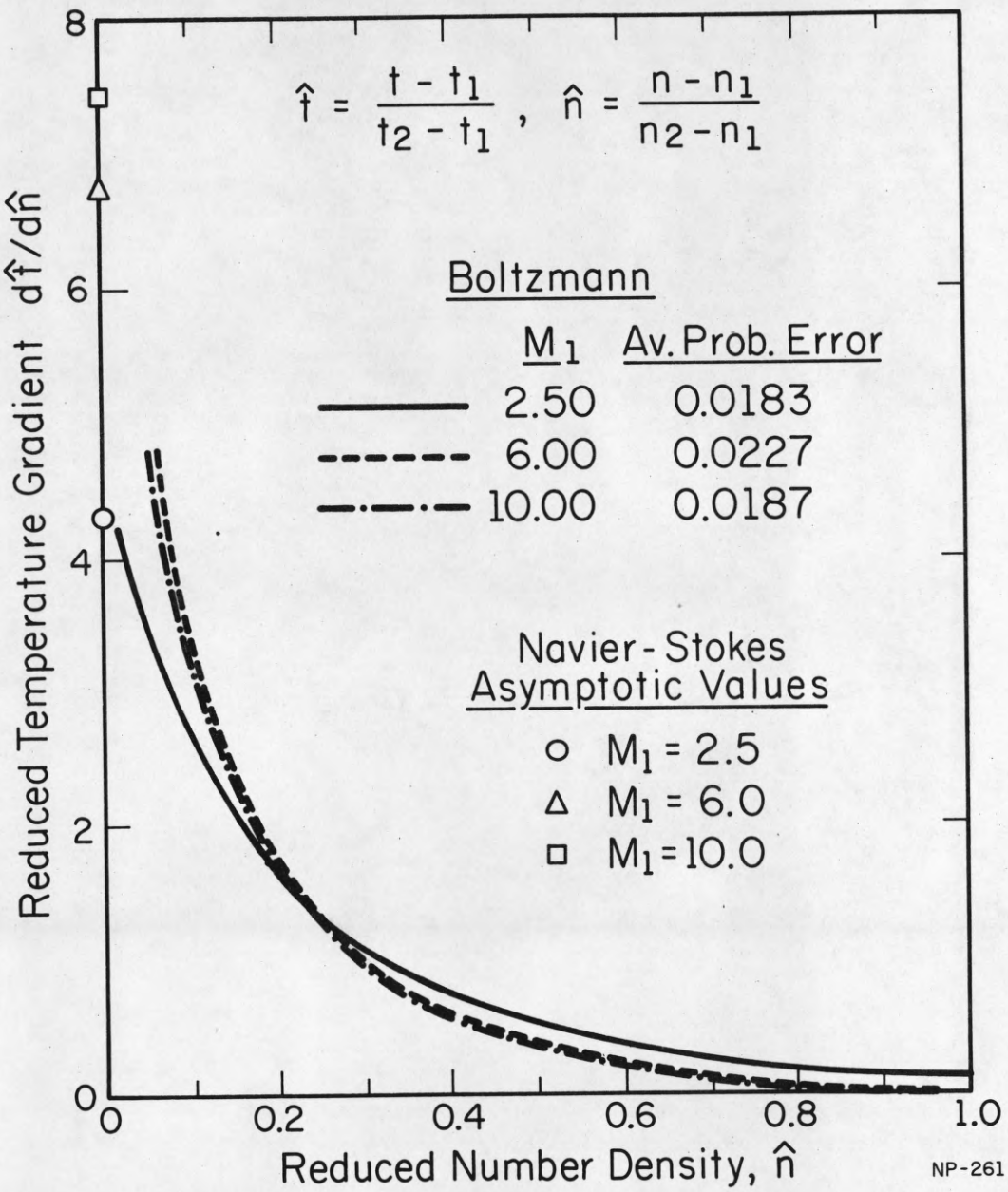

Fig. 4.3 Variation of the gradient of reduced temperature, $d\hat{t}/d\hat{n}$, with reduced density $\hat{n}$ for M_1 = 2.5, 6, and 10.

Since, as has been discussed by Baganoff and Nathenson[21] for example, the change in total temperature is rather small in a shock wave, we would then expect dt/dn to be a rather steep function of n, somewhat like inverse cube of n, as was indeed illustrated in Fig. 4.2. The values of $d\hat{t}_t/d\hat{n}$ are plotted vs $\hat{n}$ in Fig. 4.4 for M_1 = 1.1, 1.56, 2.5, and 10. As expected, they are much smaller than $d\hat{t}/d\hat{n}$, but these small values represent the part of the variation of $d\hat{t}/d\hat{n}$ with $\hat{n}$ which is <u>not</u> predictable a priori from the term $4\pi m_2^2/5n^3$ and which can only be calculated at present from solutions of the non-linear Boltzmann equation. Note also, for strong shocks, that near the hot side dt/dn is much less than either $|dt_x/dn|$ or $dt_\perp/dn$, i.e., there is a delicate balance between the large positive value of $dt_\perp/dn$ and the large negative value of dt_x/dn.

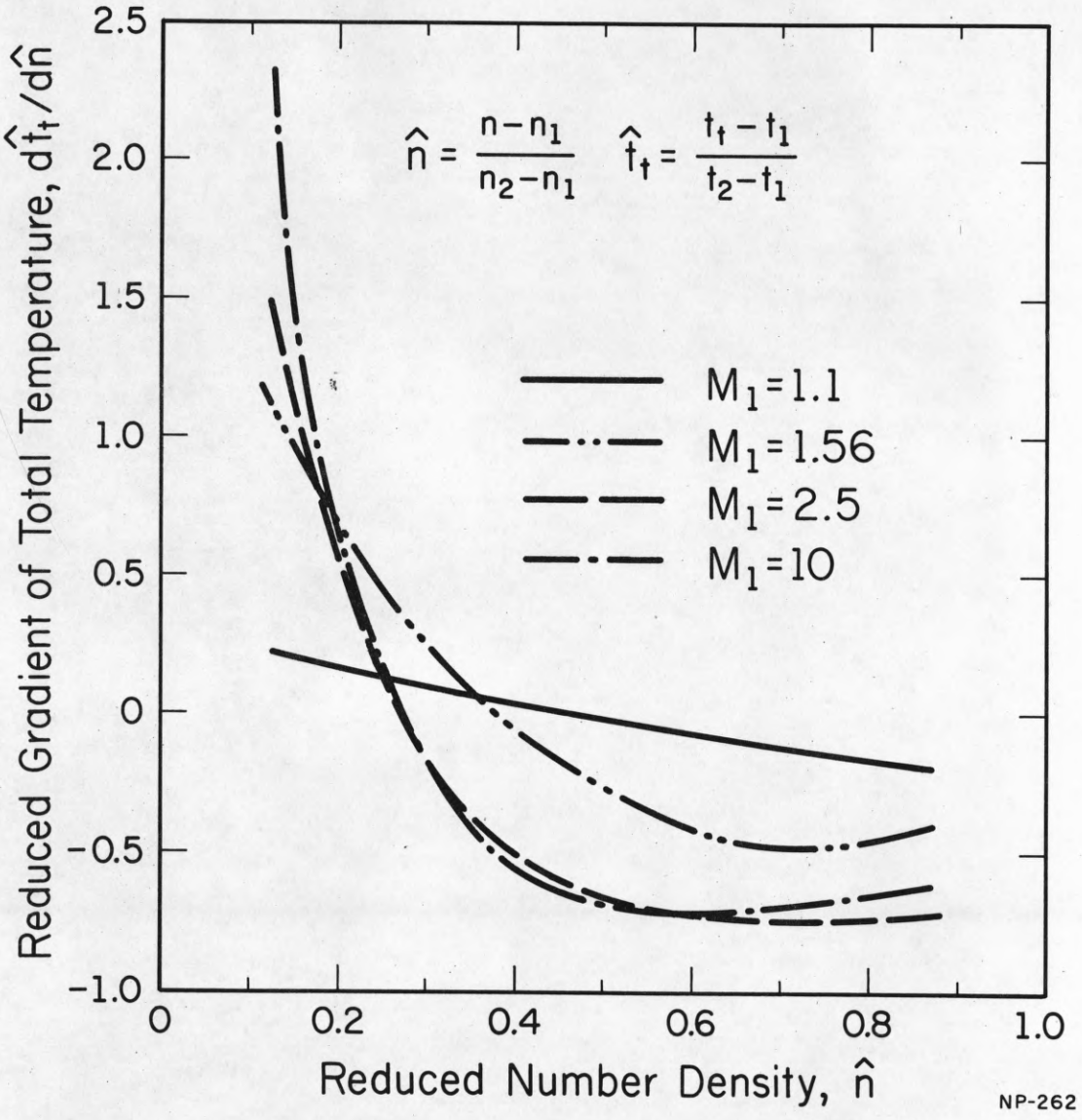

Fig. 4.4 Variation of the gradient of reduced total temperature, $d\hat{t}_t/d\hat{n}$, with reduced density $\hat{n}$ for M_1 = 1.1, 1.56, 2.5, and 10.

5. Transport Properties of Shock Waves

5.1 Properties at the Mid-Shock Position

In Section 3 we discussed the variation with Mach number of certain properties of shocks evaluated at the mid-shock position. In Section 4 we discussed the gradients of some shock properties as a function of position in the shock. In the present section we shall discuss variations of the transport properties of shock waves, both with respect to M_1 and with respect to shock position.

Three transport properties are basic to our discussion. There are τ, a measure of the total stress (or momentum flux); q, a reduced heat flux, and q_x, the part of the heat flux associated with the longitudinal random motion of the molecules. The properties are calculated from the formulae given in Section 3. As seen from Eqs.(3.1)-(3.8) in Section 3, τ and q can be derived from one moment of f, namely $\mathcal{M}_9$ (see Section 4), or from the lateral temperature $t_\perp$, together with t_g which is a known function of the conserved moments and therefore of M_1 and of n. To calculate q_x an additional moment must be known, namely, $\mathcal{M}_6$.

Let us first consider the momentum transport τ. Eq.(3.4) shows that it vanishes only when the two temperatures t_x and $t_\perp$ are equal. Fig. 5.1 shows the behavior of τ/p_1 as a function of M_1, at the mid-shock position. Its behavior is very similar to that for the Mott-Smith shock. The difference varies between 2% (near the cold side) and 6% (near the hot side).

Fig. 5.2 shows the variation of q and q_x with M_1. From earlier remarks we know that the curve of q is not independent of the τ curve in Fig. 5.1. However, within a shock wave the lack of equilibration of the longitudinal and lateral degrees of freedom makes it necessary to introduce also the second

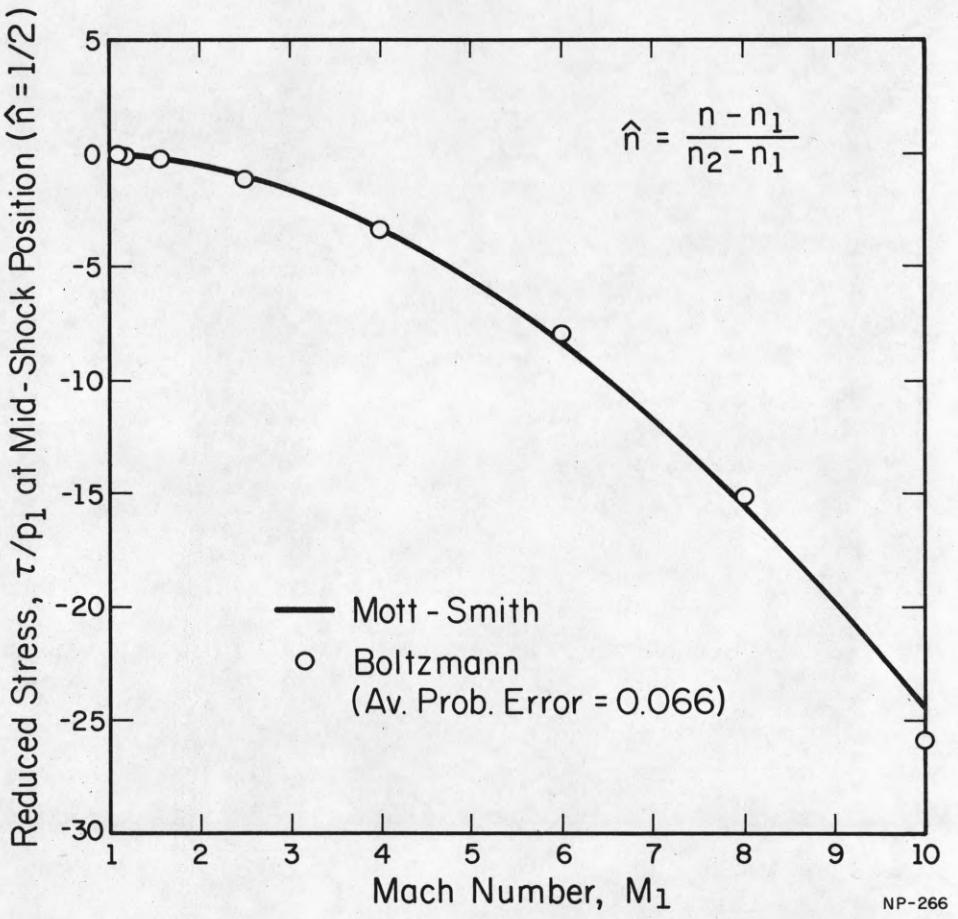

Fig. 5.1 Variation of reduced stress, τ/p_1, at mid-shock position ($\hat{n} = \frac{1}{2}$) with Mach number M_1.

quantity q_x in describing the heat flux. As shown in Fig. 5.2, the Mott-Smith values of q_x are larger than the Boltzmann values, and their difference increases as M_1 increases.

The ratio q_x/q is also of interest. As pointed out by Baganoff and Nathenson[21] the Chapman-Enskog approximation yields a constant value of $q_x/q = 0.6$. Baganoff's model[23] gives $q_x/q = 15M^2/(7+18M^2)$ where M = local Mach number. Our solutions of the Boltzmann give the curve shown in Fig. 5.3 which is in good agreement with Baganoff's model. Note that even for low Mach numbers, the ratio q_x/q is not a constant as predicted by Chaptman-Enskog approximation, but is a function of the local Mach number. We have found also that we can correlate the Mott-Smith values of q_x/q with Baganoff's expression, but only approximately. The plot of Mott-Smith q_x/q is lower than Baganoff's curve for large M_1.

In fluid dynamics one is interested in the relation between each flux and the corresponding gradient. In Navier-Stokes fluids the relation is described by the transport coefficients σ and k, defined by

$$\mu = \tau/(dn/dx)$$
$$k = q/(dt/dx) \qquad (5.1)$$

For a gas of elastic spheres the temperature dependence of the coefficients is given by

$$\mu = \mu_1(t/t_1)^{\frac{1}{2}}$$
$$k = k_1(t/t_1)^{\frac{1}{2}} \qquad (5.2)$$

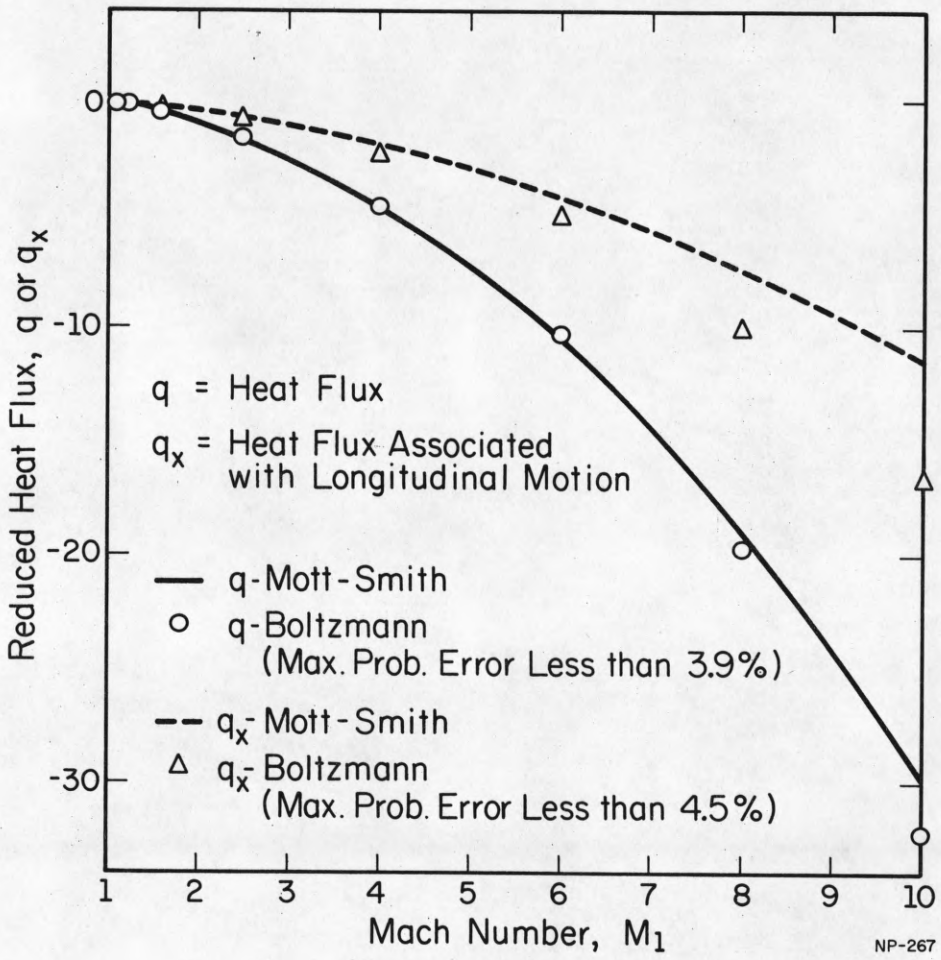

Fig. 5.2 Variation of heat flux, q, and heat flux associated with longitudinal motion, q_x, with Mach number M_1.

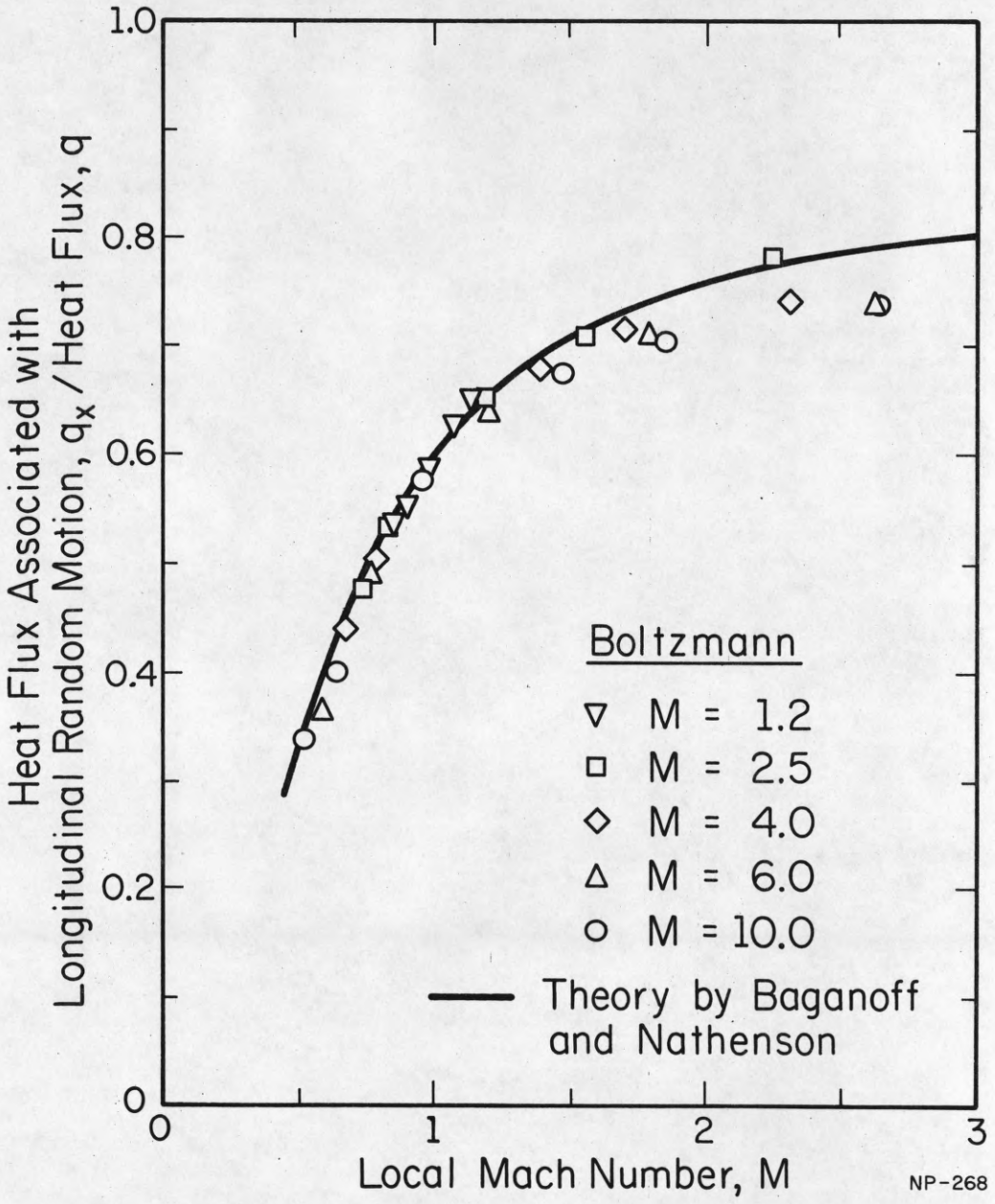

Fig. 5.3 Variation of heat flux ratio q_x/q with local Mach number M for M_1 = 1.2, 2.5, 4, 6, and 10.

In the kinetic theory of a non-equilibrium gas, like that in the interior of a shock wave, it is convenient to use the same definition of transport coefficients but to normalize them by dividing by $t^{\frac{1}{2}}$ and the upstream value of the coefficient. Thus in our discussion we shall use

$$\sigma_{rel} = (\mu/\mu_1)/(t/t_1)^{\frac{1}{2}}$$

$$k_{rel} = (k/k_1)/(t/t_1)^{\frac{1}{2}} \qquad (5.3)$$

For a Chapman-Enskog gas (i.e., small values of (M_1-1)) σ_{rel} and k_{rel} should be equal to one.

These quantities are plotted in Figs. 5.4 and 5.5 against M_1 for the mid-shock position. We notice first that, up to $M_1 = 10$, $1 < \sigma_{rel} < 1.6$ and $1 < k_{rel} < 3$ so that the near equilibrium theory predicts too small values of the transport coefficients, but not by an order of magnitude. The fact that our values of these reduced coefficients approach 1 as M_1 approaches 1 is evidence of the extreme accuracy of the Monte Carlo solutions in this region, for determination of each of the coefficients requires division of a flux by a gradient, namely, of one small number by another, since each of these numbers approaches zero as M_1 approaches 1. The Boltzmann and Mott-Smith values of σ_{rel} are in agreement within 90% confidence limit for $M_1 > 2.5$; however the Mott-Smith values of k_{rel} are significantly larger than the Boltzmann results.

In near equilibrium flows the Prandtl number $\tilde{Pr}$ characterizes the variation with density of most macroscopic properties. (See Section 6.) We therefore also calculate it for the mid-point position of the shocks, as shown

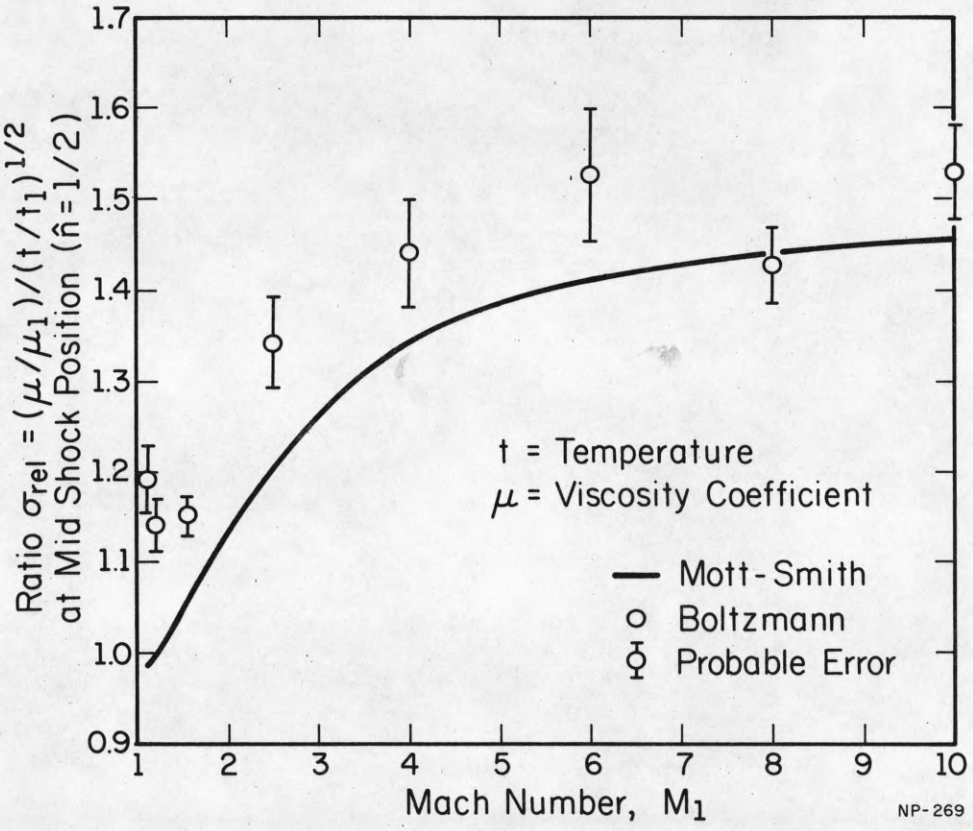

Fig. 5.4 Variation of the viscosity-temperature ratio, $\sigma_{rel.} = (\frac{\mu}{\mu_1})/(\frac{t}{t_1})^{\frac{1}{2}}$ at mid-shock position ($\hat{n}=\frac{1}{2}$) with Mach number M_1.

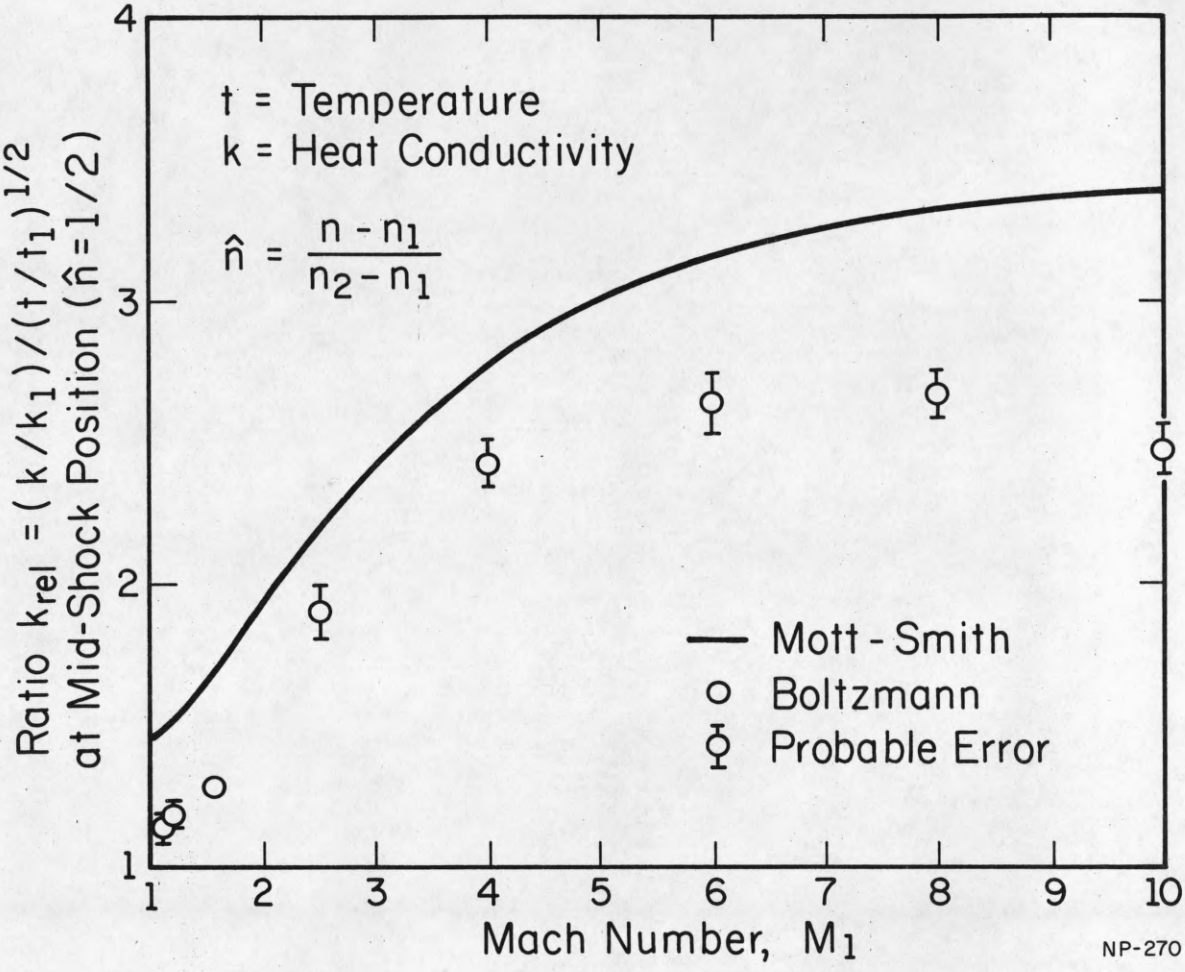

Fig. 5.5 Variation of the heat conductivity-temperature ratio, $k_{rel.} = (k/k_1)/(t/t_1)^{\frac{1}{2}}$, at mid-shock position ($\hat{n} = \frac{1}{2}$) with Mach number M_1.

in Fig. 5.6. The Chapman-Enskog value of the Prandtl number for the elastic sphere gas is 8/9. Our Monte Carlo results are not in disagreement with this value for weak shocks except near the hot side. The Mott-Smith values for $\tilde{Pr}$ are nearly constant for weak shocks but are considerably lower than 8/9 (40% for $M_1 = 1.1$ and 1.2). The Monte Carlo results suggest that the asymptotic value for the Prandtl number, as $M_1 \to \infty$, may lie near 0.5 for elastic spheres.

5.2 Profiles of Transport Properties ($M_1 = 4$)

We next look at the variation of the transport properties within a shock wave for $M_1 = 4$. Figs. 5.7 and 5.8 show the variation of three fluxes, τ, q, and q_x for the Boltzmann shock and the Mott-Smith. At the upstream and downstream boundaries of the shock the Monte Carlo values of the three fluxes are consistent with the zero values expected there. As shown in the two figures, the three profiles of the Boltzmann shock are similar to those of the Mott-Smith shock; however, the differences are significant, especially near the upstream boundary. The maximum percentage differences are 9.8% (at $\hat{n} = 0.125$), 21% (at $\hat{n} = 0.25$), and 6.5% (at $\hat{n} = 0.1875$) for τ, q, and q_x respectively.

Figs. 5.9 and 5.10 show respectively the variation of σ_{rel} and k_{rel} in a shock wave for $M_1 = 4$. The values of σ_{rel} are larger near the boundaries than in the interior of the shock wave and therefore depart quite significantly from the values expected for near equilibrium flow.[14] This departure is much larger for k_{rel} near the downstream boundary. Whether this disagreement is due to systematic errors in our solutions of the Boltzmann equation near the shock boundaries or due to errors in the (first order) Chapman-Enskog theory cannot be decided without further investigation. As shown in Figs. 5.9 and 5.10, the

Boltzmann σ_{rel} and k_{rel} are in agreement with the Mott-Smith values at most positions for this shock wave.

The variation of $\tilde{Pr}$ vs $\hat{n}$ is given in Fig. 5.11. The Boltzmann value of $\tilde{Pr}$ is consistent with the C-E value of 8/9 at the upstream boundary; however it is very much smaller at the downstream boundary. Except very near the downstream boundary, the Boltzmann and Mott-Smith values of $\tilde{Pr}$ are in good agreement.

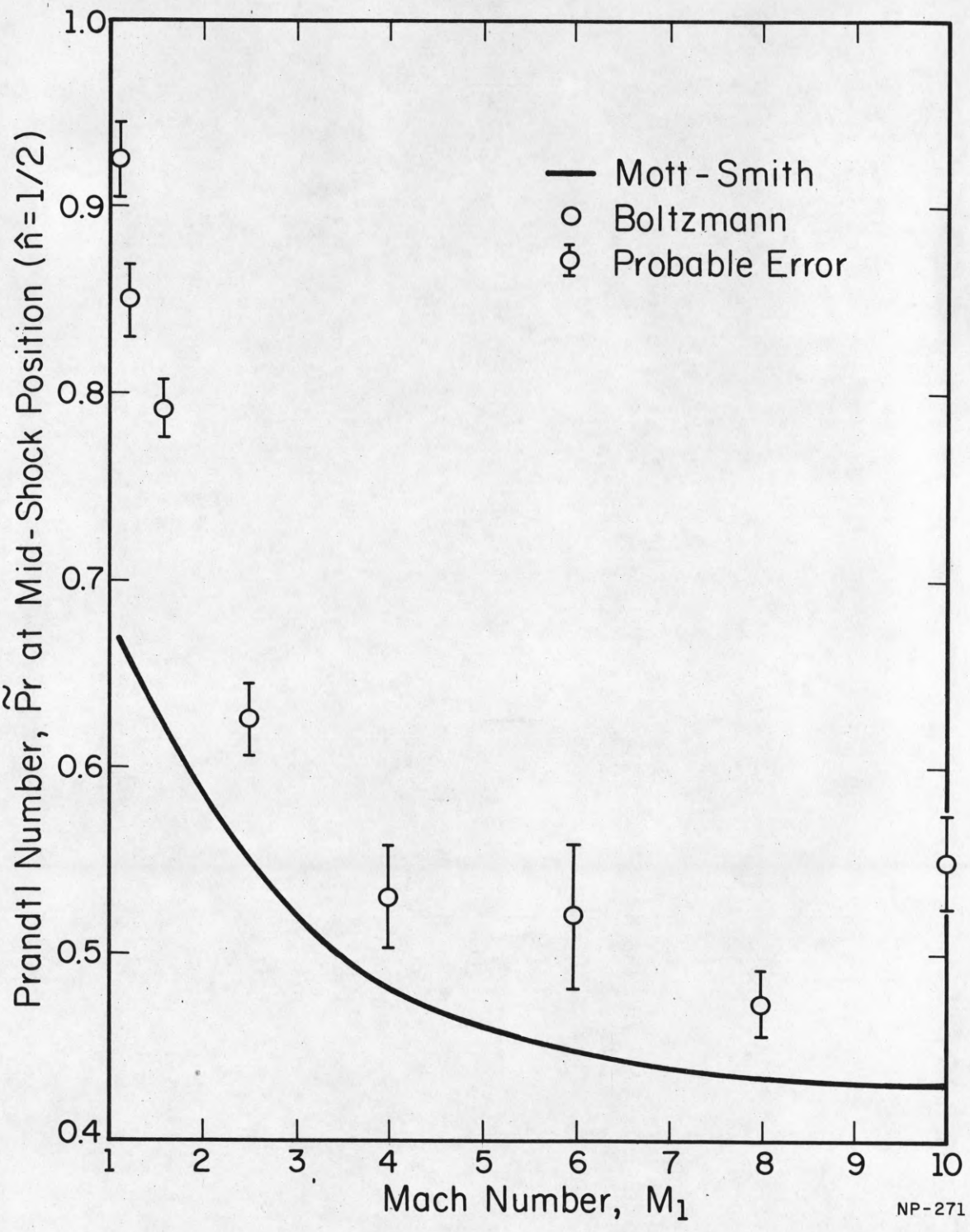

Fig. 5.6 Variation of Prandtl number $\tilde{P}r$ at mid-shock position ($\hat{n} = \frac{1}{2}$) with Mach number M_1.

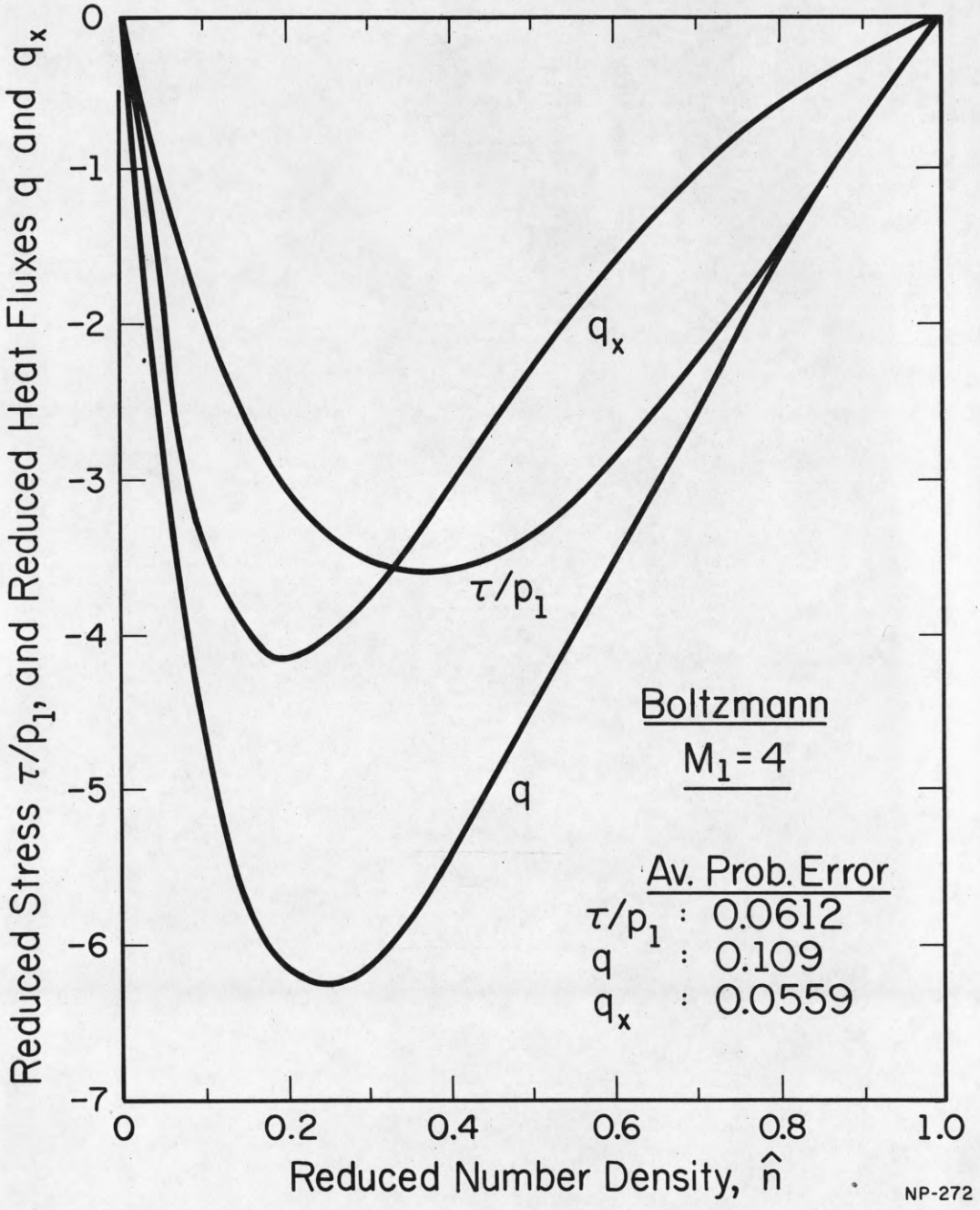

Fig. 5.7 Variation of stress τ/p_1, heat flux q, and heat flux associated with longitudinal motion q_x with reduced density $\hat{n}$ for $M_1 = 4$.

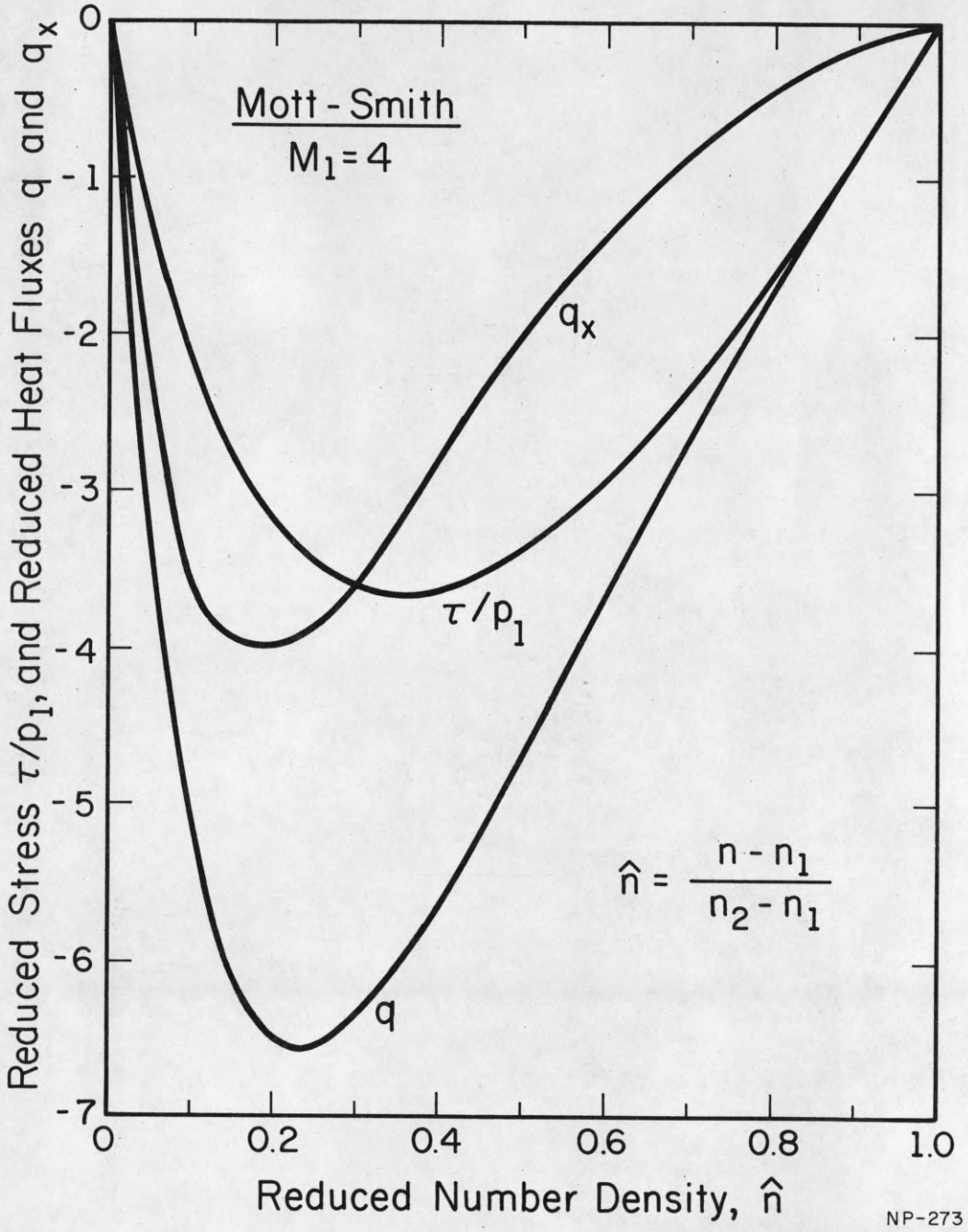

Fig. 5.8 Variation of stress τ/p_1, heat flux q, and heat flux associated with longitudinal energy q_x with reduced density $\hat{n}$ for a Mott-Smith shock of $M_1 = 4$.

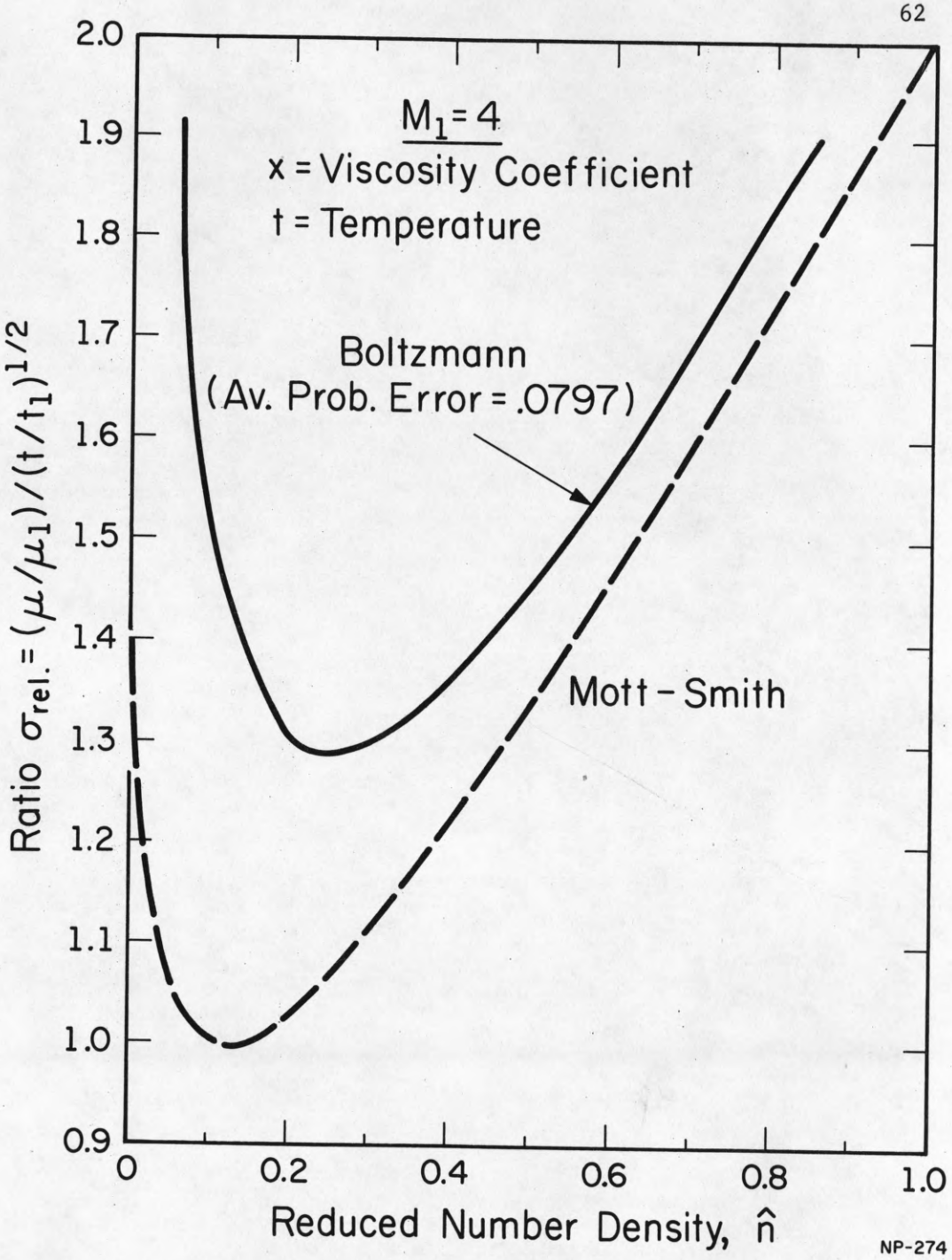

Fig. 5.9 Variation of viscosity-temperature ratio, $\sigma_{rel.} = (\frac{\mu}{\mu_1})/(\frac{t}{t_1})^{\frac{1}{2}}$ with $\hat{n}$ for a shock wave of $M_1 = 4$.

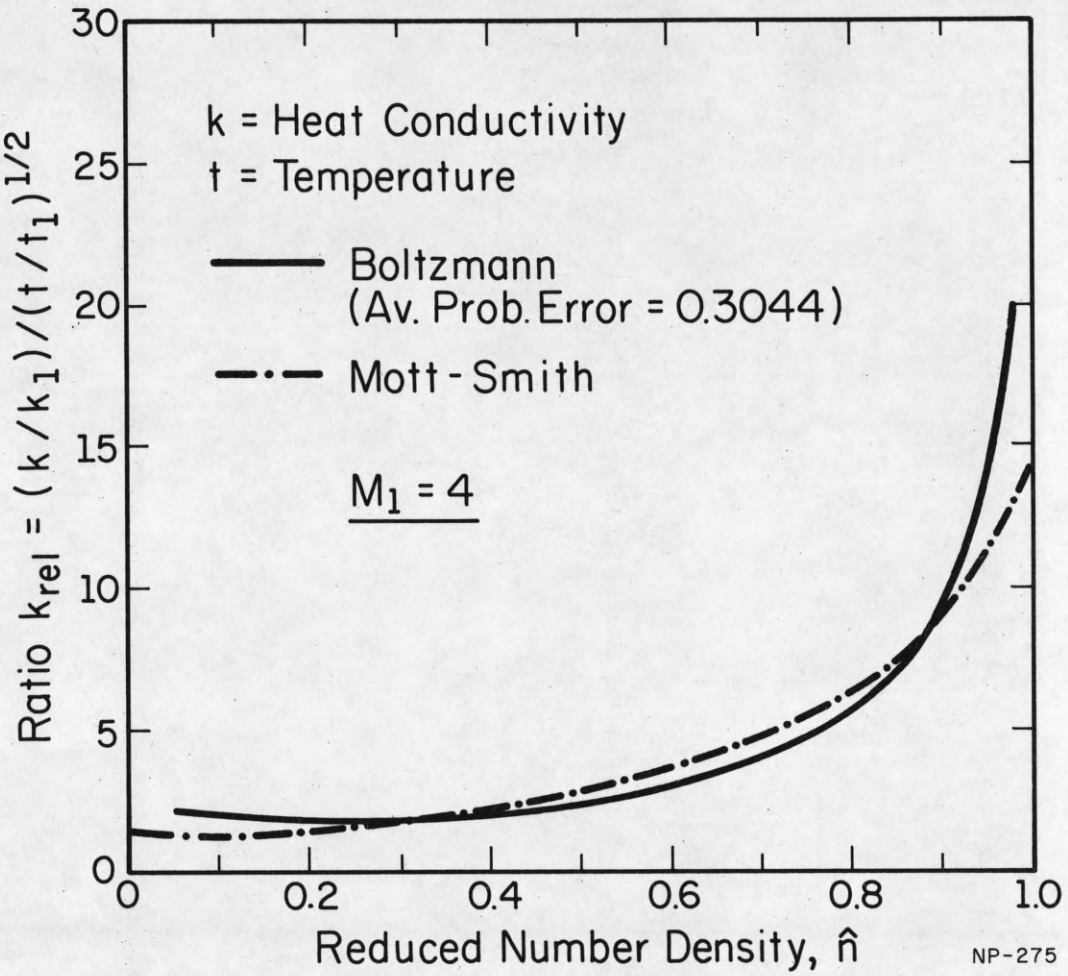

Fig. 5.10 Variation heat conductivity - temperature ratio $k_{rel.} = (\frac{k}{k_1})/(\frac{t}{t_1})^{\frac{1}{2}}$ with $\hat{n}$ for a shock wave of $M_1 = 4$.

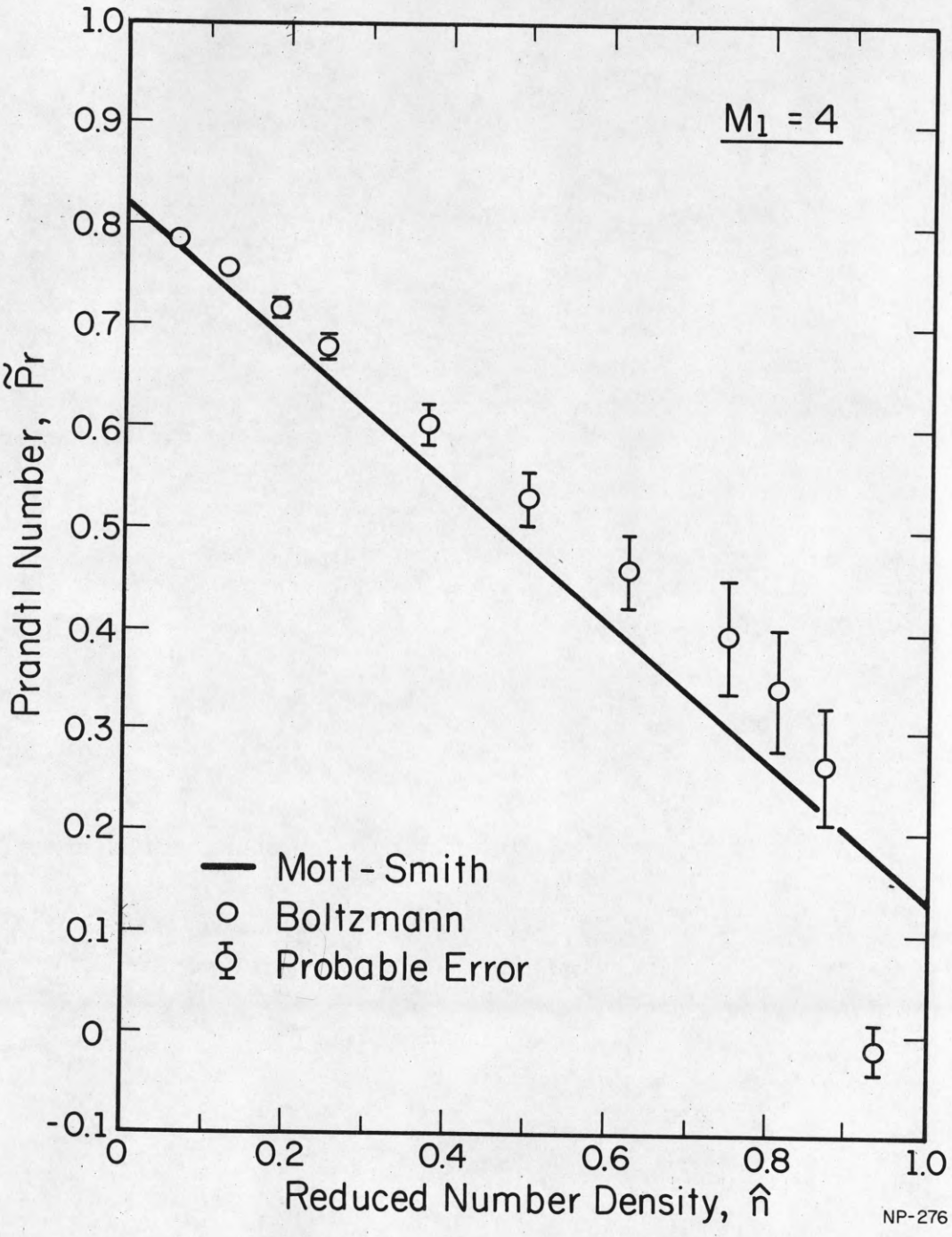

Fig. 5.11 Variation of Prandtl number $\tilde{Pr}$ with $\hat{n}$ for a shock wave of $M_1 = 4$.

6. Comparison with Navier-Stokes Shock at a Low Mach Number ($M_1 = 1.2$)

In Section 2, we have found that the Boltzmann results on RST are smaller than the Navier-Stokes values for low Mach numbers. In order to extend our comparative study, we will look at four additional properties in detail for $M_1 = 1.2$: the density gradient dn/dx, the profile of temperature t vs density n, the Prandtl number $\tilde{P}r$ as a function of n, and the viscosity coefficient μ as a function of n.

It is worthwhile to review how the Navier-Stokes shock solution is usually obtained. The first step is to obtain the integral curve for constant $\tilde{P}r$, yielding either the t-n or the t-v profile. As indicated in Section 3, several properties including temperature are functions of $\mathcal{M}_9 = \int v_\perp^2 f \, d\bar{v}$; therefore, the t-n relation determines also many other shock properties as functions of density n. The second step is to obtain the density profile, the density n vs the distance x, by using a viscosity-temperature (μ-t) relation consistent with the collision law of a gas.

In our comparative study of the Boltzmann and Navier-Stokes for $M_1 = 1.2$ we need (1) to look at the difference in dn/dx, (2) to compare the dt/dn profile, (3) to examine the variation of $\tilde{P}r$ in the Boltzmann shock, and (4) to see if the viscosity coefficient in the Boltzmann shock is proportional to the square root of temperature, a relation derived from the linearized theory for hard sphere gases.

Fig. 6.1 shows the variation of reduced density gradient dn/dx vs reduced density $\hat{n}$. For $\hat{n} > 0.2$, the Boltzmann values of dn/dx are significantly lower than the Navier-Stokes results. The value of RST for $M_1 = 1.2$ shown in Fig. 2.2 is proportional to the maximum value of dn/dx in this figure.

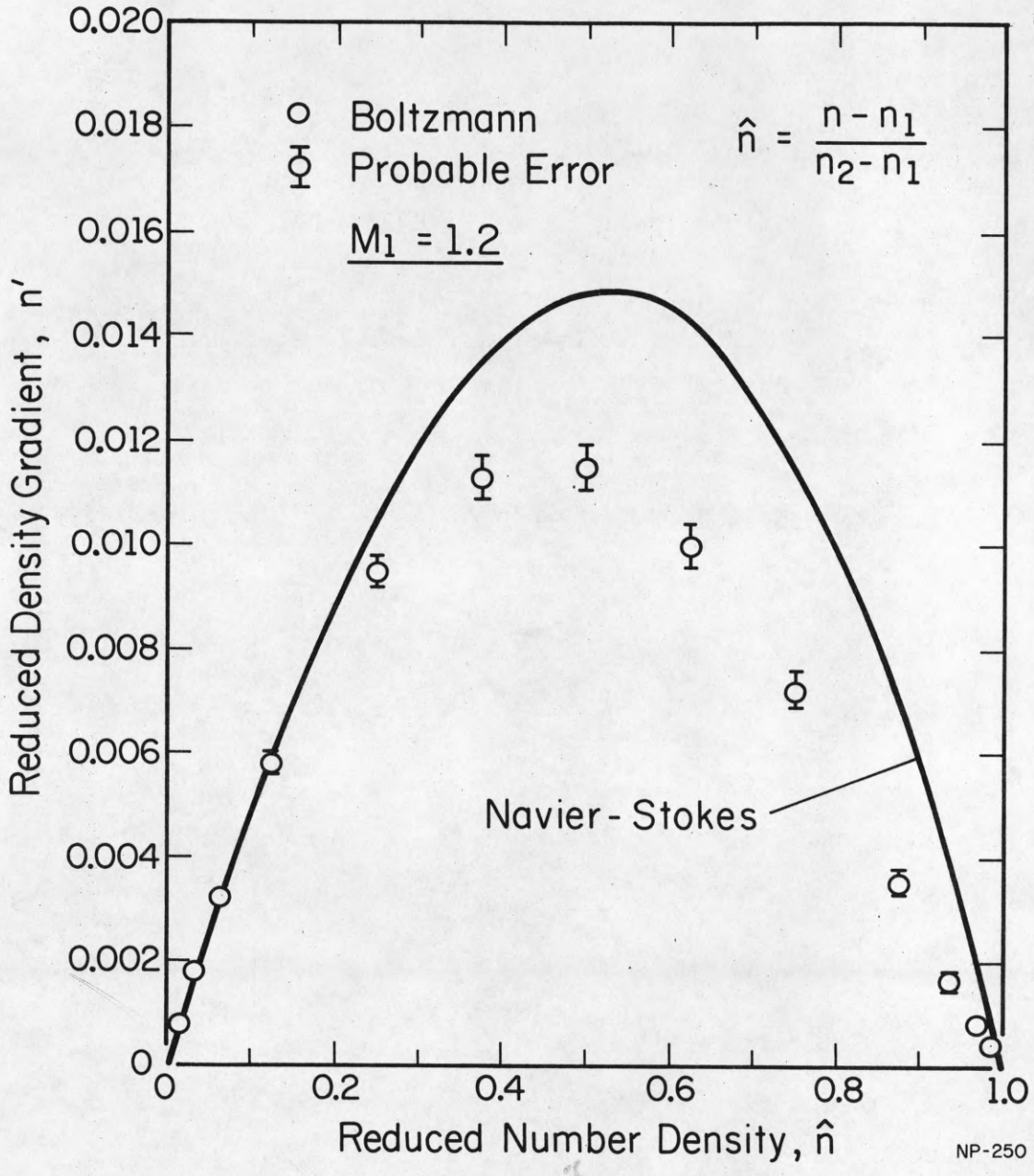

Fig. 6.1 Comparison of density gradients n' of Boltzmann with Navier-Stokes results for $M_1 = 1.2$.

The results on the reduced temperature gradient $d\hat{t}/d\hat{n}$ are compared in Fig. 6.2 which shows good agreement for the two shocks. This agreement implies good agreement also for the variation of the properties such as t, $t_\perp$, τ, and q (which are functions of $\mathcal{M}_9$) as functions of density n. Fig. 6.3 shows the variation of $\tilde{Pr}$ vs $\hat{n}$ in the Boltzmann shock. The significant variation of $\tilde{Pr}$, except near the cold and hot sides, is less than 10%. Since the Navier-Stokes dt/dn was obtained on the basis of constant $\tilde{Pr}$ of 8/9 (corresponding to Pr = 2/3), our result on Prandtl number are also in accord with that of the Navier-Stokes shock.

The ratio $\sigma_{rel.} = (\mu/\mu_1)/(t/t_1)^{\frac{1}{2}}$ is one for gas of elastic spheres. We have studied this ratio for the Boltzmann shock (see Section 4). The variation of this ratio for $M_1 = 1.2$ is given in Fig. 6.4. We note that this ratio is appreciably greater than unity, with a maximum departure of 40%. The fact that the ratio $\sigma_{rel.}$ is greater than one for the Boltzmann shock is the reason why the Boltzmann dn/dx and RST are smaller than the Navier-Stokes results for $M_1 = 1.2$ and other lower Mach numbers.

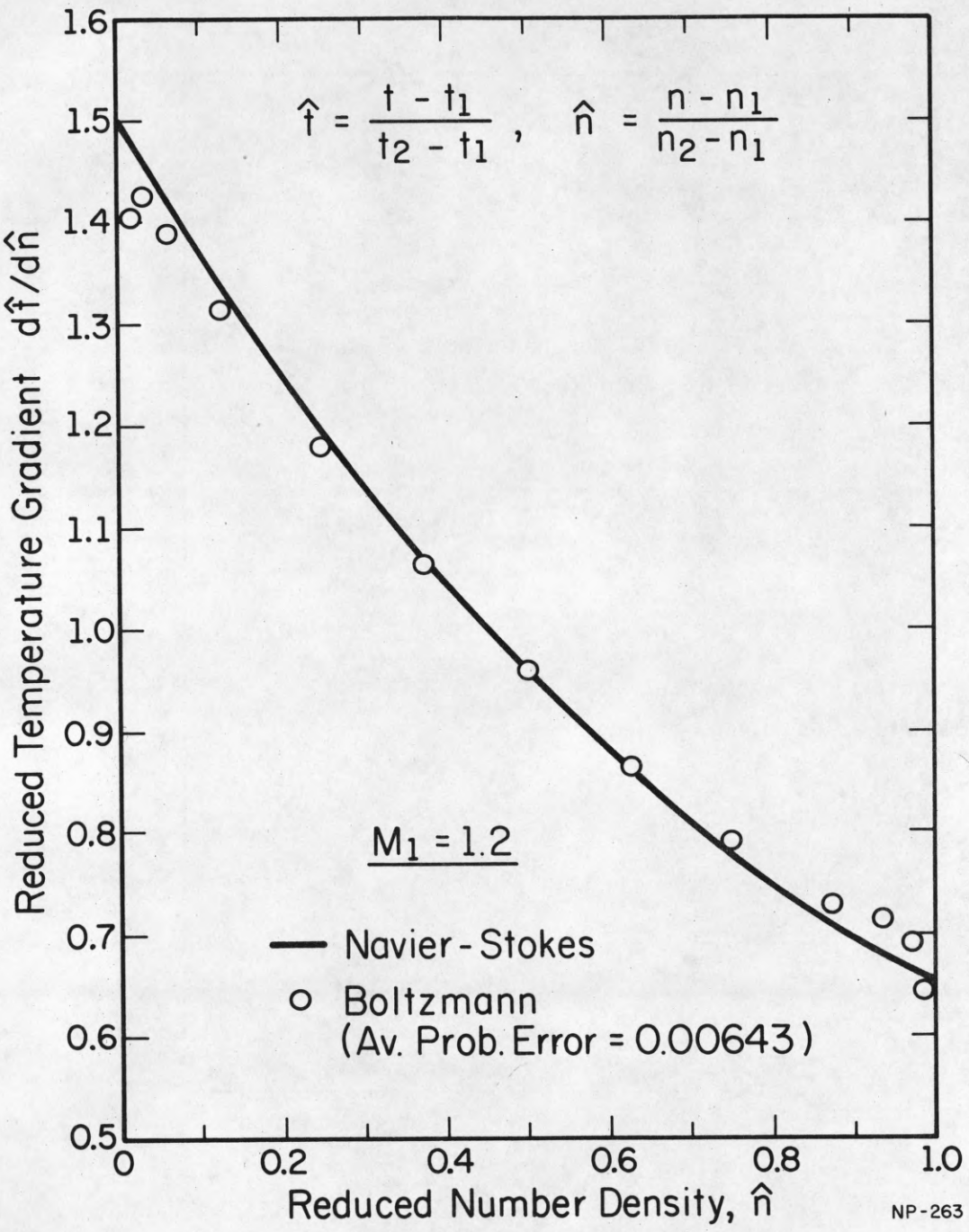

Fig. 6.2 Comparison of Boltzmann gradient of reduced temperature, $d\hat{t}/d\hat{n}$, with the Navier-Stokes values for $M_1 = 1.2$.

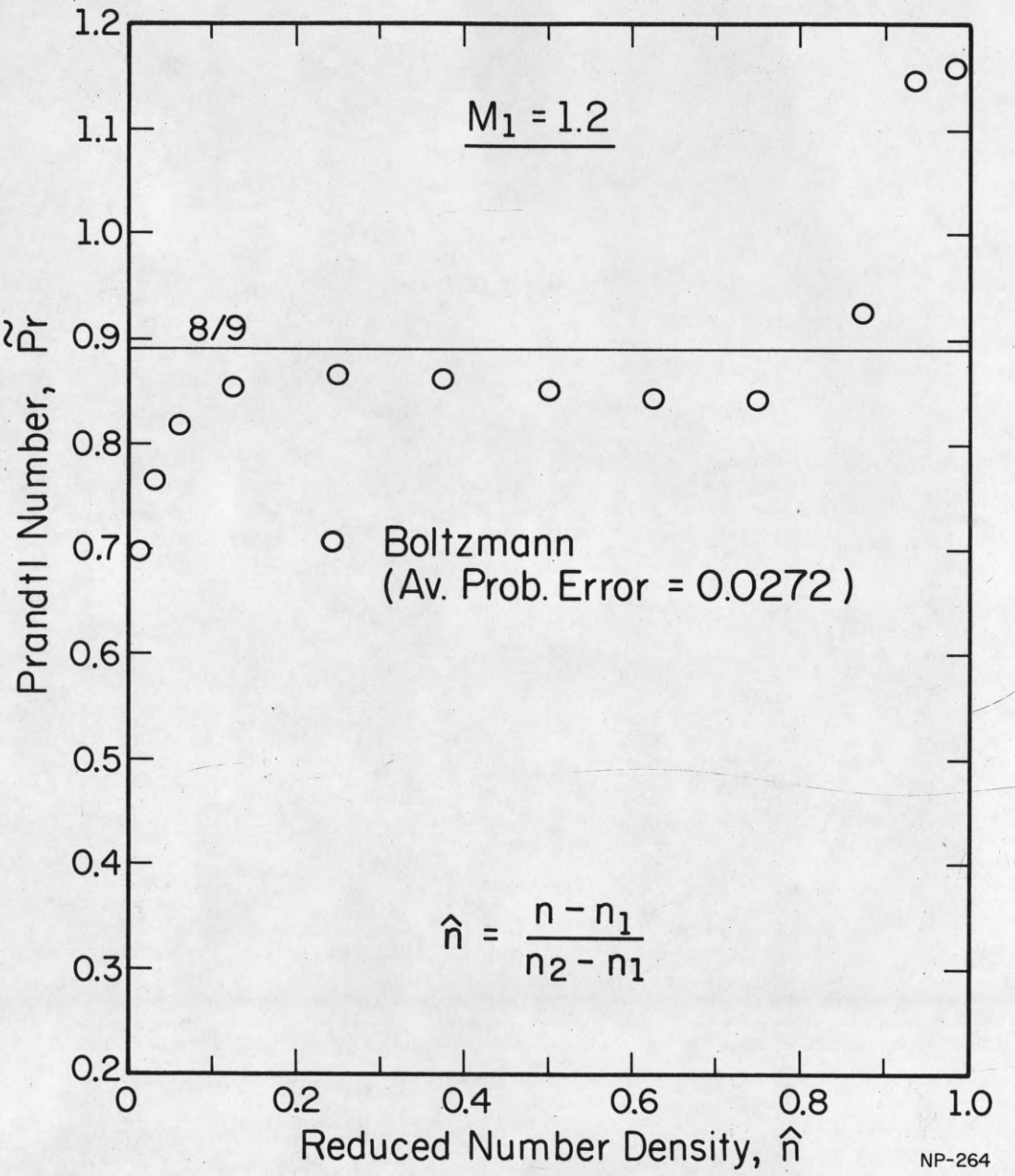

Fig. 6.3 Variation of Prandtl number $\tilde{Pr}$ with reduced density $\hat{n}$ for $M_1 = 1.2$.

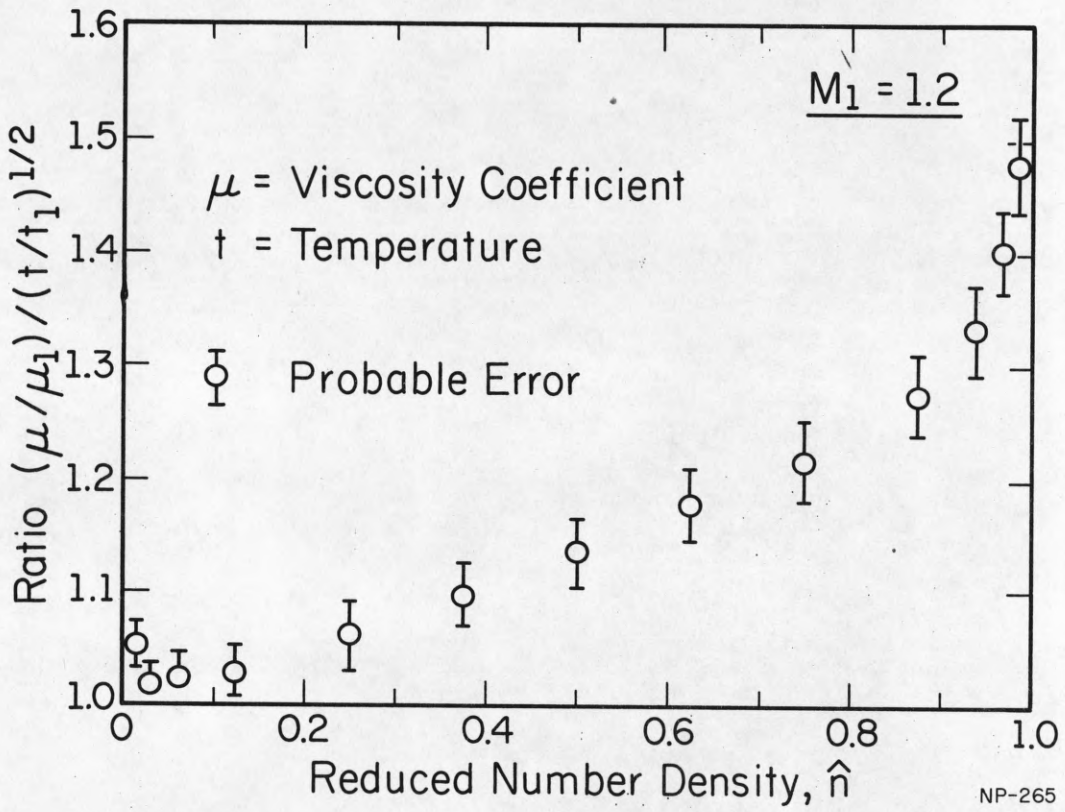

Fig. 6.4 Variation of the viscosity-temperature ratio $\sigma_{rel.} = (\frac{\mu}{\mu_1})/(\frac{t}{t_1})^{\frac{1}{2}}$ with reduced density $\hat{n}$ for $M_1 = 1.2$.

7. The Velocity Distribution Function (M_1=4)

In the previous sections we have discussed the dependence on Mach number and shock position of many moments of f, the velocity distribution function, and of other functions derived from f. In this section we shall describe the behavior of f as a function of position in velocity space for one Mach number (M_1=4) and at several positions in the shock.

The qualitative feature of the distribution function was monitored by the CSL computer graphical display system.[22] The layout of the velocity space for the display of our velocity dependent functions is shown in Fig. 7.1. A representative distribution function f at the mid-shock position ($\hat{n} = \frac{1}{2}$), given in Fig. 7.2 for $M_1 = 4$, shows well its bimodal characteristics.

For the reasons explained in the Introduction we shall present our results in the form of comparisons of the Boltzmann values of f with the Mott-Smith values. We shall also compare our results with the special distribution functions measured by Muntz and Harnett.[23] Before making these comparisons we should interpolate remarks about approximate theoretical methods.

Direct comparisons of our solutions of the non-linear Boltzmann equation for shock waves with various approximate descriptions of shock waves, like those based on the Mott-Smith or the Krook model, are obviously of interest. One comparison of Krook and Boltzmann collision integrals is made in Section 8. Otherwise we defer detailed comparisons until later papers, remarking, however, that the Krook solutions for the shock waves are obtained very easily by our Boltzmann program and for exactly the same values of those parameters which control the nature of the numerical methods used. An auxiliary program makes possible direct estimates, at any point in velocity space, of the accuracy of either the distribution function or of the collision integral calculated from the approximate shock descriptions.

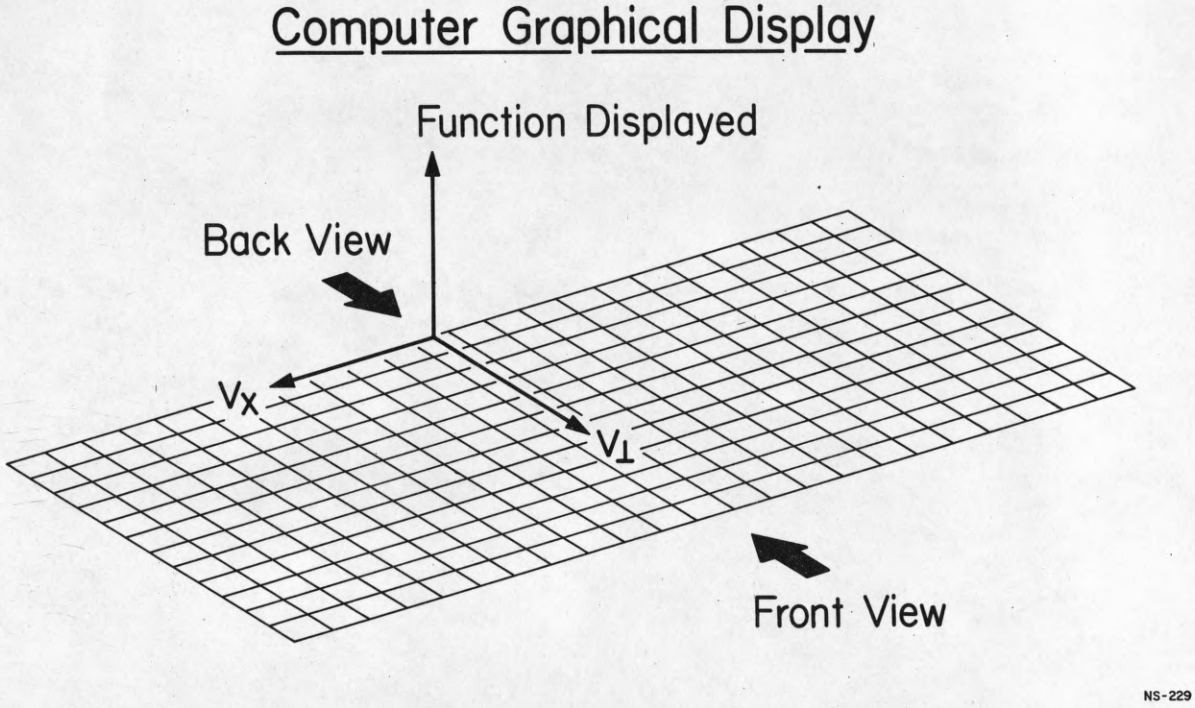

Fig. 7.1 Layout of velocity space used in the computer display system to exhibit functions of velocity.

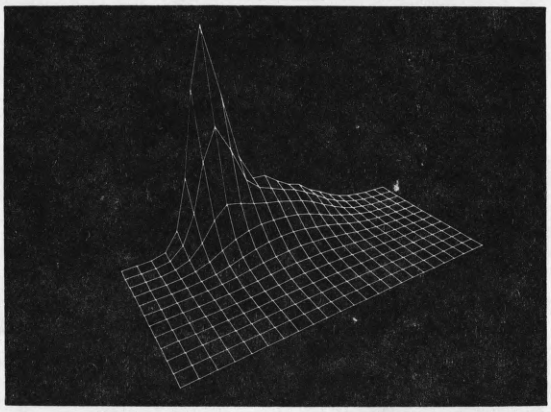

Fig. 7.2 Display of distribution function f at mid-shock position ($\hat{n} = \frac{1}{2}$) for $M_1 = 4$.

Let us now define

$$\delta f = f_{Boltz.} - f_{MS} \tag{7.1}$$

each term in the equation, of course, being calculated for the same value of $\bar{v}$ and $\hat{n}$, and for the same Mach number.

The nature of the variation of δf across velocity space for the mid-shock position ($\hat{n} = \frac{1}{2}$) is shown in Fig. 7.3. Notice that there are regions in which δf is positive and other regions in which δf is negative. These regions are well-defined at all positions within the shock but their shape and size vary with position. This figure suggests that the errors of the Mott-Smith function for this Mach number and position in the shock are indeed significant.

This opinion is confirmed when we look at values of δf for individual bins in comparison with the estimates we have made of $\epsilon_{90} f$ for the same bins. We find that for about 40% of the bins at most shock positions δf is greater than $3\epsilon_{90} f$, that is, the δf observed for these bins would occur by chance only once in 100 or more trials. Near the cold boundary these highly significant values of f occur only for about 20% of the bins, so that here the Mott-Smith Ansatz gives fewer large deviations from the solution of the Boltzmann equation than elsewhere.* Nevertheless the largest individual deviations also occur near the cold side of the shock.

The rms values of both δf and $\epsilon_{90} f$ are approximately constant across the shock. The rms value of δf for all stations (1.34×10^{-2}) is 1.7 times larger than the average value of $\epsilon_{90} f$ (0.79×10^{-2}) and is a 6.3 times smaller than the rms value of f throughout the shock.

---

*Essentially the same result was found earlier for the $M_1 = 2.5$ shock.[9]

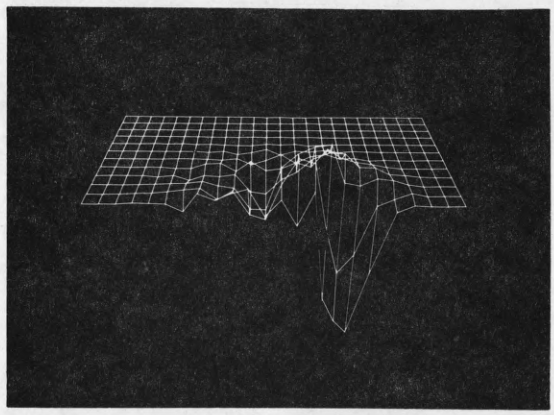

Fig. 7.3 Display of the difference between the Boltzmann distribution function and the Mott-Smith distribution function $\delta f = f_{Boltz.} - f_{MS}$ at mid-shock position ($\hat{n} = \frac{1}{2}$) for $M_1 = 4$.

A qualitative summary of the characteristics of δf, and therefore of f itself, would be useful in guiding the future development of analytical or analytical-numerical methods of describing the properties of shock waves. Let us therefore summarize the qualitative features of the solution $f(\bar{v},n)$ of the Boltzmann equation for the shock wave. To do this we shall again use δf, the departure of f from the corresponding Mott-Smith function, because the fractional deviation $\delta f/f$ is generally small, though not small in each local region in velocity space and in the shock. What are the qualitative properties of δf obtained from our solution of the Boltzmann equation?

1) $\delta f = 0$ at the up and downstream boundaries of the shocks.

2) $\delta n = \int \delta f d\bar{v}$ must = 0 because the values of f_{Boltz} and f_{MS} in Eq.(7.1) are calculated for the same value of n. Therefore, δf must have both positive and negative values for each position in the shock.

3) The three conserved moments of δf, like those of f and of $f_{M\text{-}S}$, must be constant across the shock.

4) δf cannot be represented as a product of a function of n and a function of $\bar{v}$, because the shape of the isolines of δf changes with n, i.e., with position in the shock.

5) In particular, δf is not simply proportional to $\hat{n}(1-\hat{n})$, because analysis of three of the non-conserved moments of f show that it cannot be represented by quadratic functions of n.

Muntz and Harnett[23] have recently made two experimental measurements for $M_1 = 1.59$: $F(v_x) = \int f\, dv_x dv_y$ and $F(v_y) = \int f\, dv_x dv_z$. They found that $F(v_x)$ deviates significantly from that of the corresponding Chapman-Enskog's first iterate. In order to find if similar deviations exist between our Boltzmann results and those of C-E first iterate, we have made a similar comparison for

$M_1 = 1.59$ for hard spheres. The results on half-width of $F(v_x)$ are shown in Fig. 7.4.

It was indeed interesting to find that we have obtained the following detailed agreements with Muntz's findings: (1) the half-widths of $F(v_x)$ overshoots in the region $\hat{n} > \frac{1}{2}$; (2) the half-widths of $F(v_x)$ are smaller than the C-E values in the region $\hat{n} < \frac{1}{2}$ but are larger in the remainder of the shock, (3) the departure of profiles of $F(v_x)$ from those of C-E, are significant, depending on the location in the shock, (4) the results on $F(v_x)$ indicates there is a significant enhancement of high speed molecules (large v_x) in comparison with C-E results.

We should like to point out that Muntz's results are for Argon gas with different collision cross-section than that of hard spheres; therefore, it would not be possible to make direct, quantitative comparison of our Boltzmann results with Muntz's values. However, we are pleased to find the detailed qualitative agreement mentioned above, especially for a relatively low Mach number of $M_1 = 1.59$ in which a high accuracy of the calculation of the small Boltzmann collision integrals is required.

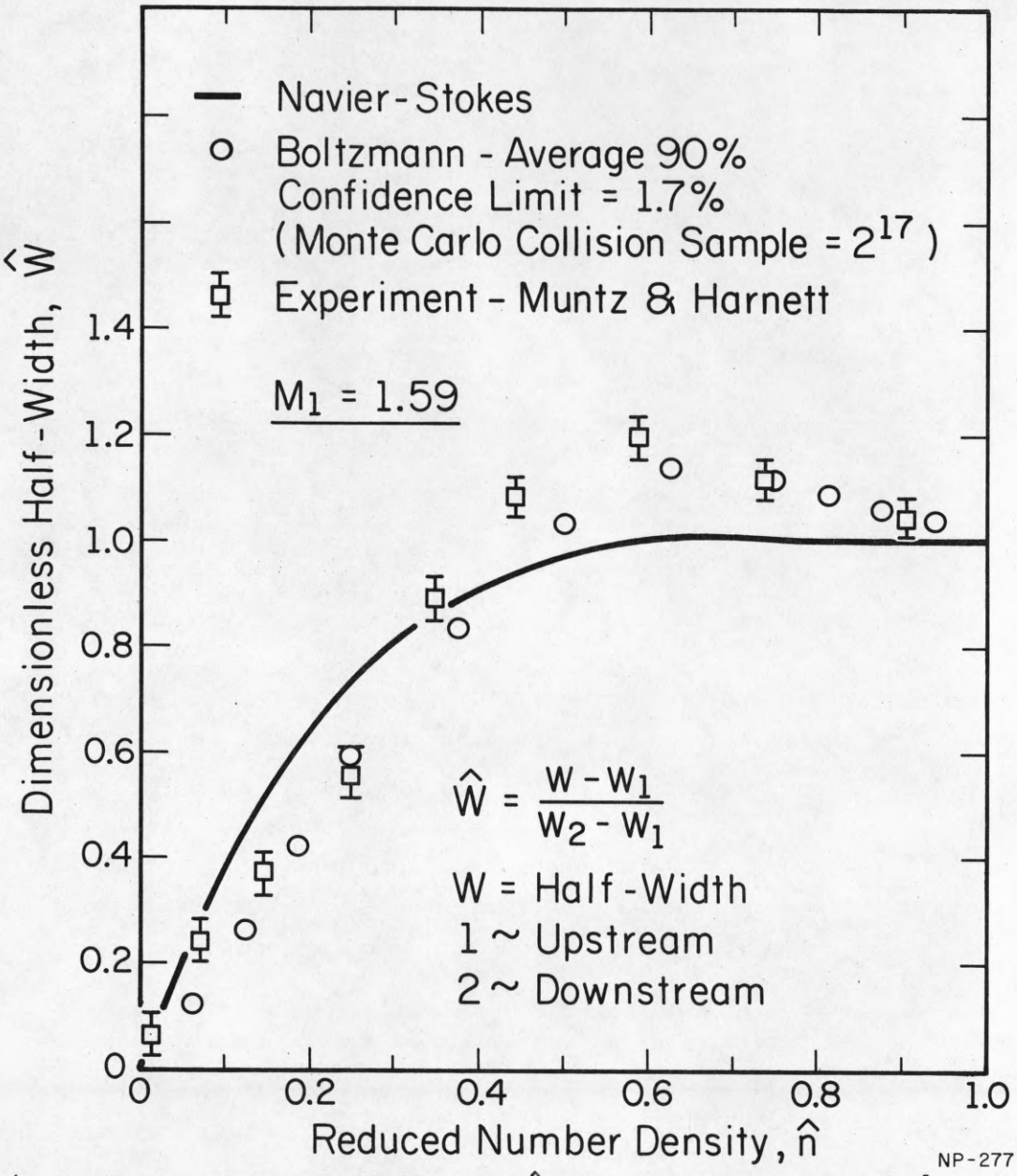

Fig. 7.4 Variation of reduced half-width $\hat{W}$ of the function $F(v_x) = \int f \, dv_y \, dv_z$ with reduced density $\hat{n}$ for $M_1 = 1.59$.

8. The Boltzmann Collision Integral (M_1=4)

As pointed out in the Introduction, it is Nordsieck's method of evaluation of the (non-linear) Boltzmann collision integral that has made possible the solution of the Boltzmann equation for strong shock waves and other far-from-equilibrium situations. We have deferred discussion of the collision integral until this concluding section, however, because the characteristics of the function, even though fundamental to understanding the detailed behavior of rarefied gases, are less familiar to gas dynamicists than the distribution function and its moments.

We shall first describe briefly the nature of the Boltzmann collision integral, as calculated by Nordsieck's Monte Carlo method from a solution of the Boltzmann equation for M_1=4. We shall then compare this function, as well as its two parts separately, with the approximations to it associated with the names of Mott-Smith and Krook in order to discover how far these approximations may be useful as descriptions of the solutions of the Boltzmann equation for strong shocks.

In Fig. 8.1 are shown the isolines of the function $v_\perp(a-bf)$ (the function calculated directly by our numerical solution of the Boltzmann equation) at the mid-shock position ($\hat{n} = \frac{1}{2}$) for M_1=4. The negative values of the function for large positive v_x correspond to $df/dx < 0$ and to the scattering loss of molecules with high forward velocity, like those characteristic of the cold side of the shock. The negative values for $v_x < 0$ (molecules moving in the upstream direction) correspond to $df/dx > 0$. The collision integral should vanish on the line $v_x = 0$ if df/dx is to be finite there. This requirement is a strong test of the reliability of numerical solutions of the Boltzmann equation or of approximations like those of Mott-Smith and Krook.

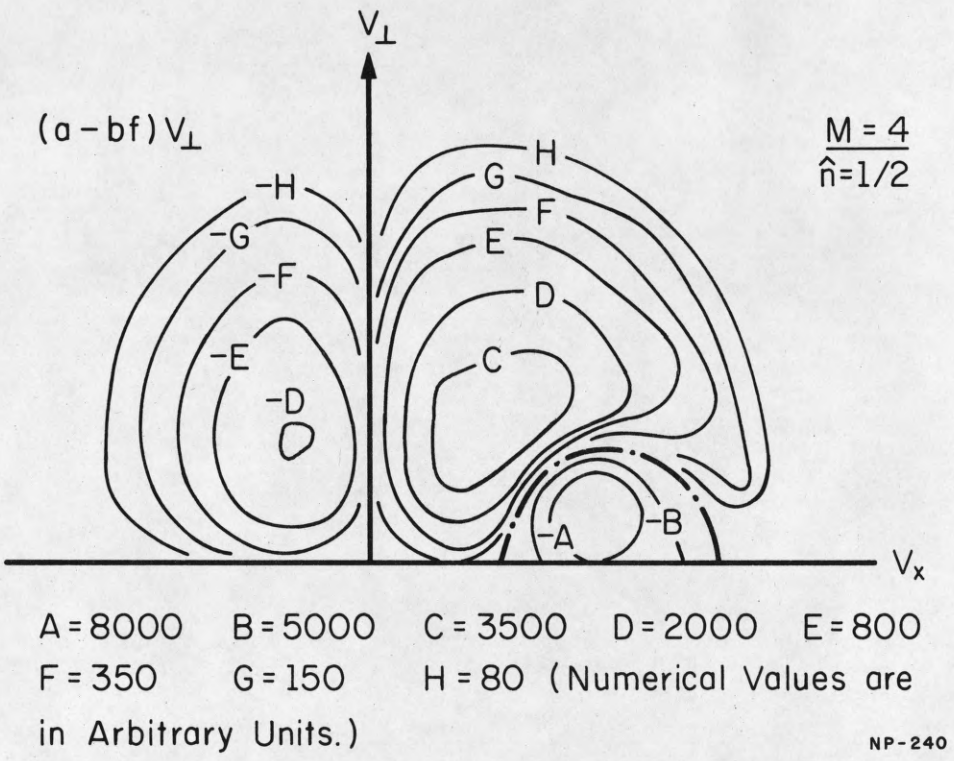

Fig. 8.1 Isolines of the function $v_\perp(a\text{-}bf)$ at the mid-shock position for $M_1 = 4$. $v_\perp(a\text{-}bf)$ is the function calculated directly by Nordsieck's Monte Carlo method.

Except in the case of a few velocity bins the values of (a-bf) obtained by Monte Carlo solution of the Boltzmann equation satisfy this criterion well.

A graphical representation of (a-bf) is given in Fig. 8.2. The negative peak is again in evidence. The values of the ordinate elsewhere are all positive except for $v_x < 0$. The function f increases in the downstream direction, as noted in the preceding paragraph, except near the cold peak.

Now let us look at the situation for the Mott-Smith approximation. Mott-Smith's Ansatz does not, of itself, provide values of the collision integral from solution of the Boltzmann equation.* We therefore compare the values of $(a\text{-}bf)_{MS}$ calculated from our solution of the Boltzmann equation, with a given Monte Carlo collision sample, to values of $(a\text{-}bf)_{MS}$ calculated from Mott-Smith values of the velocity distribution function using the same collision sample. We already know from the discussion in Section 2 that $(a\text{-}bf)_{MS}$ calculated from the Mott-Smith f is proportional to $\hat{n}(1\text{-}\hat{n})$ and that this proportionality does not hold for the Boltzmann values of (a-bf) calculated from solution of the Boltzmann equation. We could now show, in full detail, how the Boltzmann and Mott-Smith values differ from one another over velocity space. Instead, we will just comment here on two features of the Mott-Smith values.

We find, first, that the curve along which $(a\text{-}bf)_{MS}=0$ is displaced from the line $v_x=0$ by about 10% of the upstream gas velocity. The Mott-Smith (a-bf) thus does not satisfy the criterion that it should vanish on the

*The collision integrals of the Mott-Smith distribution function could be evaluated analytically and were obtained by Narasimha.[24]

Shock
($M_1 = 4$, $\hat{n} = 1/2$)

Boltzmann Collision Integrals, (a - bf)

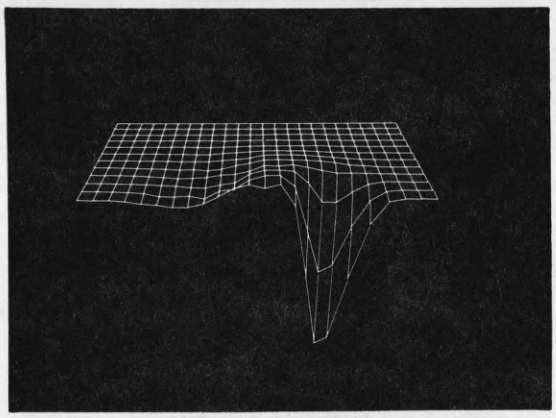

(Back View)

NP-280

Fig. 8.2 Graphical display of the Boltzmann collision integral (a-bf) at the mid-shock position ($\hat{n} = \frac{1}{2}$) for $M_1 = 4$.

line $v_x=0$. Aside from this strong defect of the Mott-Smith (a-bf), its qualitative features like the negative peak, for example, agree well with the Boltzmann (a-bf).

The Krook Ansatz says that the collision integral should be replaced by $\bar{b}(f_{eq}-f)$, where $\bar{b}$ = average collision frequency. The function f_{eq} is the Maxwell-Boltzmann distribution function for the same values of the density, temperature and gas velocity as obtained locally for the gas in the shock wave, that is, the values calculated from the Monte Carlo velocity distribution f. If the Krook collision term accurately describes the variation over velocity space of the Boltzmann collision term, even if only in part of the shock wave, then in this part the Krook equation can be used to replace the Boltzmann equation.*

We look first at the behavior of the Krook term near the line $v_x=0$. We find that for $\hat{n}$ in the range 0.6 to 0.8 the Krook term vanishes near this line. For other positions in the shock the curve on which the Krook term vanishes is displaced by 5 to 30% of the upstream gas velocity, the greatest displacement being near the cold side of the shock. From this qualitative evidence we conclude that a solution of the Krook equation can satisfy the Boltzmann equation, for $M_1 = 4$, only near $\hat{n} = 0.7$. Aside from this major defect the Krook expression is similar, in its qualitative features, like the negative peak, to the Boltzmann term.

It would be of interest also to see if the gain term a is symmetrical with respect to u, the local average speed as predicted by the Krook model.

---

*Solutions of the Krook equation for the shock waves are easy to obtain with our program. Detailed comparison of the "Krook shock" and the "Boltzmann shock" is, however, a large topic that will be treated elsewhere.

Fig. 8.3 shows the behavior of "a" in the velocity space for the unit shock position ($\hat{n} = \frac{1}{2}$) for $M_1 = 4$. (As mentioned in the Introduction, the gain term "a" and the loss term bf in the collision integral are calculated separately.)

We also may ask how well values of the Krook expression, for given velocity bins, agree with the Boltzmann values. We find that for $v_x < 0$ the Krook values are generally too large by a factor of about 1.6. Thus if each of the Krook values, for all bins for which $v_x < 0$, and for each station in the shock, were multiplied by 0.6, these values would agree with the Boltzmann values, within about 15% on the average. The situation is quite different for the bins for which $v_x > 0$. Here the values of the Krook expression are too large on the average by factors which vary, from 2.6 at the upstream side of the shock ($\hat{n}$=1/8) to 1.4 at the downstream side ($\hat{n}$=7/8). We might say then that the Krook expression overestimates the collision rate more seriously on the upstream side of the shock than on the downstream side.

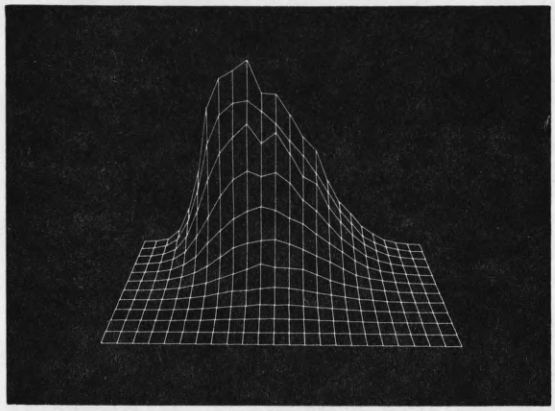

Fig. 8.3 Graphical display of the Boltzmann gain term "a" at the mid-shock position ($\hat{n} = \frac{1}{2}$) for $M_1 = 4$.

References

1. A. Nordsieck and B. L. Hicks, "Monte Carlo Evaluation of the Boltzmann Collision Integral," Proceedings of the Fifth International Symposium on Rarefied Gas Dynamics, 1967, Academic Press, pp. 675-710. (CSL Report R-307).

2. B. L. Hicks and S. M. Yen, "Solutions of the Non-Linear Boltzmann Equation for Plane Shock Waves," Proceedings of Sixth International Symposium on Rarefied Gas Dynamics, Academic Press, Vol. 1, 313-317, 1969.

3. S. M. Yen and H. J. Schmidt, "Monte Carlo Solutions of the Boltzmann Equation for Heat Transfer Problems," Proceedings of Sixth International Symposium on Rarefied Gas Dynamics, Vol. 1, Academic Press, 205-213, 1969.

4. S. M. Yen and B. L. Hicks, "On the Accuracy of Approximate Solutions of the Boltzmann Equation," Proceedings of the Fifth International Symposium on Rarefied Gas Dynamics, 1967, Academic Press, pp. 785-801. (CSL Report R-308.)

5. B. L. Hicks, "The Pseudo-Shock: A Non-Linear Problem of Translational Relaxation," CSL Report R-236.

6. S. M. Yen and B. L. Hicks, "Initial Behaviour of the Pseudo-Shock," CSL Report R-350.

7. Bruce L. Hicks and Margaret A. Smith, "On the Accuracy of Monte Carlo Solutions of the Non-linear Boltzmann Equations," Journal of Computational Physics, 3, 1, 58-79, August, 1968.

8. B. L. Hicks, S. M. Yen, and B. Reilly, "Numerical Studies of the Non-linear Boltzmann Equation. Studies of New Techniques and Error Reduction," CSL Report R-412, 1969.

9. B. L. Hicks and M. A. Smith, "Numerical Studies of Strong Shock Waves. Properties of a Strong Shock Wave for a Mach number of 2.5," CSL Report R-347, 1967.

10. M. Krook, "Continuum equations in the dynamics of rarefied gases," J. Fluid Mech., 6, p. 523, 1959.

11. H. M. Mott-Smith, "The Solution of the Boltzmann Equation for a Shock Wave," Physical Review, 82, 6, pp. 885-892, 1951.

12. F. S. Sherman, "A Low-density Wind-Tunnel Study of Shock-Wave Structure and Relaxation Phenomena in gases," NACA TN 3298, 1955.

13. S. Ziering and F. Ek, "Mean-Free-Path Definition in the Mott-Smith Shock Wave Solution," Physics of Fluids, 4, 6, p. 765, 1961.

14. B. L. Hicks and S. M. Yen, "A Simple Theory of Shock Structure," Physics of Fluids, 10, 458-460 (February, 1967).

15. C. S.-Wang-Chang, "On the Theory of the Thickness of Weak Shock Waves," University of Michigan. Report APL/JHO CM-504, UMH-3-F, 1948.

16. H. Grad, "The Profile of a Strong Plane Shock Wave," Communications on Pure and Applied Mathematics, Vol. V., p. 257, 1952.

17. H. Schmidt, "A Comparative Study of Shock Wave Solutions," M.S. Thesis, University of Illinois, 1965.

18. L. Talbot and F. S. Sherman, "Structure of Weak Shock Waves in a Monatomic Gas," NASA Memo, 12-14-58W, 1959.

19. S. M. Yen, "Temperature Overshoot in Shock Waves," Physics of Fluids, 9, 1417-1418, 1966.

20. M. Morduchow and P. A. Libby, "On the Distribution of Entropy with the Structure of a Normal Shock Wave," Pibal Report No. 759, Brooklyn Institute of Technology, 1962.

21. D. Baganoff and M. Nathenson, "Constitutive Relations for Stress and Heat Flux in a Shock Wave," Physics of Fluids, 13, 3, p. 596, 1970.

22. K. C. Kelley, "A Computer Graphics Program for the Generation of Half-Tone Images with Shadows," CSL Report R-444, University of Illinois, 1969.

23. E. P. Muntz and L. N. Harnett, "Molecular Velocity Distribution Function Measurements in a Normal Shock Wave," Physics of Fluids, Vol. 12, No. 10, p. 2027, 1970.

24. S. M. Deshpande and R. Narasimha, "The Boltzmann Collision Integrals for a Combination of Maxwellians," J. Fluid Mechanics, 36, part 3, p. 545, 1969.

Distribution List as of April 1,1970

ESD (ESTI)
L. G. Hanscom Field
Bedford, Mass 01731 2 copies

Defense Documentation Center
Attn: DDC-TCA
Cameron Station
Alexandria, Virginia 22314 50 copies

Commanding General
Attn: STEWS-RE-L, Technical Library
White Sands Missile Range
New Mexico 88002 2 copies

Mr Robert O. Parker, AMSEL-RD-S
Executive Secretary, TAC/JSEP
U.S. Army Electronics Command
Fort Monmouth, New Jersey 07703

Director, Electronic Programs
Attn: Code 427
Department of the Navy
Washington, D.C. 20360 2 copies

Naval Air Systems Command
AIR 03
Washington, D.C. 20360 2 copies

Director
Naval Research Laboratory
Attn: Code 2027
Washington, D.C. 20390 6 copies

Naval Electronic Systems Command
ELEX 03, Room 2046 Munitions Building
Department of the Navy
Washington, D.C. 20360 2 copies

Commander
U.S. Naval Ordnance Laboratory
Attn: Librarian
White Oak , Md 20910 2 copies

LTC H. W. Jackson
Chief, Electronics Division
Directorate of Engineering Sciences
Air Force of Scientific Research
Arlington, Virginia 22209 5 copies

Commander
Naval Electronics Laboratory Center
Attn: Library
San Diego, Calif 92152 2 copies

Dr. L. M. Hollingsworth
AFCRL (CRN)
L. G. Hanscom Field
Bedford, Mass 01731

Division of Engineering & Applied Physics
210 Pierce Hall
Harvard University
Cambridge, Mass 02138

Director
Research Laboratory of Electronics
Massachusetts Institute of Technology
Cambridge, Mass 02139

Miss R. Joyce Harman
Project MAC, Room 810
545 Technology Square
Cambridge, Mass 02139

Professor R. H. Rediker
Elec Engineering Professor
Mass, Institute of Technology
Building 13-3050
Cambridge, Mass 02139

Raytheon Company
Research Division Library
28 Seyon Street
Waltham, Mass 02154

Sylvania Electronic Systems
Applied Research Laboratory
Attn: Documents Librarian
40 Sylvan Road
Waltham, Mass 02154

Commanding Officer
Army Materials & Mechanics
Research Center
Attn: Dr H. Priest
Watertown Arsenal
Watertown, Mass 02172

MIT Lincoln Laboratory
Attn: Library A-082
PO Box 73
Lexington, Mass 02173

Commanding Officer
Office of Naval Research
Branch Office
495 Summer Street
Boston, Mass 02210

Commanding Officer (Code 2064)
U.S. Naval Underwater Sound Laboratory
Fort Trumbull
New London, Conn 06320

Dept of Eng & Applied Science
Yale University
New Haven, Conn 06520

Commanding General
U.S. Army Electronics Command
Attn: AMSEL-CT-A
Fort Monmouth, New Jersey 07703

Commanding General
U.S. Army Electronics Command
Attn: AMSEL-CT-D
Fort Monmouth, New Jersey 07703

Commanding General
U.S. Army Electronics Command
Attn: AMSEL-CT-I
Fort Monmouth, New Jersey 07703

Commanding General
U.S. Army Electronics Command
Attn: AMSEL-CT-L (Dr W.S. McAfee)
Fort Monmouth, New Jersey 07703

Commanding General
U.S. Army Electronics Command
Attn: AMSEL-CT-O
Fort Monmouth, New Jersey 07703

Commanding General
U.S. Army Electronics Command
Attn: AMSEL-CT-R
Fort Monmouth, New Jersey 07703

Commanding General
U.S. Army Electronics Command
Fort Monmouth, New Jersey 07703
Attn: AMSEL-CT-S

Commanding General
U.S. Army Electronics Command
Attn: AMSEL-GG-DD
Fort Monmouth, New Jersey 07703

Commanding General
U.S. Army Electronics Command
Attn: AMSEL-DL
Fort Monmouth, New Jersey 07703

Commanding General
U.S. Army Electronics Command
Attn: AMSEL-KL-D
Fort Monmouth, New Jersey 07703

Commanding General
U.S. Army Electronics Command
Attn: AMSEL-KL-E
Fort Monmouth, New Jersey 07703

Commanding General
U.S. Army Electronics Command
Attn: AMSEL-KL-I
Fort Monmouth, New Jersey 07703

Commanding General
U.S. Army Electronics Command
Attn: AMSEL-KL-SM
Fort Monmouth, New Jersey 07703

Commanding General
U.S. Army Electronics Command
Attn: AMSEL-KL-S
Fort Monmouth, New Jersey 07703

Commanding General
U.S. Army Electronics Command
Attn: AMSEL-KL-T
Fort Monmouth, New Jersey 07703

Commanding General
U.S. Army Electronics Command
Attn: AMSEL-NL-A
Fort Monmouth, New Jersey 07703

Commanding General
U.S. Army Electronics Command
Attn: AMSEL-NL-C
Fort Monmouth, New Jersey 07703

Commanding General
U.S. Army Electronics Command
Attn: AMSEL-NL-D (Dr H. Bennett)
Fort Monmouth, New Jersey 07703

Commanding General
U.S. Army Electronics Command
Attn: AMSEL-NL-P
Fort Monmouth, New Jersey 07703

Commanding General
U.S. Army Electronics Command
Attn: AMSEL-SC
Fort Monmouth , New Jersey 07703

Commanding General
U.S. Army Electronics Command
Attn: AMSEL-VL-D
Fort Monmouth, New Jersey 07703

Commanding General
U.S. Army Electronics Command
Attn: AMSEL-VL-F
Fort Monmouth, New Jersey 07703

Commanding General
U.S. Army Electronics Command
Attn: AMSEL-WL-D
Fort Monmouth, New Jersey 07703

Commanding General
U.S. Army Electronics Command
Attn: AMSEL-XL-DT
Fort Monmouth, New Jersey 07703

Commanding General
U.S. Army Electronics Command
Attn: AMSEL-XL-D
Fort Monmouth, New Jersey 07703

Mr Norman J. Field, AMSEL-RD-S
Chief, Office of Science & Technology
Research and Development Directorate
U.S. Army Electronics Command
Fort Monmouth, New Jersey 07703

Project Manager
Common Positioning & Navigation Systems
Attn: Harold H. Bahr (AMCPM-NS-TM),
Building 439
U.S. Army Electronics Command
Fort Monmouth, New Jersey 07703

U.S. Army Munitions Command
Attn: Science & Technology
Info Br., Bldg 59
Picatinny Arsenal, SMUPA-RT-S
Dover, New Jersey 07801

European Office of Aerospace Research
APO New York 09667

Director
Columbia Radiation Laboratory
Columbia University
538 West 120th ST
New York, N. Y. 10027

Dr John R. Ragazzini, Dean
School of Engineering & Science
New York University
University Heights
Bronx, New York 10453

Mr Jerome Fox, Research Coordinator
Polytechnic Institute of Brooklyn
333 Jay St.
Brooklyn, New York 11201

Airborn Instruments Laboratory
Deerpark, New York 11729

Dr W. R. Lepage, Chairman
Syracuse University
Dept of Electrical Engineering
Syracuse, New York 13210

Rome Air Development Center
Attn: Documents Library (EMTLD)
Griffiss Air Force Base, New York 13440

Mr H. E. Webb (EMBIS)
Rome Air Development Center
Griffiss Air Force Base, New York 13440

Professor James A. Cadzow
Department of Electrical Engineering
State University of New York at Buffalo
Buffalo, New York 14214

Dr A. G. Jordan
Head of Dept of Elec Engineering
Carnegie-Mellon University
Pittsburgh, Penn 15213

Hunt Library
Carnegie-Mellon University
Schenley Park
Pittsburgh, Penn 15213

Lehigh University
Dept of Electrical Engineering
Bethelehem, Penn 18015

Commander (ADL)
Naval Air Development Center
Attn: NADC Library
Johnsville, Warminster, Pa 18974

Technical Director (SMUFA-A2000-107-1)
Frankford Arsenal
Philadelphia, Penn 19137

Mr M. Zane Thornton, Chief, Network
Engineering, Communications and
Operations Branch, Lister Hill
National Center/ Biomedical Communications
8600 Rockville Pike
Bethesda, Maryland 20014

U.S. Post Office Dept
Library - Room 6012
12th & Pennsylvania Ave. N.W.
Washington, D.C. 20260

Technical Library
DDR&E
Room 3C-122, The Pentagon
Washington, D.C. 20301

Director for Materials Sciences
Advanced Research Projects Agency
Department of Defense
Washington, D.C. 20301

Asst Director (Research)
Rm 3C128, The Pentagon
Office of the Sec of Defense
Washington, D.C. 20301

Chief, R & D Division (340)
Defense Communications Agency
Washington, D.C. 20305

Distribution List (cont'd.)

Commanding General
U.S. Army Materiel Command
Attn: AMCRD-TP
Washington, D.C. 20315

Director, U.S. Army Material
Concepts Agency
Washington, D.C. 20315

Hq USAF (AFRDD)
The Pentagon
Washington, D.C. 20330

Hq USAF (AFRDDG)
The Pentagon
Washington, D.C. 20330

Hq USAF (AFRDSD)
The Pentagon
Washington, D.C. 20330

AFSC (SCTSE)
Andrews Air Force Base, Maryland 20331

Dr I. R. Mirman
Hq AFSC (SGGP)
Andrews AFB, Maryland 20331

Naval Ship Systems Command
Ship 031
Washington, D.C. 20360

Naval Ship Systems Command
Ship 035
Washington, D.C. 20360

Commander
U.S. Naval Security Group Command
Attn: G43
3801 Nebraska Avenue
Washington, D.C. 20390

Director
Naval Research Laboratory
Washington, D.C. 20390
Attn: Dr A. Brodizinsky, Sup. Elec Div

Director
Naval Research Laboratory
Washington, D.C. 20390
Attn: Maury Center Library (Code 8050)

Director
Naval Research Laboratory
Washington, D.C. 20390
Attn: Dr W.C. Hall, Code 7000

Director
Naval Research Laboratory
Attn: Library, Code 2029 (ONRL)
Washington, D.C. 20390

Dr G. M. R. Winkler
Director, Time Service Division
U. S. Naval Observatory
Washington, D.C. 20390

Colonel E.P. Gaines, Jr
ACDA/FO
1901 Pennsylvania Ave. N.W.
Washington, D.C. 20451

Commanding Officer
Harry Diamond Laboratories
Attn: Mr Berthold Altman (AMXDO-TI)
Connecticutt Ave & Van Ness St., N.W.
Washington, D.C. 20438

Central Intelligence Agency
Attn: CRS/ADD Publications
Washington, D.C. 20505

Dr H. Harrison, Code RRE
Chief, Electrophysics Branch
National Aeronautics & Space Admin
Washington, D.C. 20546

The John Hopkins University
Applied Physics Laboratory
Attn: Document Librarian
8621 Georgia Avenue
Silver Spring, Maryland 20910

Technical Director
U.S. Army Limited War Laboratory
Aberdeen Proving Ground
Aberdeen, Maryland 21005

Commanding Officer (AMXRD-BAT)
US Army Ballistics Research Laboratory
Aberdeen Proving Ground
Aberdeen, Maryland 21005

Electromagnetic Compatibility
Analysis Center (ECAC)
Attn: ACOAT
North Severn
Annapolis, Maryland 21402

Commanding Officer
U.S. Army Engineer Topographic Laboratories
Attn: STINFLO Center
Fort Belvoir, Virginia 22060

U.S. Army Mobility Equipment Research
and Development Center, Bldg 315
Attn: Technical Document Center
Fort Belvoir, Virginia 22060

Director (NV-D)
Night Vision Laboratory, USAECOM
Fort Belvoir, Virginia 22060

Dr Alvin D. Schnitzler
Institute for Defense Analyses
Science and Technology Division
400 Army-Navy Drive
Arlington, Virginia 22202

Director
Physical & Engineering Sciences Division
3045 Columbia Pike
Arlington, Va 22204

Commanding General
U.S. Army Security Agency
Attn: IARD-T
Arlington Hall Station
Arlington, Virginia 22212

Commanding General
USACDC Institute of Land Combat
Attn: Technical Library, Rm 636
2461 Eisenhower Avenue
Alexandria, Virginia 22314

VELA Seismological Center
300 North Washington St
Alexandria, Virginia 22314

U.S. Naval Weapons Laboratory
Dahlgren, Virginia 22448

Research Laboratories for the Eng
Sciences, School of Engineering &
Applied Science
University of Virginia
Charlottesville, Va 22903

Dr Herman Robl
Deputy Chief Scientist
U.S. Army Research Office (Durham)
Box CM, Duke Station
Durham, North Carolina 27706

Rochard O. Ulsh (CRDARD-IP)
U.S. Army Research Office (Durham)
Box CM, Duke Station
Durham, North

Richard O. Ulsh (CRDARD-IP)
U.S. Army Research Office (Durham)
Box CM, Duke Station
Durham, North Carolina 27706

ADTC (ADBPS-12)
Eglin AFB, Florida 32542

Commanding Officer
Naval Training Device Center
Orlando, Florida 32813

Technical Library, AFETR
(ETV,MU-135)
Patrick AFB, Florida 32925

Commanding General
U.S. Army Missile Command
Attn: AMSMI-RR
Redstone Arsenal, Alabama 35809

Redstone Scientific Information Center
Attn: Chief, Document Section
U.S. Army Missile Command
Redstone Arsenal, Alabama 35809

AUL3T-9663
Maxwell AFB, Alabama 36112

Hq AEDC (AETS)
Attn: Library/Documents
Arnold AFS, Tennessee 37389

Case Institute of Technology
Engineering Division
University Circle
Cleveland, Ohio 44106

NASA Lewis Research Center
Attn: Library
21000 Brookpark Road
Cleveland, Ohio 44135

Director
Air Force Avionics Laboratory
Wright-Patterson AFB, Ohio 45433

AFAL (AVTA) R.D. Larson
Wright-Patterson AFB, Ohio 45433

AFAL (AVT) Dr H.V. Noble, Chief
Electronics Technology Division
Air Force Avionics Laboratory
Wright-Patterson AFB, Ohio 45433

Dr Robert E. Fontana
Head, Dept of Elec Engineering
Air Force Institute of Technology
Wright Patterson AFB, Ohio 45433

Dept of Electrical Engineering
Clippinger Laboratory
Ohio University
Athens, Ohio 45701

Commanding Officer
Naval Avionics Facility
Indianapolis, Indiana 46241

Dr John D. Hancock, Head
School of Electrical Engineering
Purdue University
Lafayette, Ind 47907

Professor Joseph E. Rowe
Chairman,
Dept of Elec Engineering
The University of Michigan
Ann Arbor, Michigan 48104

Dr G. J. Murphy
The Technological Institute
Northwestern University
Evanston, Ill 60201

Commanding Officer
Office of Naval Research
Branch Office
219 South Dearborn St
Chicago, Illinois 60604

Illinois Institute of Technology
Dept of Electrical Engineering
Chicago, Illinois 60616

Deputy for Res. and Eng (AMSE-DRE)
U.S. Army Weapons Command
Rock Island Arsenal
Rock Island, Illinois 61201

Commandant
U.S. Army Command & General
Staff College
Attn: Acquisitions, Library Division
Fort Leavenworth, Kansas 66027

Dept of Electrical Engineering
Rice University
Houston, Texas 77001

HQ AMD (AMR)
Brooks AFB, Texas 78235

USAFSAM (SMKOR)
Brooks AFB, Texas 78235

Mr B. R. Locke
Technical Adviser, Requirements
USAF Security Service
Kelly Air Force Base, Texas 78241

Director
Electronics Research Center
The University of Texas as Austin
Eng-Science Bldg 110
Austin, Texas 78712

Department of Elec Engineering
Texas Technological University
Lubbock, Texas 79409

Commandant
U.S. Army Air Defense School
Attn: Missile Sciences Div., C&S Dept
P.O. Box 9390
Fort Bliss, Texas 79916

Director
Aerospace Mechanics Sciences
Frank J. Seiler Research Laboratory (OAR)
USAF Academy
Colorado Springs, Colorado 80840

Director of Faculty Research
Department of the Air Force
U.S. Air Force Academy
Colorado Springs, Colorado 80840

Major Richard J. Gowen
Tenure Associate Professor
Dept of Electrical Engineering
U.S. Air Force Academy
Colorado Springs, Colorado 80840

Academy Library (DFSLB)
U.S. Air Force Academy
Colorado Springs, Colorado 80840

M.A. Rothenberg (STEPD-SC(S))
Scientific Director
Desert Test Center
Bldg 100, Soldiers' Circle
Fort Douglas, Utah 84113

Utah State University
Dept of Electrical Engineering
Logan, Utah 84321

School of Engineering Sciences
Arizona State University
Tempe, Ariz 85281

Distribution List (cont'd.)

Commanding General
U.S. Army Strategic Communications Command
Attn: SCC-CG-SAE
Fort Huachuca, Arizona 85613

The University of Arizona
Dept of Electrical Engineering
Tucson, Arizona 85721

Capt C.E. Baum
AFWL (WLRE)
Kirkland AFB, New Mexico 87117

Los Alamos Scientific Laboratory
Attn: Report Library
P.O. Box 1663
Los Alamos, N.M. 87544

Commanding Officer
(AMSEL-BL-WS-R)
Atmospheric Sciences Laboratory
White Sands Missile Range
New Mexico 88002

Commanding Officer
Atmospheric Sciences Laboratory
White Sands Missile Range
New Mexico 88002

Chief, Missile Electronic Warfare
Technical Area, (AMSEL-WL-M)
U.S. Army Electronics Command
White Sands Missile Range
New Mexico 88002

Director
Electronic Sciences Lab
University of Southern California
Los Angeles, Calif 90007

Eng & Math Sciences Library
University of California at Los Angeles
405 Hilgred Avenue
Los Angeles, Calif 90024

Aerospace Corporation
P.O. Box 95085
Los Angeles, California 90045
Attn: Library Acquisitions Group

Hq SAMSO (SMTTS/Lt Belate)
AF Unit Post Office
Los Angeles, Calif 90045

Dr Sheldon J. Wells
Electronic Properties Information Center
Mail Station E-175
Hughes Aircraft Company
Culver City, California 90230

Director, USAF PROJECT RAND
Via: Aif Force Liaison Office
The RAND Corporation
Attn: Library D
1700 Main Street
Santa Monica, California 90406

Deputy Director & Chief Scientist
Office of Naval Research Branch Office
1030 East Green Street
Pasadena, California 91101

Aeronautics Library
Graduate Aeronautical Laboratories
California Institute of Technology
1201 E. California Blvd
Pasadena, California 91109

Professor Nicholas George
California Institute of Technology
Pasadena, Califonria 91109

Commanding Officer
Naval Weapons Center
Corona Laboratories
Attn: Library
Corona, California 91720

Dr F. R. Charvat
Union Carbide Corporation
Materials Systems Division
Crystal Products Dept
8888 Balboa Avenue
P.O. Box 23017
San Diego, California 92123

Hollander Associates
P.O. Box 2276
Fullerton, California 92633

Commander, U.S. Naval Missile Center (56322)
Point Mugu, California 93041

W.A. Eberspacher, Associate Head
Systems Integration Division
Code 5340A,Box 15
U.S. Naval Missile Center
Point Mugu, California 93041

Sciences-Engineering Library
University of California
Santa Barbara, California 93106

Commander (Code 753)
Naval Weapons Center
Attn: Technical Library
China Lake, California 93555

Library (Code 2124)
Technical Report Section
Naval Postgraduate School
Monterey, California 93940

Glen A. Myers (Code 52Mv)
Assoc Professor of Elec Eng
Naval Postgraduate School
Monterey, California 93940

Dr Leo Young
Stanford Research Institute
Menlo Park, California 94025

Lenkurt Electric Co., Inc.
1105 County Road
San Carlos, California 94070
Attn: Mr E.K. Peterson

Director
Microwave Laboratory
Stanford University
Stanford, California 94305

Director
Stanford Electronics Laboratories
Stanford University
Stanford, California 94305

Director
Electronics Research Laboratory
University of California
Berkeley, California 94720

ADDENDUM

Dr Joel Trimble, Code 437
Information Systems Branch
Office of Naval Research
Department of the Navy
Washington, D.C. 20360

U.S. Naval Oceanographic Office
Attn: M. Rogofsky, Librarian (Code640)
Washington, D.C. 20390

CORRECTION

Director, Electronic Programs
Attn: Code 427
Office of Naval Research
Department of the Navy
Washington, D.C. 20360 2 copies

DELETE

Technical Director
U.S. Army Limited War Laboratory
Aberdeen Proving Ground
Aberdeen, Maryland 21005

REPLACE WITH

Technical Director
U.S. Army Land Warfare Laboratory
Aberdeen Proving Ground
Aberdeen, Maryland 21005

DELETE

USAF European Office of Aerospace Research
APO New York 09667

REPLACE WITH

European Office of Aerospace Research
Technical Information Office
Box 14, FPO New York 09510

DELETE

Dr John R. Raggazzini, Dean
School of Engineering and Science
New York University
University Heights
Bronx, New York 10453

REPLACE WITH

New York University
Engineering Library
Bronx, New York 10453

Security Classification

DOCUMENT CONTROL DATA - R & D

(Security classification of title, body of abstract and indexing annotation must be entered when the overall report is classified)

1. ORIGINATING ACTIVITY *(Corporate author)*
University of Illinois
Coordinated Science Laboratory
Urbana, Illinois 61801

2a. REPORT SECURITY CLASSIFICATION

2b. GROUP

3. REPORT TITLE
THE INTERNAL STRUCTURE OF SHOCK WAVES

4. DESCRIPTIVE NOTES *(Type of report and inclusive dates)*

5. AUTHOR(S) *(First name, middle initial, last name)*
HICKS, Bruce L.; YEN, Shee-Mang & REILLY, Barbara J.

6. REPORT DATE	7a. TOTAL NO. OF PAGES	7b. NO. OF REFS
June 1970	87	24

8a. CONTRACT OR GRANT NO.
DAAB 07-67-C-0199; also in part ONR N00015-67-A-0305-0001.

b. PROJECT NO.

c.

d.

9a. ORIGINATOR'S REPORT NUMBER(S)
R-474

9b. OTHER REPORT NO(S) *(Any other numbers that may be assigned this report)*
UILU-ENG 70-219

10. DISTRIBUTION STATEMENT
This document has been approved for public release and sale; its distribution is unlimited.

11. SUPPLEMENTARY NOTES

12. SPONSORING MILITARY ACTIVITY
Joint Services Electronics Program
thru U.S. Army Electronics Command
Fort Monmouth, New Jersey 07703

13. ABSTRACT

The non-linear Boltzmann equation has been solved for shock waves in a gas of elastic spheres. The solutions were made possible by the use of Nordsieck's Monte Carlo method of evaluation of the collision integral in the equation. Accurate solutions were obtained by the same method for the whole range of upstream Mach numbers M_1 from 1.1 to 10 even though the corresponding degree of departure from equilibrium varies by a factor greater than 1000. Many characteristics of the internal structure of the shock waves have been calculated from the solutions and compared with Navier-Stokes, Mott-Smith and Krook descriptions which, except for low Mach numbers, are not based upon the Boltzmann equation itself.

DD FORM 1 NOV 65 1473

Security Classification

14 KEY WORDS	LINK A		LINK B		LINK C	
	ROLE	WT	ROLE	WT	ROLE	WT
Solutions of Boltzmann Equation						
Shock Waves						
Mach Number =1.1-10						
Distribution Function						
Collision Integrals						
Shock Properties						
Density Gradients						
Transport Properties						
Boltzmann Function						
Entropy						